La borsa di dottorato è stata cofinanziata con risorse del
Programma Operativo Nazionale Ricerca e Innovazione 2014-2020 (CCI 2014IT16M2OP005),
Fondo Sociale Europeo, Azione I.1 "Dottorati Innovativi con caratterizzazione Industriale"

UNIONE EUROPEA
Fondo Sociale Europeo

Politecnico
di Bari

Department of Electrical and Information Engineering

ELECTRICAL AND INFORMATION ENGINEERING
PH.D. PROGRAM

SSD: ING-INF/03 – TELECOMMUNICATIONS

Final Dissertation

DESIGN AND CHARACTERIZATION OF YEAST-BASED ELECTROCHEMICAL BIOSENSORS FOR APPLICATION IN PRECISION AGRICULTURE

---

by

Ehtisham Wahid

Supervisor:
Prof. Cataldo Guaragnella, Ph.D.
Co-supervisor:
Prof. Nicoletta Guaragnella, Ph.D.

Coordinator of Ph.D. Program:
Prof. Mario Carpentieri, Ph.D.

Course n°36, 12/02/2021-11/05/2024

Politecnico di Bari

LIBERATORIA PER L'ARCHIVIAZIONE DELLA TESI DI DOTTORATO

Al Magnifico Rettore
del Politecnico di Bari

Il/la sottoscritto/a WAHID EHTISHAM nato/a a SARGODHA, PAKISTAN il 14/04/1991
residente a BARI, ITALY in via GIUSEPPE FANELLI 201/13A e-mail ehtisham.wahid@poliba.it
iscritto al 3° anno di Corso di Dottorato di Ricerca in INGEGNERIA ELETTRICA E DELL' INFORMAZIONE ciclo XXXVI ed essendo stato ammesso a sostenere l'esame finale con la prevista discussione della tesi dal titolo: DESIGN AND CHARACTERIZATION OF YEAST-BASED ELECTROCHEMICAL BIOSENSORS FOR APPLICATION IN PRECISION AGRICULTURE

DICHIARA

1) di essere consapevole che, ai sensi del D.P.R. n. 445 del 28.12.2000, le dichiarazioni mendaci, la falsità negli atti e l'uso di atti falsi sono puniti ai sensi del codice penale e delle Leggi speciali in materia, e che nel caso ricorressero dette ipotesi, decade fin dall'inizio e senza necessità di nessuna formalità dai benefici conseguenti al provvedimento emanato sulla base di tali dichiarazioni;
2) di essere iscritto al Corso di Dottorato di ricerca INGEGNERIA ELETTRICA E DELL' INFORMAZIONE ciclo XXXVI, corso attivato ai sensi del "*Regolamento dei Corsi di Dottorato di ricerca del Politecnico di Bari"*, emanato con D.R. n.286 del 01.07.2013;
3) di essere pienamente a conoscenza delle disposizioni contenute nel predetto Regolamento in merito alla procedura di deposito, pubblicazione e autoarchiviazione della tesi di dottorato nell'Archivio Istituzionale ad accesso aperto alla letteratura scientifica;
4) di essere consapevole che attraverso l'autoarchiviazione delle tesi nell'Archivio Istituzionale ad accesso aperto alla letteratura scientifica del Politecnico di Bari (IRIS-POLIBA), l'Ateneo archivierà e renderà consultabile in rete (nel rispetto della Policy di Ateneo di cui al D.R. 642 del 13.11.2015) il testo completo della tesi di dottorato, fatta salva la possibilità di sottoscrizione di apposite licenze per le relative condizioni di utilizzo (di cui al sito http://www.creativecommons.it/Licenze), e fatte salve, altresì, le eventuali esigenze di "embargo", legate a strette considerazioni sulla tutelabilità e sfruttamento industriale/commerciale dei contenuti della tesi, da rappresentarsi mediante compilazione e sottoscrizione del modulo in calce (Richiesta di embargo);
5) che la tesi da depositare in IRIS-POLIBA, in formato digitale (PDF/A) sarà del tutto identica a quelle consegnate/inviate/da inviarsi ai componenti della commissione per l'esame finale e a qualsiasi altra copia depositata presso gli Uffici del Politecnico di Bari in forma cartacea o digitale, ovvero a quella da discutere in sede di esame finale, a quella da depositare, a cura dell'Ateneo, presso le Biblioteche Nazionali Centrali di Roma e Firenze e presso tutti gli Uffici competenti per legge al momento del deposito stesso, e che di conseguenza va esclusa qualsiasi responsabilità del Politecnico di Bari per quanto riguarda eventuali errori, imprecisioni o omissioni nei contenuti della tesi;
6) che il contenuto e l'organizzazione della tesi è opera originale realizzata dal sottoscritto e non compromette in alcun modo i diritti di terzi, ivi compresi quelli relativi alla sicurezza dei dati personali; che pertanto il Politecnico di Bari ed i suoi funzionari sono in ogni caso esenti da responsabilità di qualsivoglia natura: civile, amministrativa e penale e saranno dal sottoscritto tenuti indenni da qualsiasi richiesta o rivendicazione da parte di terzi;
7) che il contenuto della tesi non infrange in alcun modo il diritto d'Autore né gli obblighi connessi alla salvaguardia di diritti morali od economici di altri autori o di altri aventi diritto, sia per testi, immagini, foto, tabelle, o altre parti di cui la tesi è composta.

Luogo e data BARI, 10/07/2024 Firma 

Il/La sottoscritto, con l'autoarchiviazione della propria tesi di dottorato nell'Archivio Istituzionale ad accesso aperto del Politecnico di Bari (POLIBA-IRIS), pur mantenendo su di essa tutti i diritti d'autore, morali ed economici, ai sensi della normativa vigente (Legge 633/1941 e ss.mm.ii.),

CONCEDE

- al Politecnico di Bari il permesso di trasferire l'opera su qualsiasi supporto e di convertirla in qualsiasi formato al fine di una corretta conservazione nel tempo. Il Politecnico di Bari garantisce che non verrà effettuata alcuna modifica al contenuto e alla struttura dell'opera.
- al Politecnico di Bari la possibilità di riprodurre l'opera in più di una copia per fini di sicurezza, back-up e conservazione.

Luogo e data BARI, 10/07/2024 Firma _____

Politecnico di Bari

Department of Electrical and Information Engineering

ELECTRICAL AND INFORMATION ENGINEERING
PH.D. PROGRAM

SSD: ING-INF/03 – TELECOMMUNICATIONS

Final Dissertation

DESIGN AND CHARACTERIZATION OF YEAST-BASED ELECTROCHEMICAL BIOSENSORS FOR APPLICATION IN PRECISION AGRICULTURE

---

by

Ehtisham Wahid

Referees:

Prof. Giuseppe Pirlo
Prof. Giovanni Attolico

Supervisor:

Prof. Cataldo Guaragnella, Ph.D.

Co-supervisor:
Prof. Nicoletta Guaragnella, Ph.D.

Coordinator of Ph.D. Program:
Prof. Mario Carpentieri, Ph.D.

Course n°36, 12/02/2021-11/05/2024

Dedicated to:
The one and only,
The Great,

"*MY MOTHER*"

Acknowledgements

I am thankful to Allah almighty who bestowed upon me the intellectual ability, courage and strength to complete this humble contribution towards knowledge. First and foremost, I deem it as my utmost pleasure to express my deepest thanks, respect and sincere gratitude to my supervisor Prof. Cataldo Guaragnella, and co-supervisor Prof. Nicoletta Guaragnella, for their invaluable guidance, support and encouragement throughout the course of this research. Their expertise and experience were instrumental in helping me to develop my research skills and shape my ideas into a cohesive project. I am deeply indebted for their patience, feedback, and commitment to my work. I would like to thank Prof. Matteo Grattieri from Department of Chemistry (DoC), for his help in designing the immobilization protocols.

I would especially like to thank Prof. Enrico Marsili from China Beacon Institute (CBI), Ningbo, China for his collaboration and guidance to help me acquire in depth knowledge related to electrochemical characterization techniques.

I am also thankful to all of my colleagues in our research group for creating a supportive and collaborative environment that facilitated my research. I extend my heartfelt appreciation to every single person who has supported and encouraged me in any possible way during my journey. Your contributions have played a vital role, and I am forever beholden.

Finally, I would like to thank my family and friends, for their support, love, and prayers.

Abstract

Ehtisham Wahid

Design and Characterization of Yeast-based Electrochemical Biosensors for Application in Precision Agriculture

In recent years, precision agriculture (PA) has garnered significant interest due to its substantial agronomical advantages. At the heart of PA lie advanced sensing technologies, which offer rapid, cost-effective, and skill-independent detection solutions. Among these cutting-edge technologies are electrochemical biosensors. These biosensors integrate bioreporters such as living cells, aptamers, DNA, peptides, and antigens within electrochemical transducers, whether electrodes or field-effect transducers. This integration facilitates easy miniaturization, mass production, and seamless incorporation with electronic acquisition systems. Additionally, the devices for collecting current and potential signals are not only affordable and portable but also exhibit low power consumption. Consequently, electrochemical biosensors are poised to deliver point-of-care diagnostics essential for precision agriculture applications. Despite their potential, the industrial adoption of electrochemical biosensors remains limited, primarily due to the insufficient affinity recognition of bioreporters towards targeted analytes. Addressing this gap necessitates the exploration of novel bioreporters. Recently, unicellular microorganisms with robust cell walls, like yeast and bacteria, have garnered significant research interest. Unlike aptamers and enzymes, which require pretreatment, whole-cell biosensors can detect analytes in bioavailable forms. Furthermore, these microorganisms thrive under less stringent growth conditions and can be genetically modified to achieve the desired responses, making them highly suitable for on-site electrochemical applications. One exemplary organism is the yeast species *S. cerevisiae*, renowned for its resilience in extreme environments, lack of biofilm formation, ethanol production instead of CO_2, accessibility, non-pathogenic nature, and, most importantly, its well-characterized metabolism and genome. Additionally, *S. cerevisiae* has demonstrated the ability to generate electrical signals during the decomposition of organic compounds, positioning it as a model organism for electrochemical sensing. Leveraging the remarkable properties of yeast-based electrochemical biosensors and aiming to pioneer IoT-enabled biosensors for precision agriculture, we developed innovative yeast-based biosensors accompanied by a handheld prototype electrochemical device for point-of-care copper detection. Complementing this, a Python-based web application has been created for the online storage, visualization, and analysis of sample data. The initial phase of this project is dedicated to the design and characterization of yeast-based electrochemical biosensors utilizing a Glassy Carbon Electrode (GCE). This section is meticulously divided into three subsections. The first subsection elucidates the response of the biorecognition element (*S. cerevisiae WT* cells) in the presence of $CuSO_4$, using standard optical detection techniques. The second subsection delves into the protocols employed for the immobilization of the biorecognition element onto the surface of the GCE using polydopamine (PDA) to fabricate bio-electrodes (biosensors). The final subsection investigates the performance of the developed biosensor through comprehensive electrochemical characterization utilizing a single channel potentiostat. While standard optical detection showed a significant response only at concentrations above 5 mM after 4 hours of incubation with $CuSO_4$, an impressive limit of detection (LoD) of 12.5 µM was achieved using electrochemical detection, boasting an R^2 value of 0.956 after 2500 seconds of incubation. The subsequent part of this study centers on the design and characterization of biosensors fabricated with Screen-Printed Electrodes (SPE), incorporating genetic (multiple yeast respiratory mutants) and metabolic (various growth media) approaches to enhance the overall electrochemical response. This section is further bifurcated into two primary parts. Initially, the viability and growth of three *S. cerevisiae* strains *WT*, Δ*hap4*, and Δ*rtg2* in varying concentrations of $CuSO_4$ using standard optical detection are evaluated. In the second part, biosensors prepared with immobilized *S. cerevisiae WT* cells under different growth conditions, and Δ*hap4* and Δ*rtg2* cells cultured in standard media are

examined through electrochemical characterization using a multichannel potentiostat for $CuSO_4$ detection. The SPE-based biosensors with metabolically and genetically manipulated yeast cells exhibit superior performance, achieving a LoD as low as 2.2 μM and an R^2 of 0.998. Subsequently, a prototype handheld electrochemical device, capable of in-house biosensor mounting, was assembled. A complementary web application was also developed for the online storage, visualization, and analysis of data acquired from the prototype. The prototype was tested with biosensors prepared by immobilizing *WT* cells on the SPE surface in the presence of copper, achieving a LoD of 2.9 μM and an R^2 of 0.998, closely mirroring the results obtained with a standard laboratory potentiostat.

During this work, we also developed a Matlab-based application which provides a rapid and robust quantitative yeast growth analysis from spot plating assay images. The spot plating assay represents a common method for assessing yeast growth in low-throughput laboratory environments, encompassing growth on various nutrient substrates or exposure to particular stressors. The application features a straightforward one-step installation process, an intuitive interface, and streamlined analysis steps in contrast to traditional methods, rendering it a valuable resource for quantifying growth and viability, suitable for both experienced and inexperienced yeast researchers alike.

Publications

Journal Papers

1. Wahid, E., Ocheja, O. B., Guaragnella, N., & Guaragnella, C. (2024). A Matlab-based application for quantification of yeast cell growth on solid media. *Journal of the Royal Society Interface*, *21*(212), 20230695.
2. Ocheja, O. B., Wahid, E., Franco, J. H., Trotta, M., Guaragnella, C., Marsili, E., ... & Grattieri, M. (2024). Polydopamine-immobilized yeast cells for portable electrochemical biosensors applied in environmental copper sensing. *Bioelectrochemistry*, *157*, 108658.
3. Wahid, E., Ocheja, O. B., Marsili, E., Guaragnella, C., & Guaragnella, N. (2023). Biological and technical challenges for implementation of yeast-based biosensors. *Microbial Biotechnology*, *16*(1), 54-66.
4. Di Noia, M. A., Scarcia, P., Agrimi, G., Ocheja, O. B., Wahid, E., Pisano, I., ... & Guaragnella, N. (2023). Inactivation of HAP4 accelerates RTG-dependent Osmoadaptation in Saccharomyces cerevisiae. *International Journal of Molecular Sciences*, *24*(6), 5320.

Conference Presentations

1. Wahid, E., Ocheja, O. B., Guaragnella, N., & Guaragnella, C. "A Matlab-based application for quantification of yeast cell growth on solid media". *XVI Federation of Life Sciences (FISV) congress, Naples, September 2022.*
2. Wahid, E., Ocheja, O. B., Guaragnella, N., & Guaragnella, C. "A Matlab-based application for quantification of yeast cell growth on solid media". *International Forum on Industrial Biotechnology and Bioeconomy (IFIB), Bari, September 2022*.
3. Ocheja, O. B., Wahid, E., Guaragnella, N., & Guaragnella, C. "Comparison of Yeast cells immobilization procedures for biosensor applications". *31st International Conference on Yeast Genetics and Molecular Biology (ICYGMB31), Florence, August 2023*.
4. Ocheja, O. B., Wahid, E., Guaragnella, N., & Guaragnella, C. "Exploring the potential of yeast cells as biosensors for environmental monitoring". *Federation of European Biochemical Societies (48FEBS), Milan, June – July 2024*.

Table of contents

List of Figures

List of Tables

Thesis Organization

Chapter 1: A review of the state of the art topics covered in this thesis is presented. Basics of yeast based biosensors, are briefly explained. The effect of $CuSO_4$ on yeast cells along with cell immobilization techniques is discussed. Finally, classification of electrochemical biosensors based on transduction mechanisms is described.

Chapter 2: This chapter covers the methods for the growth of biorecognition element (yeast cells) and basic theory of characterization techniques used in this thesis, to provide a better understanding of underline knowledge gained during this study.

Chapter 3: Details on design and characterization of yeast based biosensor developed using GCE (transducer) as well as the numerical results obtained are provided in this chapter. The first part covers the preliminary experiments performed to study the response of biorecognition element (yeast) in liquid media in the presence of $CuSO_4$ along with the morphological study. In the second part, the protocols for immobilization of biorecognition element on transducer (GCE) surface as well as electrochemical analysis of biosensor using techniques like CV, EIS and CA is explained.

Chapter 4: This chapter explains the design and characterization of yeast based electrochemical biosensors prepared with SPE using metabolic and genetic manipulations on biorecognition elements. Initially, the viability assessment and growth analysis of multiple biorecognition elements in the presence of $CuSO_4$ is provided using optical detection. Later, biosensors design along with electrochemical characterization and numerical results are discussed in detail.

Chapter 5: This chapter covers the state of the art topic related to prototype and web application design. The first part deals with the description of prototype and numerical results obtained after testing of biosensors using prototype device. The second part deals with explanation of design and working of Python-based web application.

Chapter 6: Details on design and working of Matlab-based application for spotting assay quantification application are provided in this chapter. Basic of spotting assay along with material and method used to perform it are briefly explained. Insight about application and protocols to perform analysis using application are discussed. Finally, numerical result and discussion on obtained by quantification of certain yeast strain in the presence of NaCl stress are described.

Chapter 7: The main results obtained during this work are summarized, the conclusions are drawn, and some future aspects are proposed.

Chapter 1

INTRODUCTION TO BIOSENSORS

The agricultural sector of the world is facing a wide spectrum of challenges like lack of water management, declining soil organic matter, diseases, pests, and chemicals management [1, 2]. Therefore, it is necessary to consider methods to make agriculture sustainable. This concept is related to the field in research called Precision Agriculture (PA). PA concept is completely reliant on modern day technologies [3]. The backbone of implementation of PA is a sustainable detection system for collection of accurate data [4-8]. PA involves the application of technology and agronomic principles to control variations in temporal, spatial and individual aspects related to production [9, 10]. The International Society of Precision Agriculture has described PA as "a management strategy that takes account of temporal and spatial variability to improve sustainability of agricultural production" [11]. Some specific advantages offered by PA practices, also recognized by the European Commission, include the increase in accuracy of field work, higher operation speed, remote monitoring, precise application of crop management inputs such as fertilizer, seeds, and pesticides, resulting in lower costs and enhances outputs as well as increase in water efficiency and optimal use of irrigation water [12, 13]. Beyond the certain advantages, the adoption of PA models still requires time, *ad hoc* competences, education, support, and investments. However, the core network of PA is made by three main actions: data acquisition, communication technology and decision processes [12]. For this reason, PA tools involve a vast array of technologies including hardware and software, such as portable sensors, mobile devices, Internet of Things (IOT) and many more. For PA agriculture, the sensing layer is the most important as it is responsible for the data acquisition [9, 11]. Generally, these sensors are coupled with smart transmission systems such as NB-IoT, LoRa and Sigfox for IoT, allowing the development of a dense and "culture specific" data acquisition system [14]. In recent years, specific in-situ IoT sensors, connected to a centralized system, able to periodically acquire data have been developed [15]. However, most of them are mainly used to monitor physical parameters, others have been presented as methods but are not yet ready to be used in applications as they are still at the stage of laboratory devices and only few are available as commercial systems [14, 16, 17]. Recently, a relevant part of the scientific research dealing with the development of PA sensors has dedicated its attention to biological systems, because of their high specificity and sustainability. Among the emerging novel trends and streams in agriculture related detection and sensing technologies, biosensors are now considered most significant in all fields concerning agriculture. As they provide efficient means for detection of hazardous pollutants and chemicals. The schematic diagram of a biosensor is shown in Fig. 1.1. Biosensors are defined as analytical devices that use biorecognition elements (such as enzymes, antibodies, nucleic acids, aptamers, cells, tissues etc) to interact with the target analyte in order to produce an input biochemical signal. This signal is then converted, by the transducer element, into a different output signal (electric, optical, acoustic etc.), proportional to the concentration of the analyte [18-20]. Biosensors have gained immense interest from researcher in past few years [19, 21]. The main reason behind this significant increase is the need to develop portable, simple, rapid, and cost effective analytical devices for detection of environmental pollutants, disease markers and potential toxic molecules to improve quality of life and to minimize health risk to living beings [19, 22-24]. Conventionally, techniques like high performance liquid chromatography (HPLC), ion-exchange chromatography (IEC) and optical methods like calorimetry are mainly carried out for analysis. Although the conventional techniques provide better sensitivity and selectivity, they are complex, time consuming and expensive. Moreover, they require sample purification, extraction and/or derivation steps before analysis [24].

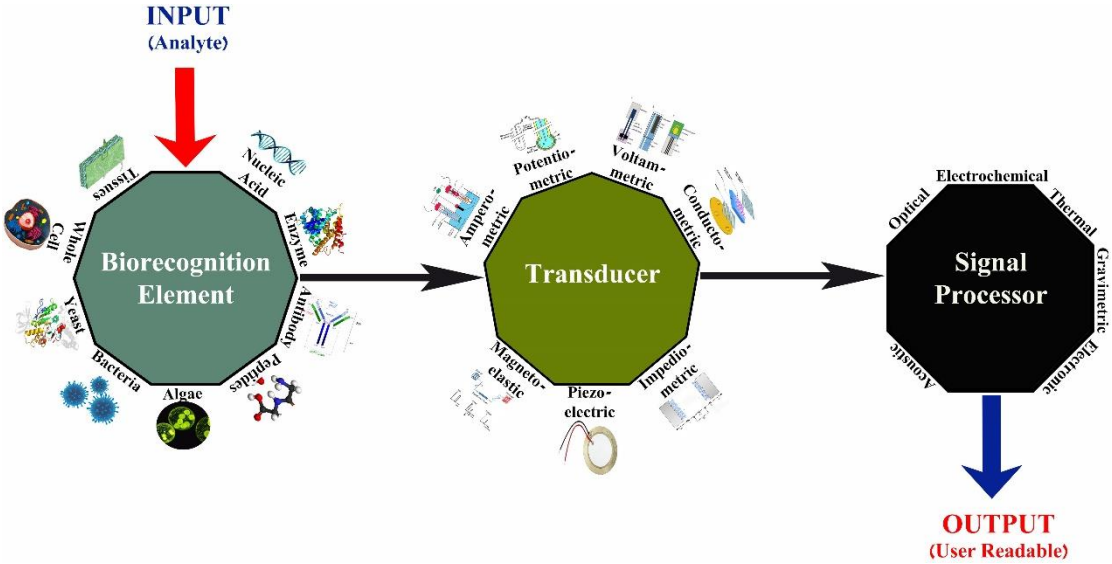

Figure 1.1: Schematic diagram of a biosensor. A biosensor includes biorecognition element for sensing, transducer for conversion of representative response into a detectable signal connected to signal processing unit to obtain a quantifiable output.

Due to these reasons, the conventional techniques require specialized operator and hence they are not considered the best solution for repetitive, continuous, online and point-of-cure analysis applications. Ideally speaking, biosensors have the capability to mitigate the drawbacks in conventional techniques by providing rapid, low cost, point-of-cure detection without skilled user. Typical example of biosensor with all above-mentioned characteristics is glucometer (for detection of glucose in blood), whose first commercial piece, developed by Yellow Spring Instruments (YSI), dates back to 1975 [19, 24]. Since the development of amperometric glucose electrode, electrochemical biosensors are widely used for clinical, environmental, industrial, and agricultural applications [25]. Generally, electrochemical biosensors present ease of miniaturization, batch fabrication and integration with electrical acquisition systems. Moreover, the signal collection devices for current and potential are low cost, portable and have low power consumption [26-28]. Thus hold the promise to provide point-of-care diagnosis. However, electrochemical biosensors who reach industrial stage are very limited, and one of the reasons is lack of affinity recognition of bioreporter (whole cells, protein, nucleic acid) towards analyte of interest. This short coming requires search for new bioreporters. Recently, unicellular microorganisms with developed cell wall like yeast and bacteria have attracted the attention of researchers. Unlike aptamers and enzymes (need pretreatment), whole cell biosensors are capable of detection in bioavailable forms. Moreover, they need less demanding growth conditions and can be generally modified to obtain required response. Thus, making them more suitable for on-site electrochemical applications [29-32]. One of such organisms is yeast species *Saccharomyces cerevisiae (S. cerevisiae)*, tolerate extreme environment, lack biofilm formation, produce ethanol instead of CO_2, provide ease of access, is non-pathogenic and above all has a well characterised metabolism and genome [33]. It is well known for its use of fermentable and non-fermentable carbon sources for energy production like glucose and ethanol, glycerol respectively for energy production [34]. Moreover, *S. cerevisiae* have also shown to produce electrical signal while decomposing organic compounds and is considered as one of the model organisms for electrochemical sensing [33, 35, 36]. However, in electrochemical biosensors extra cellular electron transfer (EET) play a pivotal role for detection [37] and microorganisms usually display low efficiency of EET at biological/inorganic interface which is a bottleneck for practical applications [38]. Microorganisms like yeast that lack adhesion to have effective EET, cell immobilization is necessary not only for sensory application but for other applications as well [39]. In this regard, single cell encapsulation using adhesive nanomaterials is suggested as a solution (such as Pd

and Au) [38, 40, 41]. Although, nanomaterials provide high conductivity, but they usually have week bonding, low cytocompatibility and usually environmental unfriendly. So, while immobilizing one should also consider biocompatibility along with stability requirements and one of such material is polydopamine (PDA). PDA is a naturally derived polymer that is organic with low toxicity, it has previously been used to immobilize yeast cells and have the ability to act as redox mediator as well [42]. Therefore, yeast cells immobilised with biocompatible and EET facilitating coating like PDA provides a promising option for electrochemical biosensing applications such as copper detection in agricultural circuits as fungicides used widely in organic farming have excessive copper contents [43]. For example, according to European regulations the maximum residual level (MSL) for grapes and vine is 20mg/kg and 1mg/l respectively [44], and soil in vineyard of some Germany [45]and Czech [46], and raw grapes and wine in Italy [44, 47] exceed local MSL regulations for Cu2+. As such, there is need for development of sensors for point-of-cure (POC) applications. Although, copper in low concentration is essential even for organisms [47-49] but a higher concentration of copper like as 0.1 mM inhibits metabolic activities in yeast and lead to sluggish fermentation [50-52]. Thus, making yeast a potential choice as bioreceptor for electrochemical biosensing for such applications. In this regard, we did an extensive study of available literature and put up a review article on biological and technical challenges for implementation of yeast-based biosensors with a citation score of 14 in one year showing the interest of research community in this topic. Moreover, owing to the advantages of electrochemical biosensors, promising features of yeast and challenges of toxicity detection in agriculture, this work is dedicated for development of efficient and portable IoT based biosensing detection system that can be used for environmental samples particularly detection of copper in soil and water from agricultural circuits. However, the development of biosensors using whole cell as biorecognition element is a lengthy process, involving multidisciplinary research as it includes the selection and manipulation of biorecognition elements, (particularly yeast strains in our case) able to respond to analyte of interest, methods of immobilization, selection of transduction mechanism and design of miniaturized devices appropriate to quantify the response generated by biosensors. In this project, we designed yeast-based biosensors paired with a handheld prototype electrochemical device to enable point-of-care detection of copper. Additionally, we developed a Python-based web application for online storage, visualization, and analysis of sample data.

1.1 Yeast as biorecognition element

Recently, yeast one of the fungi that has attained the attention of researchers to develop biosensors as it provides in-field applicability due to the intrinsic tolerance of its strains for adverse environmental conditions like salinity [53] and by elimination of sample preparation steps like concentration and extraction [54-56]. The presence of well-defined cell wall and membrane bounded organelles in yeast provides opportunity for specialized metabolism assessment in biosynthetic applications. The ability to genetically modify yeast due to separation and compartmentalization of genetic and metabolic events have provided an opportunity to be used for engineering of actuators, genetically modified biosensors and yeast based synthetic biology platform [57]. The construction of yeast based biosensors is made possible by selecting the yeast cells that are sensitive to a particular analyte of interest and then coupling them with transducers. According to biosensor design the transducer is responsible for detecting the specific response generated by yeast cells when biorecognition molecules are triggered by chemicals or analyte of interest after entering yeast cells. The specific response can be an electric current in case of amperometry or optical signal in case of color, fluorescence, or luminescence depending on reporter gene activity. The output signal is co-related to the primary biorecognition event, and thus it provides opportunity to calculate the effective concentration of the analyte of interest [58, 59]. Transduction mechanisms of yeast-based biosensors are presented in Fig. 1.2.

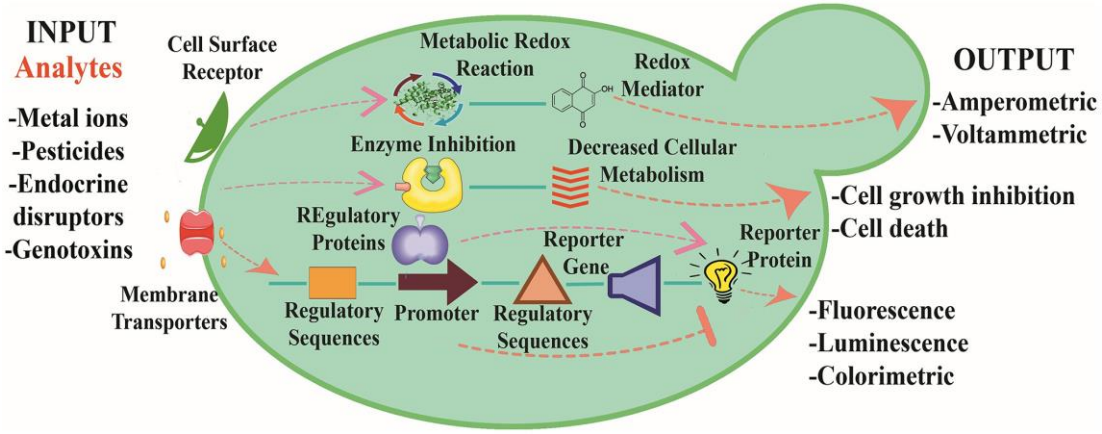

Figure 1.2: Transduction mechanisms of yeast-based biosensors. Different yeast species, genetically modified or not, can act as sensing element for analytes. Cell surface receptors and plasma membrane transporters are involved in the first interaction between the cell and the analyte. The output signals can be quantified through: amperometric/voltammetric measurements by means of intracellular metabolic redox reactions and redox mediators; cell growth inhibition and/or cell death by means of inhibition of metabolic regulatory proteins; optical measurements by means of the regulated activity of constitutive or inducible promoters fused to selected reporter genes and related proteins [60].

Generally, genetically modified yeast based biosensors present far more benefits than other techniques for in vitro models like its ability to reproduce similar results, provide scalability for high-throughput application, higher sensitivity, low-cost and robustness. Moreover, as yeast need less demanding condition of growth and they are more specific in detection in their bioavailable form they are more suitable for point-of-cure application with respect to other in vitro whole cell based biosensing systems [30, 61]. Currently, yeast based biosensors are finding their application from cytotoxins screening in surface, waste, and tap water to genotxins, endocrine disruption and heavy metal detection [62-64]. There are several yeast species that have been used for specific biosensing applications like *Arxula adenivorans*, *Pichia pastoris*, *K. marxianus*, *Kluyveromyces fragilis* and *Hansenula polymorpha* but *S. cerevisiae* is the most popular among researchers [31]. Though many yeast based biosensors have been developed over the past decade, optimal performance and applicability of yeast based biosensors is a challenge due to limitations like low concentration samples and on-site testing. Moreover, lack of knowledge about behavior of molecular organelles in yeast cells for a vast majority of toxic compound also hinders the development of sustainable yeast based biosensors [30]. However, many yeast-based biosensors have found their way to be normally used as suitable tool for detection of contaminants especially in environmental samples. For example, several biosensors with different variations in yeasts (because of ability to catabolize many substrates like nitrogenous and aromatic compounds) have been developed for BOD sensing and to target different organic compounds [65] .

Moreover, in case of inorganic contaminants like heavy metals that pose a serious threat to environment, yeast based biosensors have been developed for detection of copper using genetically modified yeast with the *CUP1* promotor attached to either *LacZ* gene [66] and *GFP* in case of fluorescent output [67] and luciferase [61], or *ADE2* gene to have colorimetric detection [63]. Similarly, *Hansenula polymorpha* (yeast) genetically modified cells have been used to detect Cd ranging from 1 M to 900 M in a dosage dependent manner [68]. The same assembly was found to respond to arsenic contamination as well. Yeast cells have also been found to work in mixed microbial consortiums for the detection of multiple analytes such as *S. cerevisiae* together with *E. coli* and *B. subtilis* bacterial species are used together for detection of Cu^{2+} and Cd^{2+} by a whole-cell electrochemical biosensor [69]. Furthermore, yeast cells are

observed to respond accumulating methyl mercury which is known to produce adverse health and neurological affects, thus providing a suitable cellular model for engineering biosensors targeting this pledge [70]. Finally, for detection of wide range of contaminants present in the environment that have toxic effects to eukaryotic cells, low specificity yeast-based biosensors have also been engineered, notably by Hollis and colleagues [71]. Surprisingly, this biosensor, when applied on herbicides and heavy metals managed to screen toxic effect of elements that were not detected by prokaryotic biosensors. In the same way, the vacuolar metabolism of yeast is also used as a biomarker for the screening of heavy metals, pesticides, and toxic pharmaceuticals in a recently developed test based on the oxidative stress due to presence of these compounds [72]. Out of all the yeast species used for development of biosensors, *S. cerevisiae* yeast is the most popular among researchers [31]. *S. cerevisiae* a single cell anaerobic microorganism with fully sequenced genome [73, 74]. Like most eukaryotic cells, *S. cerevisiae* cells are surrounded by well-defined cell walls, that provide stability to cell structure and promote protection against environmental stress. The cells of *S. cerevisiae* reproduce rapidly in favorable environment (approximately 90 minutes for a single generation) and under harsh environmental condition, the cells can become dormant and undergo sporulation [75, 76]. Moreover, *S. cerevisiae* is low cost and easy to grow in real and laboratory settings [77]. All these characteristics makes *S. cerevisiae* an ideal candidate for studies on fundamental processes that have provided information for better understanding of cellular biology [78, 79]. To date, several copper biosensors have been generated in *S. cerevisiae* by genetic engineering, using common laboratory strains equipped with different reporter systems, expressing various types of probes, detected by either amperometry [66, 80], luminometry [41], colorimetry [63, 81] or fluorescence analysis [67]. All these biosensors were shown to be specific to copper with different levels of copper sensitivity. Keeping the advantages in mind, in this work we selected *S. cerevisiae* yeast strains to act as biorecognition element.

1.2 Yeast and Copper

Copper is an essential microelement to many biological activities, e.g., it is the catalytic cofactor for various proteins or enzymes of oxidative pathways [82] since it can be present in two different redox states (Cu^{2+} and Cu^{+}). However, excessive levels can have detrimental effects on yeasts, possibly leading also to cell death. Among copper-dependent damages, oxidative stress and enzymatic inhibition have to be mentioned: the redox reaction of free copper especially with molecular oxygen results in the formation of reactive oxygen species (ROS), directly causing oxidative stress and cellular damage; the excessive copper levels may interfere with the function of metal-dependent enzymes by displacing other metals from their active sites, resulting in impaired metabolic pathways. Therefore, copper homeostasis is highly controlled process in the cell, occurring by high and low-affinity membrane transporters such as the proteins encoded by the *CTR1* and *FET4* genes, respectively, which may finely regulate the import and export fluxes. Accordingly, the expression rate of copper transporters mainly depends on the metal availability in the medium [83, 84]. Importantly, yeast cells also possess specific mechanisms to defend themselves when the external level of copper exceeds the safe zone and starts to become dangerous, mainly by producing protective molecules, such as the antioxidant tripeptide glutathione (GSH) [85], or expressing specific proteins called metallothioneins. Since the presence of multiple cysteine residues, carrying thiol groups (-SH) with significant affinity for metal cations, such as copper, metallothioneins are able to efficiently bind and sequester free copper ions, decreasing their excessive levels, and thus acting as primary detoxification agents for yeast cells [86, 87]. In *S. cerevisiae*, the metallothionein protein is encoded by the *CUP1* gene that can also be present in multiple copies in yeast genomes. Its expression is mainly regulated at transcriptional level by the Acel activator protein [88]. Notably, the Acel factor directly binds copper ions, leading to the formation of a metal-protein complex which is transcriptionally active and induces the transcription of the *CUP1* gene [89, 90]. Relevantly, observations made in different strains of *S. cerevisiae* indicated the

direct link between the high copper tolerance and the high number of copies of the *CUP1* gene present in the strain genome, supporting the role it can play in detection of copper [91].

1.3 Challenges in development of yeast-based biosensors

Although biosensors using yeast as biorecognition element have various advantages on their counterparts, nonetheless only few have reach prototyping scale, pointing out limitations for development of full-scale biosensors such as response time, stability and operation of assembly, genetic modifications, and transduction mechanisms [53, 92, 93].

1.3.1 Safe deployment and shelf life

For the swift operation of sensors based on microorganisms, cell viability and stability are two of the key factors and these aspects are primarily related to immobilization strategies used for development of these analytical devices [92]. For in field application, where the devices need mechanical stability while keeping biological activity, liquid cell cultures are not appropriate [94, 95]. In recent years, several different immobilization techniques have been assessed keeping in mind the final goal of transition from laboratory scale to field application. Among these strategies hydrogels such as agarose and alginate are most promising as they form polymers that are hydrophobic in nature with the ability to retain water which is beneficial for cell growth [96, 97]. Nevertheless, to observe appropriate response from the biorecognition element it is imperative to optimize the ratio of matrix and cell suspension, and these immobilizations are not stable for longer periods of time [98]. For long used an alternative proposed by researchers is the use of lyophilization. In this technique, under vacuum the water is removed from frozen sample keeping the integrity of cells [92] For practical applications cryoprotectant solution housing sensory cells are spotted on transduction mechanism prior to lyophilization [99]. The long-term storage capabilities enabled by using lyophilization as immobilization strategy is an attractive feature as various authors have reported maintenance of cell viability and sensitivity after months and even years of storage [100-102]. Lyophilization techniques address some of the long-term storage issues. However, the preservation of physiologically active microorganisms presents a significant bottleneck in its efficiency. In this regard, the use of inactive microorganisms, for example, spore form, is a possible solution. *S. cerevisiae* and other microorganisms, such as *Bacillus subtilis* or *Clostridium difficile*, can form spores when exposed to nutrient deficient or harsh conditions unfavorable for their growth [103, 104]. Notably, it was found that the analytical performance of spore-based sensors did not change significantly after subjecting them to several sporulation-germination cycles. Recently, a spore-based sensor has been reported with high storage capability of up to 6 months at room temperature in yeast for acetic acid detection. Aside from long-term storage capabilities, the use of spores presents an opportunity to deploy biosensors in harsh environments [105].

1.3.2 Analytical performance

The assessment of the accuracy of biosensors still relies on its comparison with the results of well-established and highly accurate analytical methods, such as liquid chromatography, mass spectrometry (LC–MS), gas chromatography, mass spectrometry (GC–MS), inductively coupled plasma mass spectrometry (ICP–MS) and other techniques. As accurate as these methods may be, the corresponding instrumentation is costly and requires high technical expertise for utilization. On the other hand, selectivity, sensitivity, time of response and limit of detection of biosensors is still under question. Selectivity and sensitivity, which in turn determine the time of response and the dynamic range, can be addressed by improving both the sensor strain and the transducer. Currently, methods aimed at manipulating genetic circuitries to improve or alter the activity of biomolecules have given investigators the opportunity to enhance the analytical performance of engineered microbial sensor strains. Directed evolution, a cyclic process mimicking natural selection and aimed at identifying functional biomolecules variants by genetic diversification tools and screening, is one of such technique [106].

Throughout the years, numerous fluorescent proteins have been developed with altered wild-type genetic makeup to increase their brightness and even modify their excitation and emission wavelengths [107]. It has been reported that small differences in cell viability between analytical runs can result in signal fluctuations, affecting read-out reproducibility and detection limits. To address this, investigators have largely relied on the use of optical density measurements and cell counting techniques to determine the quantity of cells in an analytical run. However, these techniques provide no information on the quantity of viable cells that produce a signal and therefore are not the best methods to ensure reproducibility of the measurements. Other approaches, such as the duplex reporter methodologies, have been explored to improve the analytical reproducibility of the sensors. It has been reported that the introduction of a second constitutive reporter gene acting as internal reference for correction of nonspecific response [108]. In the context of variable experimental conditions, the analyte concentration values were corrected by considering the expression of the second reporter gene, providing an internal baseline referred to cell viability and metabolic activity. Another challenge is the growing interest in engineering sensor strains for use as multiplex assays, in which various analytes can be detected from a single analytical run. This could be achieved by engineering cells with multiple differentiable reporters, each under the control of distinct promoters specific to each analyte of interest. For this purpose, both bacterial and yeast cells have been used. Recently, a multiplex biosensor for the simultaneous detection of Cd and arsenic in contaminated soils has been reported in which *E. coli* cells were transformed with two sets of plasmids, one for the detection of arsenic via expression of a red fluorescent protein and another for arsenic detection via *GFP* expression [109]. Similarly, *S. cerevisiae* cells have also been genetically modified with different fluorescent reporters for simultaneous detection of estrogenic or androgenic activities in wastewater samples via high-performance thin-layer chromatography (HPTLC) coupled to an optical based bioassay [110]. Finally, biosensors can vary greatly in their time of response. In inducible biosensors, microbial cells must first detect a bioavailable analyte and subsequently produce a quantifiable signal. Many factors can play a role that will affect the response time of an inducible sensor strain. This includes the permeability of the cells to a given analyte, the diffusion rate of an analyte through the sample matrix, the complexity of genetic circuitries employed, the strength of the underlying molecular recognition events, the metabolic rate of the microbial cell and the type of reporter molecule employed. Efforts aimed at improving the analytical parameters of a sensor strain, such as incorporating additional regulatory components which could result in lengthening the time of response due to increased metabolic load. In certain cases, the response can be quite rapid. For example, certain nonspecific and specific biosensors can produce result within 1–15 min [111] . However, time of response and detection limits are intimately related. In many cases the time of response needs to be lengthened to allow for improved detection limits via increased production of the reporter protein, yielding higher signal-to- noise ratios. Thus, the trade-off between time of response and detection limits allows for tailoring of these parameters to the needs of a given biosensors application.

1.3.3 Technical aspects

Apart from the bio-recognition element, the role of the transduction mechanism is crucial in the analytical performance of biosensors and their transition to prototype stage. In this regard, ion sensitive field effect transistors (ISFETs) have several advantages and are considered most promising over conventional transducers due to their simple and low-cost design [112-117]. As the channel region is isolated from the ionic solution, ion-induced instabilities of sensors such as hysteresis, drift and dissolution of channel materials are prevented, thus extending the durability of the biosensor device [118-121]. Field effect transducers (FETs) are reusable, while the sensing parts are disposable, which simplifies the device fabrication and reduces the cost [68, 115, 116]. However, the application of such transducers is limited to devices dealing with ionic solution. Another challenge that biosensor face is time of response, and it is related to mass transport to transducer [122]. The most common method for extending the sensing interface involves the use of magnetic nanoparticles or redox mediators that facilitate

extracellular electron transfer. As dispersing the nanoparticles throughout the sample reduces the distance over which species must diffuse, the response time is thus decreased. This approach switches the sensing paradigm from making the analyte find the sensor to making the sensor find the analyte [123]. For cost-effectiveness, researchers consider biosensor miniaturization for simple, affordable, and efficient detection and quantification of analytes. Microfluidic platform-assisted miniaturized biosensing systems show promises in this regard. A miniaturized biosensor will also ease the integration, automation, multiplex detection, and transmission of data for use in areas where well-trained personnel may not be available [124, 125]. Nevertheless, further research is needed to enhance the transduction mechanisms, which in turn can help to improve miniaturizing biosensors technologies for field applications. Notably, most of the yeast-based biosensors developed in the last years are based on an optical transduction mechanism, where fluorescence, luminescence or color are the output signals. Nevertheless, in view of real applications, the implementation of yeast biosensors based on amperometric detection may be taken into consideration given that amperometric biosensors present some advantages in terms of sensitivity, cost of equipment and integration into portable devices [126]. For amperometric biosensors, the monitoring process implies measurement of changes in electric current, due to specific cellular reactions and use of specific electrodes. In this frame, yeast capacity to produce protons and electrons from catabolic processes is directly correlated to the biosensor activity [126]. Amperometric biosensors are not without their own challenges. Different substrates oxidation processes, aerobic or anaerobic conditions and cellular growth phases have different impact on the electron transfer rate and consequently current output [127, 128]. Another important aspect affecting the electric signal is the cell adhesion to the working electrode which in turn is influenced by the electrode material. Electrode surface should be chemically inert and easy to produce. A wide range of materials have been used such as carbon, cloth, graphite foil, rods, metal or metal nanoparticles to modify working electrodes. Among them, graphite and carbon have been used for most proof-of-concept studies, due to its chemical inertness and ease of production. Furthermore, graphite and carbon is biocompatible and can be easily modified to increase the concentration of positively charge functional groups on the surface, which promote cell attachment and biofilm formation.

1.4 Cell immobilization

During the development of any biosensor, one of the main challenges is integration of biorecognition element (such as enzymes, antibodies, nucleic acids, aptamers, cells, tissues etc) with transducer surface [129]. Cell immobilization is a process in which the microorganism is entrapped in a suitable and stable matrix. Generally, it is one of most important steps in development of biosensors sing microorganisms as biorecognition element because in order to obtain the highest possible signal, the microorganism should be in close contact with transducer. To make it possible, the matrix used for immobilization must allow mass transfer of nutrients and metabolites while still protecting the cells from diffusion in surrounding medium and sheer forced in electrochemical cell. It should be biocompatible and provide stability to microorganism against the contamination [130]. Using immobilization structures of microscopic sizes like cells are packed and concentrated into macroscopic particles. The benefit of using immobilization is that cells can be used in non-sterile condition, and it also provides re-useability as the cells can be washed with water or buffer after each assay. This recycling advantage provided by immobilization in biosensors provides an added value in online, automatic, and continuous systems. There are several factors that need to be considered while choosing the immobilization such as nature of analyte of interest and biorecognition element, operating conditions and type of transducer used for specific sensing application. Above all the immobilizations must provide a favourable microenvironment to biorecognition element to ensuring maximum activity [131].

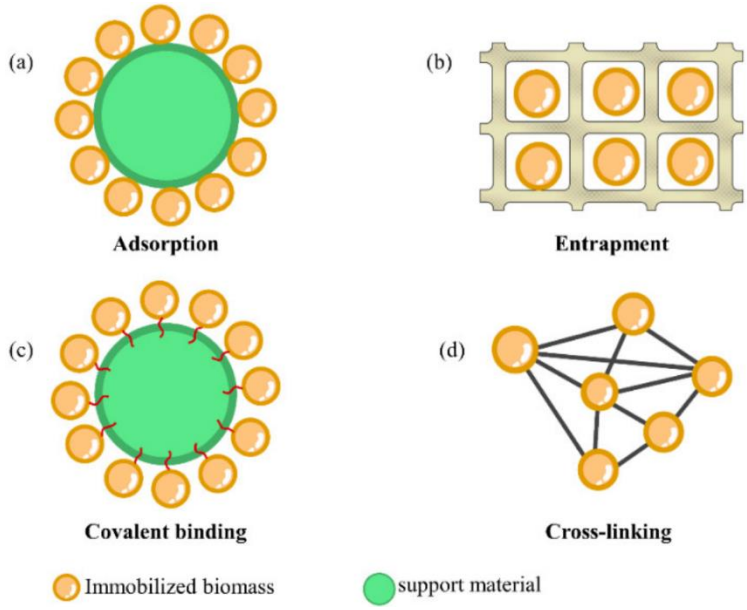

Figure 1.3: Schematic illustration showing immobilization methods: (a) Adsorption, (b) Entrapment, (c) Covalent binding, (d) Cross-linking [134].

1.4.1 Methods for cell immobilization

Immobilization of microorganisms on transducer or support matrices is achieved by both physical and chemical methods. Physical methods of immobilization include absorption and entrapment while chemical methods include cross-linking and covalent binding [132]. The successful implementation of immobilization depends on selection of type of immobilization as there are specific operating conditions for each immobilization [133] and unsuitable immobilization selection may lead to changes in structure, active site and biomass blockage, leading to loss to biochemical activity of microorganism.

1.4.1.1 Adsorption

Among all the techniques used physical adsorption is considered to be the oldest, low cost and simplest way of immobilization. Fig. 1.3 (a) shows schematic illustration adsorption. In adsorption the physical forces (van der Waals forces) of the immobilization matric keep the microorganism entrapped or attached to transducer surface [135]. Generally, a cell suspension with immobilization matrix such as alumina and glass bead are drop casted on the surface of electrode or incubated with the electrode [136, 137]. The physical adsorption-based immobilizations are achieved by ionic, polar, hydrogen or hydrophobic interactions. However, these immobilizations are generally not very stable due to long term use due to desorption of microorganism [138]. Immobilization using adsorption have advantages such as easy preparation, simple operating conditions, and reliability, however such immobilization usually displays decreasing efficiency due to loss of biomass over time as a result of weak affinity between carrier and cell. Therefore, it is necessary to develop carriers with strong adsorption capacity to improve the immobilization effect when this technology is employed.

1.4.1.2 Entrapment

For the immobilization of bio-receptors like whole cells the most preferred technique is entrapment. Fig. 1.3 (b) shows schematic illustration adsorption. In this technique, biopolymers or synthetic polymers are used to embed microorganisms. The materials used for such immobilizations include carrageenan, chitosan, collagen, polyacrylamide, poly(ethylene glycol), polyurethane or polyvinyl alcohol (PVA) [139]. A drawback of entrapment based immobilization is the presence of high diffusion resistance due to nature of entrapment material,

resulting in higher detection limit and lower sensitivity [140].

1.4.1.3 Covalent Binding

Covalent binding depends on creation of covalent bonds among nucleophilic groups on the biomass material and chemical groups on the surface of the carrier [141], it is specifically appropriate for immobilizing biomasses to increase stability. However, covalent binding at times is reported to damage cell structure i.e., cell membrane due to chemical reaction during the formation of covalent bond and thus minimizing the biological activity. Fig. 1.3 (c) shows schematic illustration adsorption. This type of immobilization is not very popular among researchers and is more favorable in conditions when the cells are in active [132]. Generally, this immobilization technique shows a better connection between the carrier and the biomass materials, resulting in better stability, but the method has a higher level of complexity [142], making it less suitable for industrialization. Covalent bonding may alter the spatial structure of the biomass materials, resulting in change of original functions and biological properties of biomass causing biological activity loss [143].

1.4.1.4 Cross-Linking

In comparison to covalent bonding, cross-linking immobilization is more commonly applied and displays better bonding, higher stability, and simpler operation. Cross linking is achieved using cross-linking agents that play pivotal role in immobilization. Fig. 1.3 (d) shows schematic illustration adsorption. Generally acknowledged cross-linking agents consist of isocyanate, glutaraldehyde, hexane diamine, maleic anhydride and diacetamide derivatives. In comparison to adsorption, the process of crosslinking is irreversible in nature and generally cytotoxic in nature. Similar to covalent binding this method is more applicable with in active cells [140]. In practical applications multiple methods are used together to address the shortcomings of a particular technique, such as adsorption–covalent [144, 145] and covalent–cross linking [146]. The use of combination of two immobilization methods can lead to improvement in stability of microorganisms as well as its adaptability to the microenvironment.

1.4.2 Polydopamine (PDA)

Polydopamine (PDA) is an emerging nature-inspired biopolymer material that possesses many interesting properties including self-assembly and universal adhesion. Recently, PDA biopolymer, a key component of protein excreted my marine mussels that forms a strong adhesion with various substrate and facilitate EET is suggested for immobilization [147, 148]. PDA being organic in nature undergoes biological self-polymerization under alkaline conditions in aqueous phase. Furthermore, it has structural properties like adhesive amino acids like 3,4-dihydroxyphenylalanine, tyrosine, and lysine [149]. PDA shells are believed to be produced by the strong covalent bonding between PDA and cell wall (glycol) protein amines or thiol moieties [150, 151]. Interestingly it was observed that PDA coating provide individual cell encapsulation, with a positive impact on the area of cell-based sensors and devices [150]. Such coating has also recently been used for biocatalytic asymmetric reduction and cytoprotection [152, 153] found to be independent of composition of substrate [154], promoting EET [155] and implemented with yeast cells as well [150]. Therefore, yeast cells immobilized with biocompatible and EET facilitating coating provides a promising option for electrochemical biosensing applications such as Cu^{2+} detection in agricultural circuits as fungicides used widely in organic farming have excessive copper contents [43]. Therefore, in this work PDA has been used as immobilization matrix for yeast cells with different growth conditions on the surface of transducers for development of biosensors.

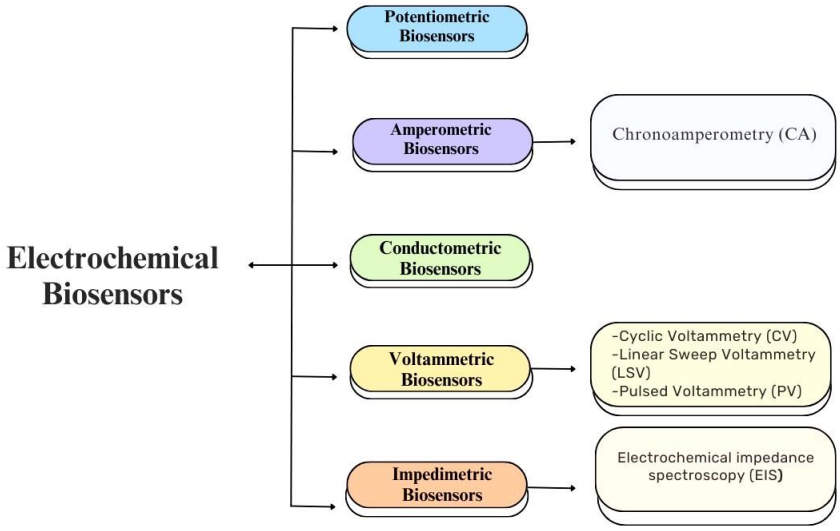

Figure 1.4: Classification of electrochemical biosensors

1.5 Electrochemical Biosensors

Electrochemical biosensors are the most extensively studied and explored biosensors. Through literature review of biosensors, it was observed that electrochemical biosensors are most promising and common ones, and thus our field of interest [156, 157]. Electrochemical biosensors present several advantages over their counterparts such as low cost instrumentation and reagents, low limits of detection (LoD), robustness, ease of miniaturization and versatility. Moreover, such devices can both be developed as "single shot" analysis tools for applications requiring disposable devices (food quality monitoring, clinical analysis etc.) and "long-term monitoring" analysis tools for applications (such as pollution monitoring) requiring devices that should operate for continuous monitoring. The operation of these biosensors depends on electrochemical properties of the analyte of interest and transducer. Electrochemical biosensors offer high selectivity, sensitivity, and the low cost detection.
In these biosensors, an electrochemical interaction takes place on surface of transducer between biorecognition element and analyte generating quantifiable electrochemical output in the form of voltage, current, impedance, and capacitance [156, 157]. Therefore, we focused on the development of electrochemical yeast based biosensors in this work.

1.5.1 Classification of Electrochemical Biosensors

On the basis of transduction principle, electrochemical biosensors are subdivided as: potentiometric, amperometric, conductometric, voltametric and impedimetric [156-159]. Fig. 1.4 illustrates the classification (a) Potentiometric, (b) Amperometric, (c) Conductometric, (d) Voltametric and Impedimetric biosensors.

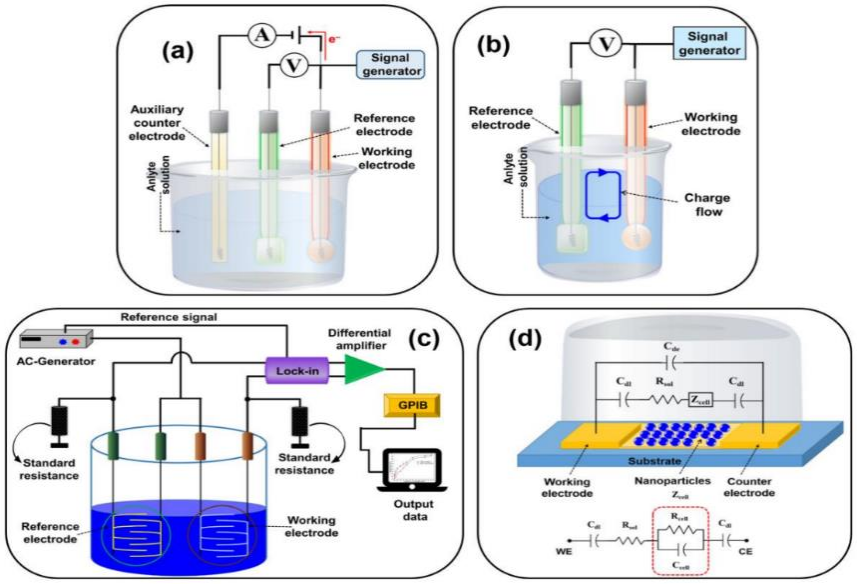

Figure 1.5: Schematic diagram of (a) Amperometric/Voltametric, (b) Potentiometric, (c) Conductometric biosensors, and (d) equivalent circuit of the Impedimetric biosensor (C_{dl} = double-layer capacitance of the electrodes, R_{sol} = resistance of the solution, C_{de} = capacitance of the electrode, Z_{cell} = impedance introduced by the bound nanoparticles, and R_{cell} and C_{cell} are the resistance and capacitance in parallel) [160].

1.5.1.1 Potentiometric Biosensors

Potentiometric transducers measure the difference in potential between working and reference electrode surface resulting from depletion of accumulation of ions. These electrodes are usually ion selective in nature (pH, ammonium, chloride and so on). To transform a biochemical reaction into a potential signal, ion-selective electrodes, and ion-sensitive field-effect transistors are used [156-159, 161]. In general, there is a logarithmic co-relation between measured signal and analyte concentration and hence these transducers provide a wide detection range. The measured signal is correlated to the analyte concentration [162-164]. A schematic diagram of potentiometric biosensors is shown in Fig. 1.5 (b).

1.5.1.2 Amperometric Biosensors

Amperometric transducers operate in a two or three electrode configuration. These sensors measure the current produced due to electrochemical oxidation or reduction of electroactive species at the working electrode when a constant potential is applied to the working electrode with respect to the reference electrode. The current produced on the surface of the working electrode is proportional to the concentration of the analyte present in the solution [156-159]. Fig. 1.5 (a) shows the schematic representation of amperometric biosensors. The materials used for manufacturing these electrodes are metals such as carbon, stainless steel, platinum, silver, or gold [162]. The most used technique for characterisation in these biosensors is chronoamperometry (CA) and same has been used in this work to observer steady state electrochemical response of our developed biosensors.

1.5.1.3 Conductometric Biosensors

Conductometric transducers measure the conductivity of electrochemical system during the course of reaction and these transducers are made up of thin-film interdigitated electrodes. These transducers are useful for reactions in which the ionic composition of the sample under consideration is changed due to consumption or production of charged species (enzyme catalyzed reactions). However, the biggest limitation in using these transducers is that of the

measurement of conductance of solution is nonspecific parameter and hence these transducers are not widely used [162, 165-167]. A schematic representation of conductometric biosensors is shown in Fig. 1.5 (c). Conductometric and impedimetric biosensors are usually used to monitor metabolic processes in living biological systems [158, 168].

1.5.1.4 Voltametric Biosensors

Voltametric transducers detect analyte by measuring the current during the controlled variation of the applied potential. Fig.1.5 (a) shows the schematic representation of voltametric biosensors. Advantages of these sensors include highly sensitive measurements and simultaneous detection of multiple analytes [158]. Basic characterization techniques used in voltametric biosensors include cyclic voltammetry (CV), linear sweep voltammetry (LSV) and pulsed voltammetry (PV). In this work CV has been used to study the electrocatalytic response of the biosensors.

1.5.1.5 Impedimetric Biosensors

A schematic diagram of potentiometric biosensors is shown in Fig. 1.5 (d). Impedimetric biosensors measure the electrical impedance produced at the electrode/electrolyte interface when a small sinusoidal excitation signal is applied. It involves the application of low amplitude AC voltage at the sensor electrode and then the in/out of phase current response is measured as a function of frequency using an impedance analyzer [158, 169]. One of the most commonly used techniques in impedimetric biosensors is electrochemical impedance spectroscopy. We have used this technique in our work for characterization of PDA immobilization on the surface of transducers.

Chapter 2

CELL GROWTH AND CHARACTERIZATION TECHNIQUES

In this chapter the methods and characterization techniques used for yeast cell (biorecognition element) growth as well as analysis of biosensors are reported, respectively. In the first section the culture media preparation and process of growing yeast cells is described which are used for the preparation of biosensors. In the second section the characterization techniques used for the sample analysis and characterization of biosensors are described briefly. This chapter provides the theory and experimental overview of fabrication and characterization techniques.

2.1 Methods

2.1.1 Preparation of culture media

In this study cells of *S. cerevisiae* strains *W303-1B* (*WT*) cells (*MAT ade2 leu2 his3 trp1 ura3*) and derivatives *rtg2* (*rtg2::LEU2*) and (*hap4:: KanMX4*) were used as biorecognition element. To culture *S. cerevisiae* strains YPD (1% yeast extract, 2% Peptone, 2% glucose) media was used in most experiments. However, in some experiments, glucose was replaced with glycerol and ethanol as well. In general, calculated weight of reagents in powdered form are dissolved in suitable volume of MilliQ water to prepare the culture media. The solution is covered with paraffin and placed in autoclave at 120 °C for 15 min for sterilization. In case of solid media, YPD mixture was further added with 2% agar and after sterilization the media was poured in Petri dishes. The plates were left at room temperature for media to solidify then stored in -4°C to avoid contamination. When needed, media (liquid or solid) were added with analytes of interest: copper sulphate and sodium chloride (Sigma Aldrich), diluted from stock solutions that were prepared by dissolving appropriate amounts of analytes of interest in milliQ water.

2.1.2 Growth of yeast strains

In general, to observe the growth in both solid and liquid media, different yeast strains were inoculated in 3mL of YPD from plate culture and incubated in shaking incubator overnight at 30 °C as preculture.

2.1.2.1 Growth of cells in solid media

For growth in solid media, the optical density (OD_{600}) of overnight yeast cultures was corrected to OD_{600} = 1.0. Five serial dilutions (1:10) were made for each strain in 1 mL eppendorfs. 5 µL of each dilution were carefully spotted with the help of micropipette under sterile conditions, on YPD ± $CuSO_4$/NaCl agar plates by placing them on a grid. The spotted plates were incubated at 30 °C for 2 days and plate images were taken every 24 h using ChemiDoc Touch Imaging System [170].

2.1.2.2 Growth of cells in liquid media

For micro and batch-culture growth assays, fresh overnight cultures were diluted in triplicate in microtiter well plates and flasks to the same initial OD_{600}. Optical density was continuously recorded using a high-precision TECAN microplate reader provided with a shaker and a temperature control environment and by using spectrophotometer at regular intervals of time. Growth curves from both assays were analyzed in Origin and relative growth was calculated in as the percentage of the optical density values under stress conditions (with $CuSO_4$) in comparison to the control (without $CuSO_4$) at specified times. At least three replicates of each culture were analyzed for each condition in an independent experiment [171].

2.2 Characterization techniques

2.2.1 UV Spectroscopy

UV spectroscopy is one of the gold standard techniques used for microbial growth especially bacteria and yeast [172, 173]. UV spectroscopy is a quantitative, fast, flexible analytical technique that finds its application as biosensor for sensing, recognition and counting of cells. The quantification is obtained by measuring one or more wavelengths of light. Moreover, additional advantages include cost-effectiveness, simple and rapid response time. Analysis of data from spectroscopic analysis usually have four different phases, lag phase (cell growth preparations are made i.e., increase in size, replication of DNA etc), exponential phase (cells grow in number and biomass is increases), stationary phase (the number of dying cells is equal to viable cells in culture) and death phase (number of cell that are dying is more them number of viable cells). However, generally death phase is not included in lysis.
The Bouguer-Lambert-Beer law holds the basis of mathematical-physical for optical spectroscopic quantification of samples as shown in equation. 2.1. [174].

$$I_g\left(\frac{I_0}{I}\right)_{\tilde{\nu}} = I_g\left(\frac{100}{T(\%)}\right)_{\tilde{\nu}} = A_{\tilde{\nu}} = \varepsilon_{\tilde{\nu}} \cdot c \cdot d \tag{2.1}$$

where,

$$A_{\tilde{\nu}} = I_g\left(\frac{I_0}{I}\right)_{\tilde{\nu}} \quad \text{represents absorbance} \tag{2.2}$$

$$T_{\tilde{\nu}} = \frac{I}{I_0} \cdot 100 \quad \text{represents the transmittance in percentage} \tag{2.3}$$

$\varepsilon_{\tilde{\nu}}$ is the molar decadic extinction coefficient.

I_0 represents intensity of monochromatic light entering and I represent intensity of emerging light respectively. c represents the concentration of substance that is absorbing light, and d shows pathlength of the sample in cm.

Equation can also be represented as:

$$\varepsilon_{\tilde{\nu}} = \frac{A_{\tilde{\nu}}}{C \cdot d} \tag{2.4}$$

Where $\varepsilon_{\tilde{\nu}}$ has a dimension of: 1 mol^{-1} cm^{-1} for "c" in mol l^{-1} or 1000 cm^2 mol^{-1} for "c" in mol 10^{-3} cm^{-3}
The molar decadic extinction coefficient, $\varepsilon_{\tilde{\nu}}$, is a quantity characteristic of the substance which also depends on wavenumber $\tilde{\nu}$ (cm^{-1}) wavelength λ (nm). The standard Bouguer-Lambert-Beer law displays a direct relationship between I_0 and I, however, while measure in the real-world environment using cuvettes made from quartz or optical glass, the is a loss of incident light due to reflection from the surface of cuvettes. To eliminate this error, during experimentation, a standard/reference measurement in the same cuvette (containing pure solvent) in the absence of substance to be measured is made keeping same path length. This value is subtracted from the sample to account for loss due to refraction form the cuvette and solvent. However, before spectroscopic analysis, the users should ensure that the size of cuvettes used for reference and actual sample and, the path length is same. Furthermore, UV spectroscopy relies heavily on the nature of solvent. For that reason, care must be taken while selecting solvent used during analysis [175].

2.2.2 Epifluorescence microscopy

Epifluorescence microscopy, the word "epi" comes from Greek origin meaning "same" (emitted and illuminated light both pass through the same lens). In this type of microscopy, a beam of parallel light is passed in upwards direction through the sample, intensity of light source used in this technique is extremely high that help produce increased illumination for the sample. For the same reason this techniques is also named as wide-field fluorescence microscopy (WFM) [176]. This technique provides much higher resolution then optical microscopy and is usually used for imaging of thick samples [176, 177]. Epifluorescence microscopy helps to obtain images of cell morphology, subcellular/cellular separation along with markers of disease or phenotype [176]. In yeast particularly, due to smaller size and presence of well-developed cell wall it is particularly challenging to image cells using normal optical microscope. However, the higher resolution of epifluorescence microscopes along with the presence of sensitive digital cameras have made the analysis of yeast up to cellular level by capturing high quality imaging and improved the quality of gained information [177, 178].

2.2.3 Scanning Electron Microscopy (SEM)

Scanning electron microscopy (SEM) is highly sensitive technique that is used to obtain images of high-resolution of biological samples [179]. In SEM to obtain an image, cathode emits an electron beam that is attracted and accelerated by anode. These accelerated electrons then hit the sample; the kinetic energy is dispersed producing secondary electrons that are captured by the sensor to produce the images. It must be noted that the resolution of image obtained depends on the wavelength of incident electrons and usually it is kept shorter than visible light to obtain high resolution images [180]. The magnification of SEM usually can be around 10 to 300.000 times and the resolution could be below 1 nm even smaller based on the type of SEM. The basic function of SEM is usually to find out morphology, topography, even the composition of a material by different in colorations of images [181]. SEM is thus applied to observe the viability of cells and morphology of coatings with outstanding magnification [179, 182].

2.2.4 Electrochemical impedance spectroscopy (EIS)

In this work all the electrochemical characterizations were carried out by using three techniques cyclic voltammetry (CV), chronoamperometry (CA) and Electrochemical impedance spectroscopy (EIS). Particularly, cyclic voltammetry is used for the electrochemical polymerization of the monomers and detection of initial electrocatalytic response and chronoamperometry and electrochemical impedance spectroscopy (EIS) for quantitative analysis. EIS is an in-depth electrochemical technique where impedance of a circuit is deployed for the investigation of interfacial properties associated to bio-recognition events taking place at the surface of electrode, like whole cell capturing, interaction of substrate-enzyme or recognition of antibody-antigen etc. Over other electrochemical technique EIS is considered more beneficial as it is a steady-state technique that can provide analysis using a small signal over a wide range of frequencies. It must be noted that the impedance in EIS is different from resistance in a DC circuit that obeys Ohm's law. In this case a small sinusoidal voltage is applied, and electrochemical cell response is pseudo-linear in which a phase-shift is acquired while measuring the current [183].

Here the applied potential/voltage in terms of function of time is given as:

$$E_t = E_0 \cdot \sin(\omega t) \tag{2.5}$$

when E_t is the potential at time t, E_0 is the amplitude of the signal, and ω is the radial frequency. The relationship between the radial frequency (ω) and the applied frequency (f) is obtained by as:

$$\omega = 2 \cdot \pi \cdot f \tag{2.6}$$

In a linear system, due to the phase shift the current output is given as:

$$I_t = I_0 \, sin(\omega t + \Phi) \tag{2.7}$$

Therefore, the impedance of the whole system can be stated as:

$$Z = \frac{E}{I} = Z_{0^{exp(i\Phi)}} = Z(cos\,\Phi + isin\Phi) \tag{2.8}$$

where *Z, E, I, ω,* and *Φ* are impedance, potential, current, frequency, and phase shift between *E* and *I*, respectively. The impedance is expressed in terms of a magnitude, Z_0, and a phase shift, *Φ*. In electrochemical cells while performing EIS fixed potential at different frequencies is applied to working electrode and corresponding current is recorded to obtain impedance as shown in expression above. From these two waves, *Z, Φ,* $Z_{real,}$ and Z_{imag} are obtained and plotted. There are two types of plots that can be sketched using obtained impedance data. i.e., Nyquist Plot and Bode plot. When we plot the real r part (Z_{real}) on the *X*-axis and the imaginary part (Z_{imag}) the curve obtained is called "Nyquist Plot" that display the impedance values at certain frequency. Alternatively, "Bode plot" is obtained by two separate logarithmic plots: magnitude vs. frequency and phase vs. frequency. This plot is more common than Nyquist plot in the engineering community. In a traditional electrochemical cell, the interaction of electrode with matter (redox species) comprises of charge transfer, transfer of mass to electrode surface for bulk solution, concentration of electroactive species and electrolyte resistance. All these factors are distinguished by electrical circuits that consist of resistances, capacitors, or constant phase elements and connected in series and parallel to form an equaling circuit with the response similar to Nyquist Plot EIS. Therefore, EIS can be used to observed processes like diffusion, charge transfer and mass transfer in an electrochemical system [183, 184] .

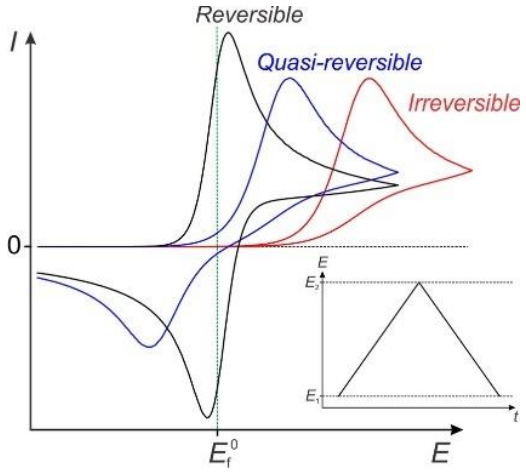

Figure 2.1: A comparison of cyclic voltametric wave-shapes for reversible, quasi-reversible, and irreversible electron transfer process with the same formal potential, E_f^0 , on an electrode. The inset shows the triangular potential "ramp" applied to the working electrode during measurements [185].

2.2.5 Cyclic Voltammetry (CV)

CV is one of the most powerful techniques used for electrochemical characterization of a compound, a biological material or electrode surface that has been modified. Information such as reversibility of redox process, stability of extro-generated species and chemical reactions following electron transfer can be obtained from CV (Fig. 2.1). For CV analysis working electrode is usually carbon, graphite, gold, or platinum while the reference electrode can be a platinum mesh or wire or a graphite rod. In an electrochemical cell a three-electrode configuration is used for CV analysis connected with a potentiostat where a ramp of potentials in a triangular trend is applied to working electrode (WE) dipping in the electrolyte solution and the reference electrode (RE) is kept at constant potential overtime. In three electrode configurations, a voltage generator applies a potential difference between WE and counter electrode (CE) while a galvanometer is used to observe current between the electrodes. For the measurement of variations in potential a voltmeter placed between WE and RE. For a standard CV analysis, the potential ramp starts from open circuit potential (OCP) and ends at catho-anodic window of interest. The voltage is applied in cyclic manner and the obtained current-voltage diagram is called cyclic voltammogram. In case redox reaction is reversable or quasi-reversible similar peak are observed in both positive and negative cycles. However, if the associated peaks are not similar when negative potential is applied it shows that the reaction is irreversible. During the analysis of voltametric response there are some specific parameters that need to be considered particularly in case the reversibility of redox reaction is being investigated. Some specific parameters can be considered in the analysis of the voltametric response. In particular, the reversibility of the redox process can be investigated by the potential difference (ΔE) between the cathodic (*Ec*) and the anodic peak potential (*Ea*):

$$\Delta E = |Ec - Ea| \tag{2.9}$$

For a reversible reaction system $\Delta E[m_v] \approx \frac{59.1}{n}$ where n = number of electrons exchanged.

Randles-Sevcik equation describes the peak current of a reversible system as:

$$i_p = (2{,}69 \cdot 105) n^{3/2} A D^{1/2} C v^{1/2} \tag{2.10}$$

when i_p = peak current [A], n = number of electrons, A = electrode area (cm^2), D = diffusion coefficient ($cm^2\ s^{-1}$), C = concentration of the species ($mol\ cm^{-3}$) and v = scan rate ($V\ s^{-1}$).

It must be kept in mind that Randles-Sevcik equation is not applicable for quasi-reversible reactions as there is a much slower electron exchange rate observed between working electrode and redox species. In an electrochemical cell the faradic current flowing at any time is the direct measure of electrochemical reaction accruing at the electrode. There are two main factors on which the current depends: the rate at which mass transfers to electrode from the solution, followed by the laws of mass transport, and the rate at which electrons transfer between electrode surface and solution. There are three primary mechanisms through which the mass transfer takes place towards the electrode surface: convection, migration, and diffusion. However, as the gradient of concentration is directly related with concentration of electroactive species thus diffusion is considered the most significant phenomenon for mass transfer.

Diffusion process in electrochemical cell is followed by Fick's laws:

$$\text{1st Fick's Law: } \frac{dN}{dt} = DA\frac{\delta C(x;t)}{\delta x} \tag{2.11}$$

$$\text{2nd Fick's Law: } \frac{\delta C(x;t)}{\delta t} = D\frac{\delta^2 C(x;t)}{\delta x^2} \tag{2.12}$$

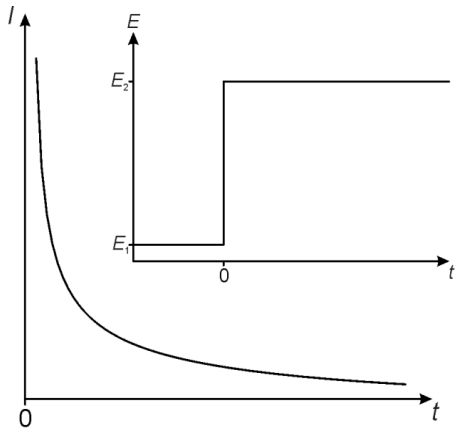

Figure 2.2: Chronoamperometry output signal obtained on an electrode (obeying Cottrell equation), following the input potential step waveform applied [185].

The first law of Fick's provides co-relation between concentration gradient and flow of matter towards surface *A* (electrode surface). The second law describes dependence of the concentration on time and distance from the electrode. While designing an electrochemical experiment care must be taken to mitigate the effect of migration and convection. For this reason, it is necessary to use an inert supporting electrolyte whose concentration is 10-100 times higher than the concentration of analyte to reduce migration, in a quiescent and thermostated solution to reduce phenomena of convection. It must be kept in mind that CV is a multifunctional technique, and it is not only limited to being used for kinetic or thermodynamic studies, or for analytical purposes but it can also be used for processes such as electrochemical polymerization. In such cases, looking at the voltammogram it can be observed that the intensity of current peaks increases with each subsequent scan [186, 187].

2.2.6 Chronoamperometry (CA)

Chronoamperometry is a simple yet powerful technique in which the potential is varied sharply from a value E_0 (no faradic process) to a value E_1 (faradic process starts) and the current flowing through the electrode is measured as a function of time during each variation of potential. This technique provides proper analytical and mechanistic investigations of the phenomenon following the variation in currents as a function of time according to the Cottrell equation (Fig. 2.2):

$$i(t) = \frac{nFAD_0C_0^b}{(\pi_1 D_0 t)^{\frac{1}{2}}} \tag{2.13}$$

when n = number of electrons, F = Faraday's constant [C mol^{-1}], A = electrode area [cm^2], D_0 = diffusion coefficient [cm^2 s^{-1}], C_0^b = concentration of the analyte in the bulk of the solution [mol cm-^{3}], t = time [s].

At a given potential E_1 an exponential decay in current is observed over time as the electroactive species around the electrode are reduced resulting in a decrease in concentration of electroactive species near electrode with time and the concentration gradient become gradually bigger due to the fact that the flow of matter arrives from longer distance, thus taking longer time thus causing a decrease in current [186, 187].

Chapter 3

DESIGN AND CHARACTERIZATION OF YEAST BASED BIOSENSOR DEVELOPED USING GLASSY CARBON ELECTRODE

In this chapter we describe the development and characterisation of biodelectrodes that serves as biosensor, strarting from growth and morpological analysis of yeast cells in the presence of different concentrations of $CuSO_4$ to observe the response of biorecognation element using optical detection. Then we describe the protocoles used for immobilization of yeast cells on the surface of transducers (GCE) to make a biosensor. Later electrochemical charactrisation using cyclic votametry, electrochemical impedance spectroscopy and chronoamperometry to observe effectivity of coating and to evaluate the sensitivity, R^2 and LoD of biosensor are presented.

3.1 UV Spectroscopic growth analysis of biorecognition element

For the development of bioelectrode acting as biosensors, initially the effect of different concentrations of $CuSO_4$, namely 0.01, 0.1, 1, 5, 7, 9, 10, and 20 mM, on the constantly growing batch cultures of *S. cerevisiae WT* cells (biorecognition element) were analyzed. Optical densities were continuously monitored by using UV spectrophotometer at fixed intervals of time. Growth curves were analyzed using Origin and calculations for relative growth were made as the percentage of the optical density values under stress conditions (with $CuSO_4$) in comparison to the control (without $CuSO_4$) at specified times. For each culture at least three replicates were analyzed for each condition in an independent experiment [171].

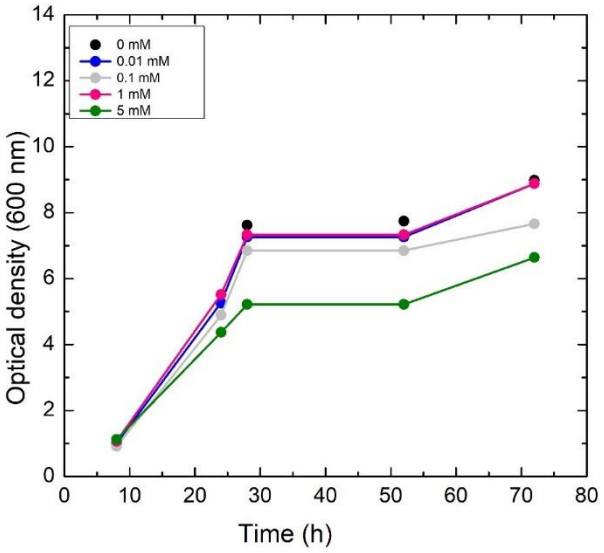

Figure 3.1: Growth curves of *S. cerevisiae WT* cells treated with $CuSO_4$. Cells were grown overnight and then inoculated in YPD under constant shaking at 30 ℃ in the presence of 0 (black), 0.01 (blue), 0.1 (grey), 1 (red), 5 mM $CuSO_4$ (green). Optical density was measured at regular intervals using a spectrophotometer [177].

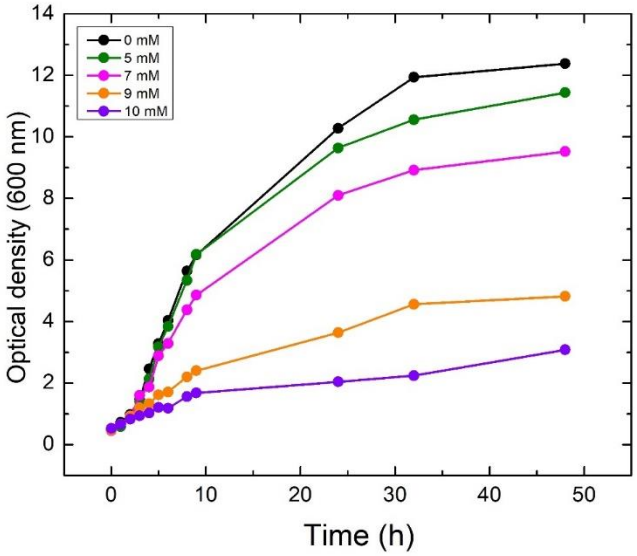

Figure 3.2: Growth curves of *S. cerevisiae WT* cells treated with $CuSO_4$. Cells were grown overnight and then inoculated in YPD under constant shaking at 30 ℃ in the presence of 0 (black), 5 (green), 7 (pink), 9 (orange), and 10 mM CuSO4 (purple). Optical density was measured at regular intervals using a spectrophotometer [177].

3.1.1 Numerical results and Discussion

Fig. 3.1. shows the optical density values at 600 nm for *S. cerevisiae* growth as a function of time in the presence of 10 µM – 5 mM $CuSO_4$. Interestingly, it was observed that at low concentrations of $CuSO_4$, from 10 µM to 1 mM there was no significant effect on growth. However, starting from 5 mM $CuSO_4$ a significant growth inhibition of 13.4 % was obtained after 4 h of incubation. Keeping the preliminary results in mind, the effect of $CuSO_4$ concentrations above 5 mM were investigated, as shown in Fig. 3.2.

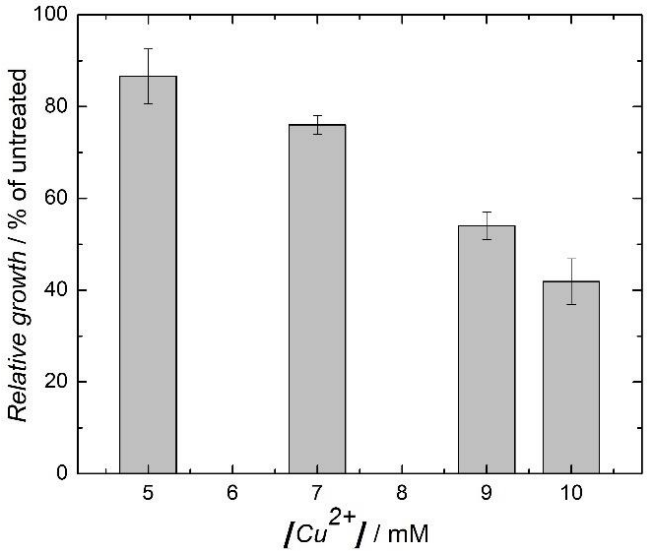

Figure 3.3: The percentage relative growth of the cells in the presence of different concentrations of $CuSO_4$ after 4 h of incubation. Percentage relative growth was calculated against the control cell growth. R^2: 0.986. Error bars indicate one standard deviation [177].

The experimental results showed that above 5 mM as the concentrations of $CuSO_4$ increased, there was a proportional decrease in growth of the cells with respect to time in 7, 9, and 10 mM $CuSO_4$ cultures causing 24.0, 45.9, and 58.1 % growth inhibition at 4 h of incubation, respectively with an $R^2 = 0.986$ as can be seen in Fig 3.3. The results indicate that there is a concentration dependent inhibition in growth at higher copper concentrations. However, the concentrations of $CuSO_4$ above 10 mM completely inhibited the growth of *S. cerevisiae* cells.

3.2 Assessment of cell morphology

Based on the obtained growth curves, we directed our attention to investigate the effect of exposure to high concentrations of $CuSO_4$ on morphology of yeast cells. The morphology of yeast cells before and after treatment with $CuSO_4$ was analyzed by epifluorescence microscope. Freshly prepared overnight cultures (control and treated) were inoculated in YPD medium with a starting $OD_{600} = 0.15$ and placed it shaking in incubator at 180 rpm for 4 h at 30 ^{0}C to grow. 1 mL of control and treated cells were collected and resuspended in YPD. 5 µL of the resuspended cells from each group were immobilized on a glass slide by mixing with 5 µL volume of 3 mM solution of low melting point agarose (Sigma-Aldrich; A-9414). Cells were analyzed at 25 ^{o}C on a Zeiss Axiovert 200 inverted epifluorescence microscope equipped with a 100X/1.30 Ph3 oil objective. Images were acquired with a CoolSNAP HQ CCD camera (Roper Scientific, Trenton NJ, USA) using MetaFluor 6.1 software (Universal Imaging Corporation, Downington, PA, USA) [177]. Fig. 3.4. shows representative images of yeast cells observed in brightfield treated with $CuSO_4$ concentrations ranging from 0 to 10 mM. The microscopy analysis did not reveal significant morphological differences among the cells after 4 h of exposure to the contaminant. It should be noted that based on the current results it cannot be excluded that minor morphological changes took place but could not be identified due to the resolution of the utilized microscope however there was no major damage to the cell structure.

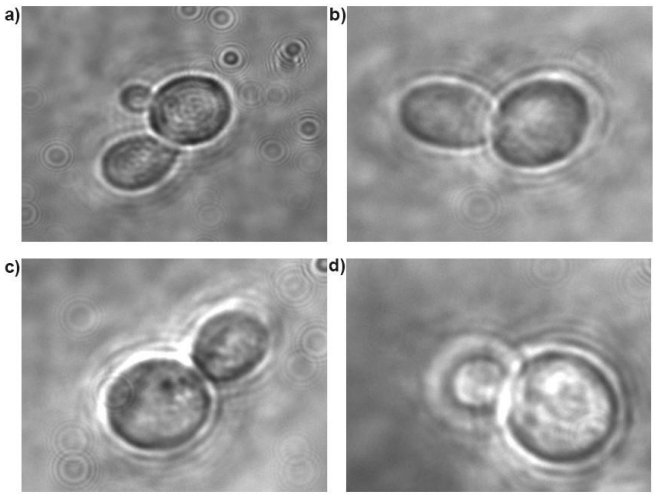

Figure 3.4: a): Representative pictures of yeast cells (*WT*) grown in YPD medium in the presence of 0 (a), 5 (b), and 10 mM $CuSO_4$ (c & d) [177].

3.3 Biosensor design

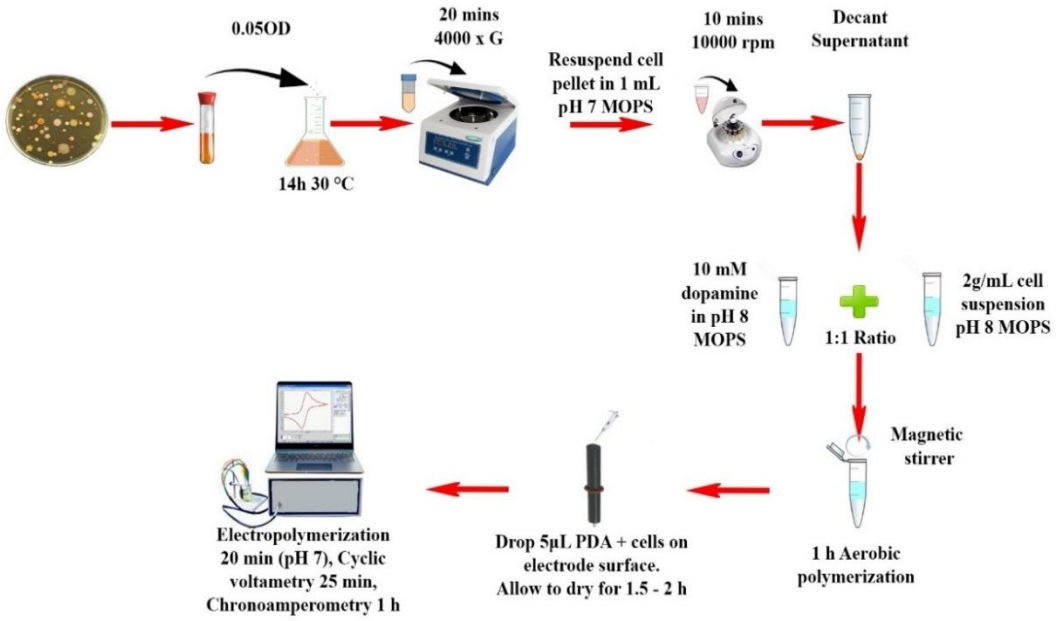

Figure 3.5: Protocol for the entrapment of *S. cerevisiae* yeast cells in PDA matrix and immobilization on GCE [177].

With the aim to develop biosensors operating at concentrations lower than 1 mM, which are of interest for agricultural and environmental monitoring, and based on the response that we observed during growth analysis using optical detection that shows dosage dependent response from biorecognition element (*S. cerevisiae* cells) at higher concentration we decided to explore the electrocatalytic features of *S. cerevisiae WT* cells immobilized on a GCE with PDA. It must be noted here that we undergo a through literature review about different transducers used for biosensors design and GCE was selected as the transducer for initial biosensor design because GCEs are composed of a stable, percolated graphenic network that is corrosion-free, chemically inert, and thus biocompatible [188-190]. Moreover, they are found to withstand extreme conditions and are made of a material that are readily available [189]. Following selection of transducer, using our previous knowledge with PDA and review of literature we formulated specific protocols for immobilization of yeast cells on the surface of transduce (SPE) to develop bioelectrodes serving as biosensors for electrochemical detection of $CuSO_4$. Fig. 3.5 shows the schematic representation of working protocols for the immobilization of *S. cerevisiae WT* yeast cells in PDA matrix on the GCE. For immobilization, cells were pre-inoculated overnight culture in YPD medium and then incubated in fresh YPD (ODstart 0.05) for about 14h at 30 °C and 180 rpm. The culture was centrifuged at 4000 rpm for 20 min and the cell pellets were resuspended in 1 mL solution containing 20 mM MOPS buffer (pH), 10mM $MgCl_2$, and 50 mM glucose, the solution was vortexed slightly and centrifuged at 10000 rpm for 10 min to further remove culture debris.

Figure 3.6: GCE with immobilized *WT* yeast cells.

Next, a 2 g mL^{-1} cell suspension was prepared by mixing appropriate weight of cell pellets with a defined volume of electrolyte solution containing 20 mM MOPS buffer (pH 8), 10 mM $MgCl_2$, and 50 mM glucose. This suspension was further mixed with 10 mM dopamine hydrochloride (in MOPS buffer at pH 8.0) solution in 1:1 ratio to obtain a concentration of 1 gmL^{-1} cell and 5 mM dopamine hydrochloride in a 2 mL Eppendorf tube (it is worth mentioning here that to have right composition of cell/immobilization is really imperative for proper response of biosensor. In this regard, we experimented with different ratios such as 1:1, 1:2 and 1:3 to finally adopt 1:1). The resulting solution was magnetic stirred at 250 rpm for 1 h under aerobic conditions for polymerization. Post aerobic polymerization, 5 µL of the solution was drop casted on the 3 mm working GCE and left to dry at a controlled temperature of 26 ℃ for maximum of 1 to 1.5 hr as shown in Fig. 3.6. Following aerobic polymerization, electrochemical polymerization was performed by 20 repeated cyclic voltammetry between -0.3 and +0.5 V with a scan rate of 20 mV s^{-1} in an electrolyte at pH 7, completing the preparation of the biohybrid electrode. Control group experiments were performed following the same procedure for bio-electrode (biosensor) preparation stated above with dead cells (viable cells placed in a hot water bath for 1 hour at 100 ℃) and PDA coating only. The biosensor was then characterized using cyclic voltammetry, electrochemical impedance spectroscopy (EIS) and chronoamperometry (CA) and [177].

3.4 Electrochemical characterization of biosensor

Following the development of protocols, *S. cerevisiae WT* cells were immobilized on the surface of 3 mm GCE to prepare biohybrid electrode using the protocols explained in previous section. After the electrochemical polymerization step, the obtained biosensors were characterized by cyclic voltammetry, electrochemical impedance spectroscopy and chronoamperometry in a three-electrode setup. Fig. 3.7. displays the working assembly used for electrochemical characterization of biosensors prepared using immobilization of *WT* yeast cells on the surface of GCE. The counter electrode was a Pt wire, and Ag|AgCl (3 M NaCl, Basi MF2052) electrode was utilized as a reference. All the potential reported in this section of work refer to this reference electrode. All experiments were performed at room temperature (24 ± 1 ◦C) in 25 mL of 20 mM MOPS buffer (pH 7) + 10 mM $MgCl_2$ + 50 mM glucose with the electrolyte exposed to air (aerobic conditions). $CuSO_4$ at different concentrations ranging from 20 µM to 100 µM was always added to the electrolyte after electrochemical polymerization and before starting the electrochemical characterization. The electrolyte was continuously stirred with a magnetic bar during the experiments. For all the different conditions investigated, at least three independent replicate experiments were performed, and values are reported with one standard deviation.

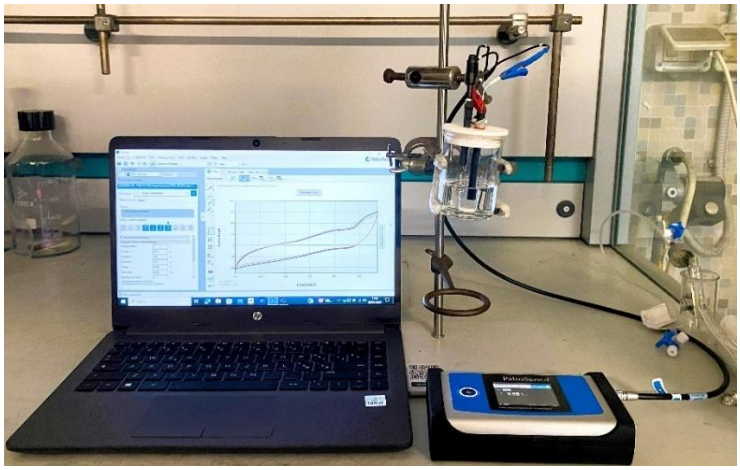

Figure 3.7: Assembly used for electrochemical characterization of biosensors prepared using immobilization of *WT* yeast cells on the surface of GCE.

3.4.1 Voltametric analysis of biosensor

After preparing bioelectrodes, at first electrochemical characterization was performed by cyclic voltammetry. Two types of control experiments were performed (i) by utilizing heat-treated yeast cells with polydopamine (metabolically inactivated cells), and (ii) by preparing electrodes with only polydopamine immobilized on the glassy carbon electrode. All other experiments were performed in the presence and absence of different concentrations of $CuSO_4$ on viable cells immobilized on electrode surface. For the best comparison of the cyclic voltammetry, only the current densities obtained during the second anodic scan were considered. We evaluated bioelectrocatalyic response of the biohybrid electrodes (biosensors) obtained by entrapping yeast-PDA through CV between - 0.1 and + 0.5 V with a scan rate of at 2 mV s^{-1} using single channel portable potentiostat (PalmSens4).

3.4.1.1 Numerical results and Discussion

Fig. 3.8 shows the CV of the bioelectrode prepared with live yeast cells (black) a clear catalytic response was observed, with an onset for the oxidative reaction at + 0.2 V in agreement with previous literature where PDA was used as a redox mediator [155]. Conversely, no catalytic response was noted from the electrode containing only PDA, and only the redox peak due to the oxidation of the redox matrix could be observed at + 0.2 V. For a comparison of the different electrodes, the current density at + 0.4 V throughout the anodic scan was used. The control electrode with only PDA had a low current density (0.3 ± 0.1 mA cm^{-2}) while the electrode with immobilized live yeast cells achieved a current density of 1.5 ± 0.2 mA cm^{-2}. Moreover, live yeast-PDA showed a two-fold higher catalytic activity compared to the heat-treated yeast-PDA (0.8 ± 0.1 mA cm^{-2}). The current generation achieved from the heat-treated yeast-PDA system may be a result of some residual active yeast in the PDA matrix. Interestingly, the enhanced current density value for the hybrid system in comparison with the electrode having heat-treated yeast with PDA or only PDA highlights crucial information about the biocatalytic role of active yeast cells. It is worth mentioning that the biohybrid electrode tolerated the 90 min of desiccation while being exposed to air, with no major negative effects on the bioelectrocatalytic response, bringing forward its facile storing and transportation given its use in the field.

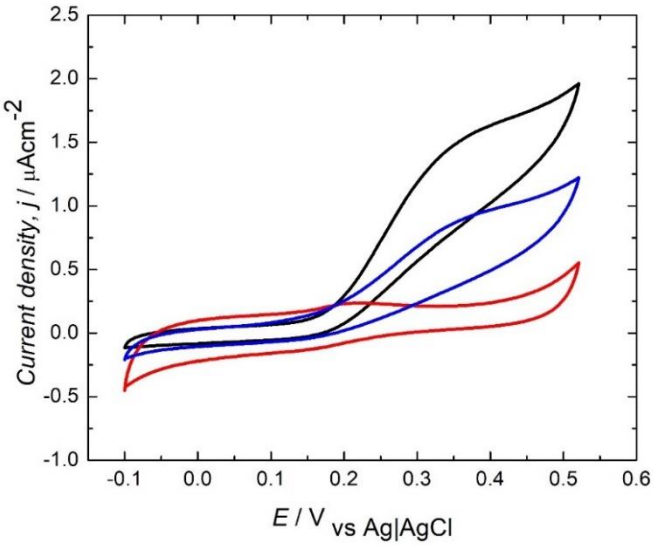

Figure 3.8: Cyclic voltammetry for the bioelectrodes prepared with live yeast cells in the PDA matrix (black), heat-treated yeast cells (blue), and sterile electrodes prepared with polydopamine alone (red).

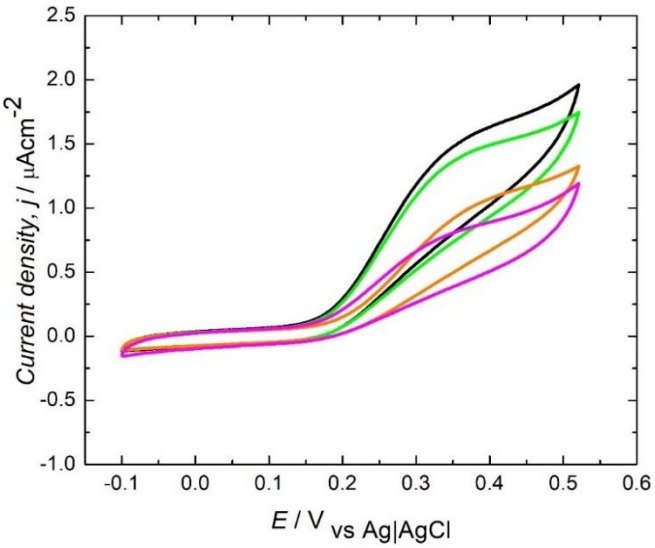

Figure 3.9: Cyclic voltammetry showing the effect of 0 (black), 20 (green), 50 (orange), and 100 μM $CuSO_4$ (purple) on the electron transfer ability of viable yeast cells immobilized with PDA on GCE.

Following control experiments, the catalytic activity of the biohybrid electrode was compared in the absence and the presence of $CuSO_4$ as shown in Fig. 3.9. The results depicted that the current density decreased considerably as the metal concentration increased. Remarkably, the addition of the highest concentration (100 μM) of $CuSO_4$ decreased the catalytic activity of the system by two-fold, confirming the effect of the $CuSO_4$ on the electron transfer ability of live yeast cells immobilized with PDA on the GCE. The dosage dependent decrease in current density during voltametric analysis depicted that the current biosensor could detect the $CuSO_4$ at lower concentration (20- 100 μM) in comparison to optical detection (5 mM and above).

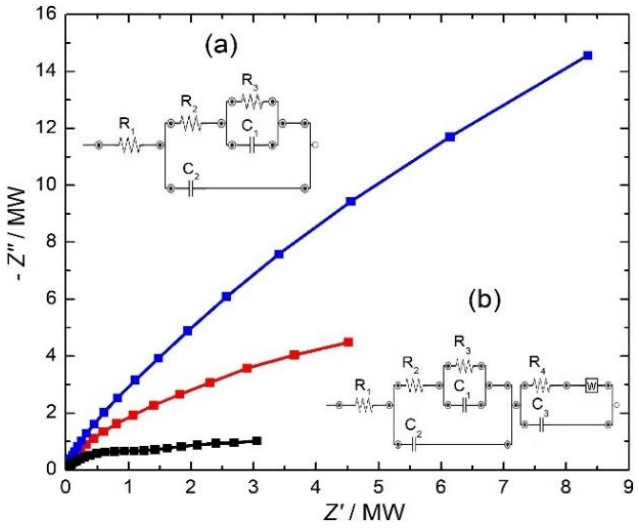

Figure 3.10: EIS spectra for only yeast (blue), only PDA (red), and yeast cells in the PDA matrix (black). Frequency range 500 kHz – 5 mHz, potential amplitude 10 mV, applied potential + 0.32 V.

3.4.2 Impedimetric analysis of PDA immobilization

Moving forward, to better understand the role of PDA in facilitating the extracellular electron transfer process, EIS analysis was performed in a three-electrode mode with working electrodes prepared with only yeast cells, only PDA, and the biohybrid system yeast-PDA. The EIS analyses were performed in a frequency range from 500 kHz to 5 mHz using an applied sinus signal of 10 mV at + 0.32 V. The impedance spectra are presented as Nyquist plots in Fig. 3.9. The complex nonlinear least square fitting of the obtained impedance data was performed using equivalent electric circuit models fitted with the PSTrace software of PalmSens.

3.4.2.1 Numerical results and Discussion

Fig. 3.10. shows the obtained EIS spectra for the three different electrodes. The yeast cells in the PDA matrix (black) showed lower impedance compared to both the system with only PDA (red) and the one with only yeast (blue). The data obtained from experiments was fitted to equivalent electrical circuit models composed of resistances and capacitance as reported in Fig. 3.10. Circuit (a) was used for fitting of PDA and yeast only system while circuit (b) for yeast cells in the PDA matrix. For all the circuits, R_1 represents the resistance of the solution, while the couple R_3 and C_2 represent the double-layer capacitance and the charge transfer resistance. In the case of the electrode prepared with only yeast (Fig. 3.10 circuit (a)), R_2 represents the resistance for the diffusion of the electrolyte in the cells deposited in parallel to a capacitance (C_1). However, for the electrode prepared with PDA only (Fig. 3.10 circuit (a)) and the one prepared with yeast- PDA (Fig. 3.10 circuit (b)), R_2 represents the resistance of the pores in the encapsulating PDA matrix that allows diffusion of the electrolyte connected in parallel to a capacitance (C_1). The third couple R_4 and C_3 present only for yeast cells in the PDA matrix (Fig. 3.6 circuit (b)) represent the PDA layer entrapping the yeast cells on the electrode. A similar model has been recently used to fit EIS spectra obtained for bacterial cells entrapped in an alginate layer on an electrode surface [191]. Accordingly, in this system, the electrons obtained from the oxidation of glucose must cross various interphases that include the yeast cell membranes, the PDA matrix, and the electrode. The various components of the circuit are further influenced by the presence of metabolically active yeast cells in the PDA matrix. Table 3.1 reports the values obtained for the fitting, highlighting that the redox mediation system in the complete biohybrid electrode allowed reducing the charge transfer resistance (R_3), enabling current generation during glucose oxidation with the biohybrid electrode.

Table 3.1: Parameters obtained for the equivalent circuit elements of the control electrodes prepared with only yeast and only PDA, and for the complete biohybrid electrode prepared with yeast and PDA. The values are calculated based on the fitted impedance spectra.

Sample	R_1 / Ω	R_2 / MΩ	R_3 / MΩ	R_4 / MΩ	C_1 / μF	C_2 / μF	C_3 / μF
Only yeast	867	10.7	32	-	1.05	1.35	-
Only PDA	867	3.35	6.80	-	1.85	4.05	-
Yeast-PDA	875	0.79	0.72	0.88	1.9	13.5	0.24

3.4.3 Amperometric analysis of biosensor

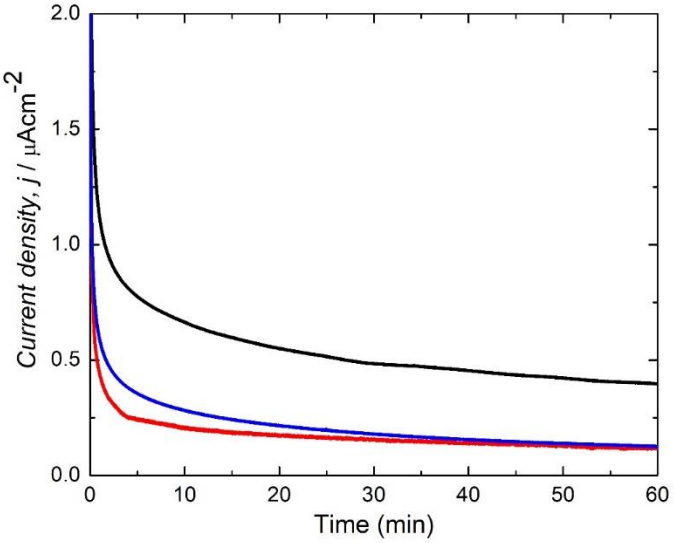

Figure 3.11: Amperometric i-t traces of PDA – yeast electrodes (black), PDA – Heat-treated yeast cells (blue), and PDA alone (red).

While the CV experiments revealed that the biosensors with live yeast-PDA efficiently provided high catalytic activity, and the EIS analysis confirmed the role of the PDA matrix in decreasing the charge transfer resistance, we aimed to further evaluate the variation in current generation over time of the biohybrid system when exposed to $CuSO_4$. Accordingly, we evaluated chronoamperometric assays (CA) of live yeast-PDA, dead yeast-PDA, and only PDA (Fig. 3.11) also in the presence of different concentrations of $CuSO_4$ (20, 50, and 100 μM) for 60 min at 0.32 V *vs* Ag|AgCl (Fig. 3.12). This potential was selected to perform the CA study as it provides a sufficient overpotential relative to the anodic oxidation peak of the redox matrix that maintains the mediator in its oxidized state.

3.4.3.1 Numerical results and Discussion

Corroborating the results obtained by CV, the bioelectrode furnished higher current density than heat-treated yeast-PDA and control electrodes with only PDA (Fig. 3.11). In addition, after 1 h of chronoamperometry, the live yeast-PDA electrode produced a three-fold higher current density (0.6496 ± 0.01 μA cm^{-2}) than heat-treated yeast-PDA and PDA-only systems (0.1521 ± 0.005 μA cm^{-2} and 0.1395 ± 0.004 μA cm^{-2}, respectively), confirming the bioelectrocatalytic role of yeast as shown in Fig. 3.11. Following, the amperometric i-t trace of the biohybrid system was evaluated under increasing additions of $CuSO_4$ as shown in Fig. 3.12.

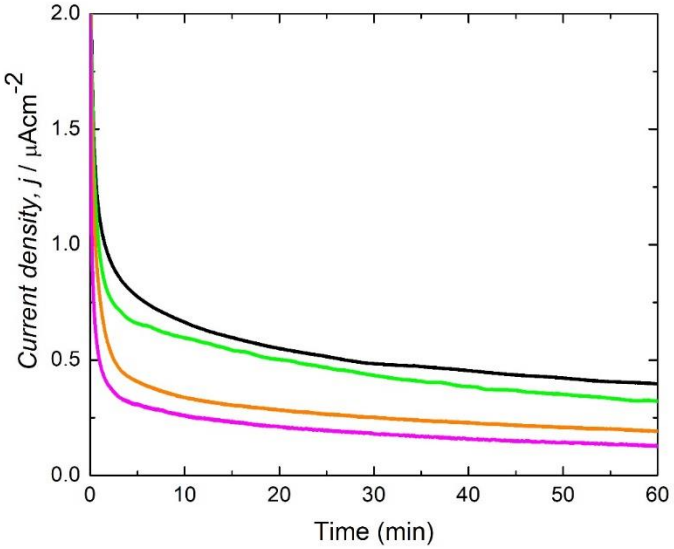

Figure 3.12: Chronoamperometry showing the effect of 0 (black), 20 (green), 50 (orange), and 100 μM $CuSO_4$ (purple) on ability of live yeast cells immobilized with PDA on GCE to transfer electrons.

Notably, the current density decreases with successive additions of $CuSO_4$, which affects the biocatalytic performance compared to the biohybrid electrode in the absence of the pollutant. When adding 100 μM $CuSO_4$, the bioelectrode showed a remarkable decrease in current density of only 0.1518 ± 0.008 μA cm^{-2}. To better correlate the catalytic activity of the biosensor and the presence of $CuSO_4$ in the electrolyte, we evaluated the relationship between the current density obtained from the amperometric i-t tests at 2500 s *vs* $CuSO_4$ concentration as shown in Fig. 3.13. As the $CuSO_4$ concentration increased, the current density decreased linearly for the hybrid system with live yeast-PDA. Remarkably, the response of the electrochemical biosensor is affected by the presence of $CuSO_4$ starting from low concentrations (20 μM), which are relevant for environmental monitoring. Linear fitting of the experimental data presented in Fig. 3.13 gives a calibration curve with a slope, corresponding to the sensitivity, of -4.8 ± 0.6 × 10^{-3} μA*cm^{-2}*L*μmol^{-1}_{CuSO4} and a LoD of 12.5 μM $CuSO_4$.

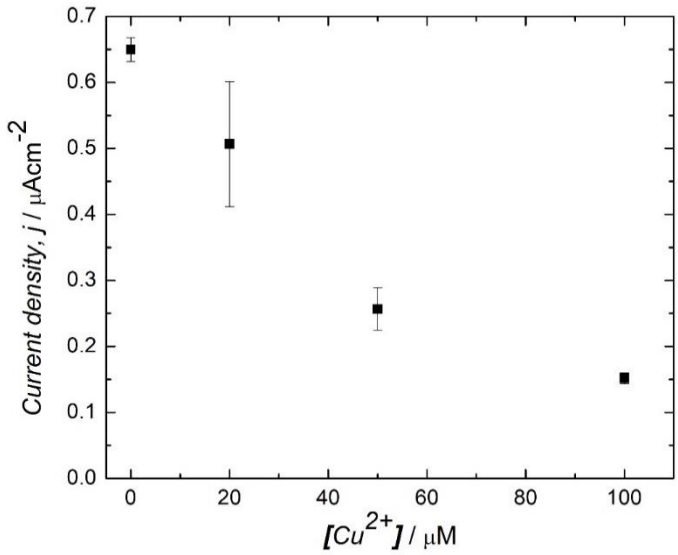

Figure 3.13: Relationship between $CuSO_4$ concentrations and current density during chronoamperometry. E_{APP}: +0.32 V. R^2: 0.956. Error bars indicate one standard deviation.

While it should be underlined that the linear relation between $CuSO_4$ concentration and current density could be improved, the obtained R^2 (0.956) is promising since the system has yet to be optimized to maximize sensitivity. In this regard, we turned our attention towards the use of metabolic and genetic approaches to improve the overall performance of biosensor.

Chapter 4

DESIGN AND CHARACTERIZATION OF YEAST BASED BIOSENSORS DEVELOPED USING SCREEN PRINTED ELECTRODES

With the motivation to develop in-situ sensor with improved sensitivity and better co-relation of $CuSO_4$ concentration and current density, in this part of research instead of using GCE as transduce, we used disposable screen printed electrode (SPE) for development of biohybrid electrodes to act as biosensors. Moreover, explored different metabolic (using different growth media) and genetic (using different yeast mutants) conditions to improve the sensitivity of the overall electrochemical response of the system. At first, viability of three *S. cerevisiae* strains namely: *WT*, Δ*hap4* and Δ*rtg2* was analyzed in the presence of different concentrations of $CuSO_4$ using optical detection. Following viability assessment, growth analysis using micro-cultures were performed in two different experimental conditions: *WT* type cells grown in YPD (fermentative carbon source) and YPG or YPE (non-fermentative carbon source), and *WT* and two mutants Δ*hap4* and Δ*rtg2* cultured in standard YPD media. These experiments were performed as preliminary screening of behavior of biorecognition element. Later bioelectrodes (biosensors) were prepared using *S. cerevisiae WT* cells having different growth conditions and with Δ*hap4* and Δ*rtg2* were cultured in standard media to act as biorecognition element for electrochemical characterization.

4.1 Viability analysis

For use of a microbe as biorecognition it is necessary that the cells remain viable. The ability to replicate and develop into colonies remains the gold standard for estimating microbial cell viability [192]. Thus, colony counting of *S. cerevisiae WT* and two mutants Δ*hap4* and Δ*rtg2* strains exposed to various $CuSO_4$ concentrations (10 - 100 µM) was performed. Cell viability was evaluated by colony forming unit (CFU) counting on YPD agar plates. From fresh culture during incubation, 100 µL aliquot was taken from each culture every 2 h until the end of the exponential growth phase. This was serially diluted in sterile milliQ water, inoculated onto YPD agar plates, and incubated at 30 °C for 48 h. Colonies formed on each plate after incubation were counted and the number of untreated colonies was considered 100%, while the viability of treated colonies was calculated as a percentage of untreated cells [193].

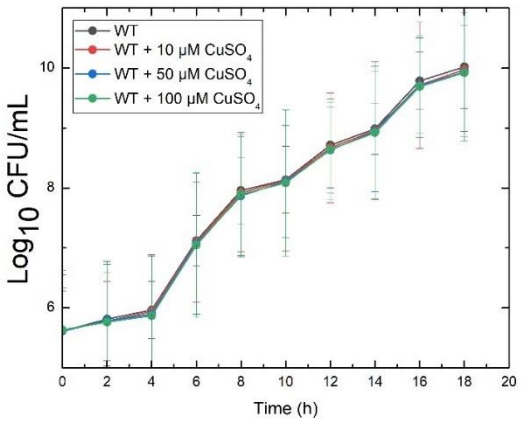

Figure 4.1: Cell viability of *S. cerevisiae WT* cells incubated in YPD medium supplemented with 10 - 100 µM $CuSO_4$ using CFU counting. Results show growth with increasing concentrations of $CuSO_4$ in each strain up to 18 h. Each dataset represents the mean and standard deviation of three independent biological replicates (n = 3).

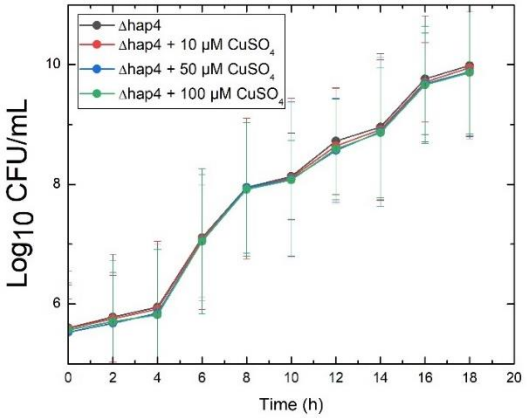

Figure 4.2: Cell viability of *S. cerevisiae* Δ*hap4* cells incubated in YPD medium supplemented with 10 - 100 μM $CuSO_4$ using CFU counting. Results show growth with increasing concentrations of $CuSO_4$ in each strain up to 18 h. Each dataset represents the mean and standard deviation of three independent biological replicates (n = 3).

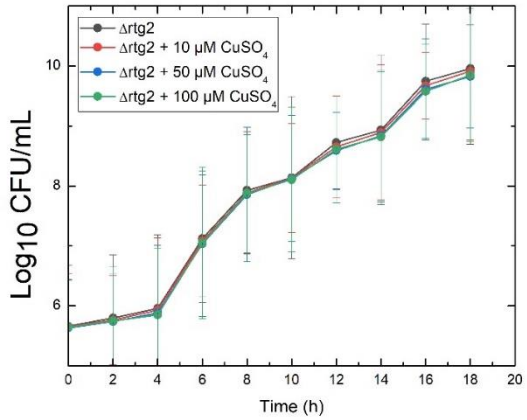

Figure 4.3: Cell viability of *S. cerevisiae* Δ*rtg2* cells incubated in YPD medium supplemented with 10 - 100 μM $CuSO_4$ using CFU counting. Results show growth with increasing concentrations of $CuSO_4$ in each strain up to 18 h. Each dataset represents the mean and standard deviation of three independent biological replicates (n = 3).

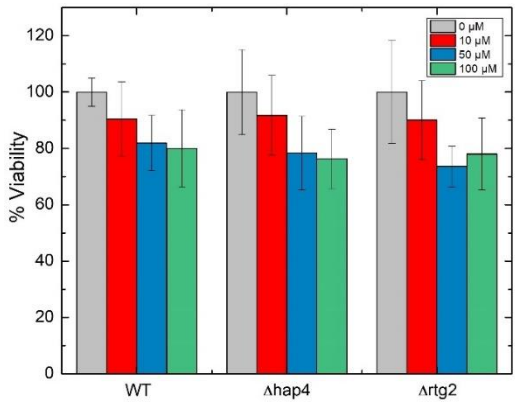

Figure 4.4: Viability of *S. cerevisiae* strains *WT, Δhap4 and Δrtg2*. Cells were grown in YPD medium supplemented with 10 - 100 μM $CuSO_4$ for 18 h. Viability was calculated as the percentage of untreated cells, set to 100%. Each bar represents the mean and standard deviation of three independent biological replicates (n = 3).

Figs. 4.1, 4.2 and 4.3 show growth curves of *S. cerevisiae* strains *WT*, Δ*hap4* and Δ*rtg2* with increasing concentrations of $CuSO_4$ in each strain up to 18 h. The results obtained showed that there was no significant difference in the viability and growth rate of the three strains tested in the presence and absence of $CuSO_4$ from 10 – 100 µM. Only a slight decrease in percentage viability with increasing $CuSO_4$ concentration in all test strains after 18 h of exposure was observed. However, the differences are not statistically significant (Turkey's test, $p<0.05$) as shown in Fig. 4.4.

4.2 UV Spectroscopic growth analysis of biorecognition elements

After testing the viability of three different strains in standard YPD media, two different type of growth analysis were performed to further analyse the growth response of yeast cells using optical detection. First, the growth analysis of *WT* cells cultured in YPD (fermentative carbon source) and YPG or YPE (non-fermentative carbon source) was performed. Followed by growth analysis of *WT* yeast strain in different growth media, yeast strains namely: *WT*, *Δhap4* and *Δrtg2* cultured in standard YPD media were evaluated for growth in micro culture in the presence of $CuSO_4$. The analysis was performed in the presence of $CuSO_4$ by measuring optical density at 600 nm with a TECAN microplate reader equipped with a shaker and a temperature control unit.

4.2.1 Numerical results and Discussion

Figs. 4.5, 4.6 and 4.7 display growth curves of *S. cerevisiae WT* cells cultured in YPD, YPG and YPE in the presence of $CuSO_4$, respectively. A representative curve from four independent biological replicates (n = 4) is shown in each panel. While Figs. 4.8, 4.9 and 4.10 show relative growth of *S. cerevisiae WT* cells cultured in YPD, YPG and YPE in the presence of $CuSO_4$, respectively from 10 to 16 h of incubation. Relative growth was calculated as the percentage of the OD_{600} of stressed/control cells. Each dataset shows the meaning of four independent biological replicates (n = 4). Relative growths are calculated in specified period (10 – 16 h) because yeast cells are expected to reach exponential phase during this time period and bioelectrode are prepared with cells cultured for 14h as well for electrochemical detection.

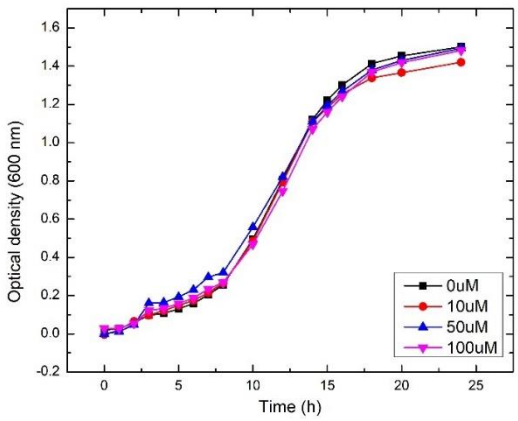

Figure 4.5: Growth curves of *S. cerevisiae WT* cells cultured in YPD in the presence of $CuSO_4$. A representative curve from four independent biological replicates (n = 4) is shown in each panel.

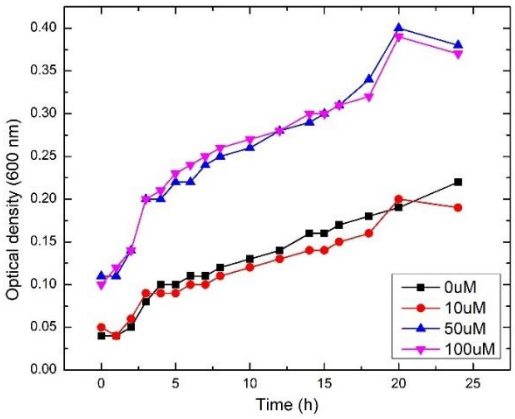

Figure 4.6: Growth curves of *S. cerevisiae WT* cells cultured in YPG in the presence of $CuSO_4$. A representative curve from four independent biological replicates (n = 4) is shown in each panel.

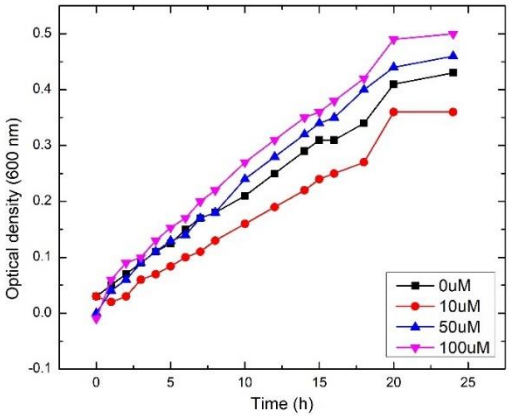

Figure 4.7: Growth curves of *S. cerevisiae WT* cells cultured in YPE in the presence of $CuSO_4$. A representative curve from four independent biological replicates (n = 4) is shown in each panel.

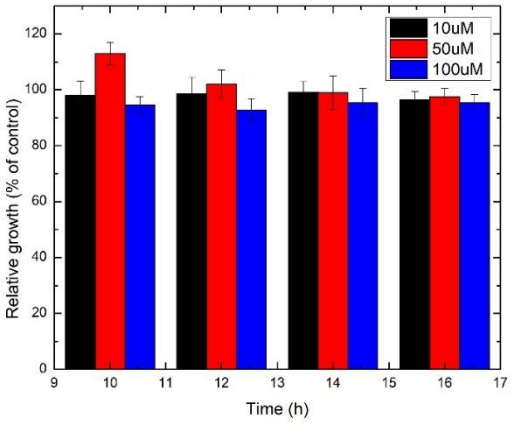

Figure 4.8: Relative growth of *S. cerevisiae WT* cells cultured in YPD in the presence of $CuSO_4$. Relative growth was calculated as the percentage of the OD_{600} of stressed/control cells. Each dataset shows the mean of four independent biological replicates (n = 4).

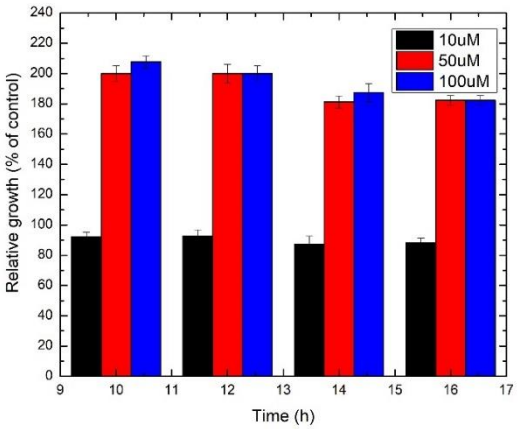

Figure 4.9: Relative growth of *S. cerevisiae WT* cells cultured in YPG in the presence of $CuSO_4$. Relative growth was calculated as the percentage of the OD_{600} of stressed/control cells. Each dataset shows the mean of four independent biological replicates (n = 4).

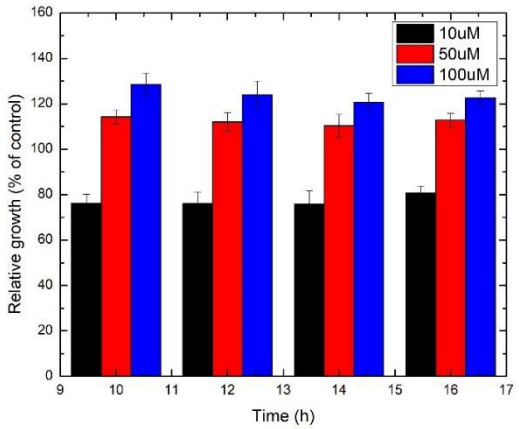

Figure 4.10: Relative growth of *S. cerevisiae WT* cells cultured in YPE in the presence of $CuSO_4$. Relative growth was calculated as the percentage of the OD_{600} of stressed/control cells. Each dataset shows the mean of four independent biological replicates (n = 4).

The results from metabolic analysis showed that there were no significant differences in growth for cultures with YPD (Figs. 4.5 and 4.8), however cultures with YPG displays a boast in growth of almost 100 % with respect to control after 12 h of incubation in the presence of both medium (50 μM) and high (100 μM) $CuSO_4$ concentration (Figs. 4.6 and 4.9). In case of YPE, there was an increase in growth of 12 and 24 % in the presence of medium and high $CuSO_4$ concentration, respectively (Figs. 4.7 and 4.10). However, a slight inhibition in relative growth was observed over time in both cases.

Figs. 4.11, 4.12 and 4.13 display growth curves of *S. cerevisiae WT, Δhap4 and Δrtg2* cells cultured in YPD in the presence of $CuSO_4$, respectively. A representative curve from four independent biological replicates (n = 4) is shown in each panel. While Figs. 4.14, 4.15 and 4.16 show relative growth of *S. cerevisiae WT, Δhap4 and Δrtg2* cells cultured in YPD in the presence of $CuSO_4$, respectively from 10 to 16 h of incubation. Relative growth was calculated as the percentage of the OD_{600} of stressed/control cells. Each dataset shows the meaning of four independent biological replicates (n = 4).

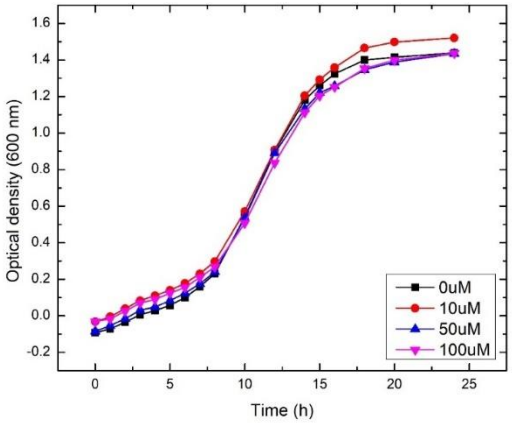

Figure 4.11: Growth curves of *S. cerevisiae WT* cells cultured in YPD in the presence of $CuSO_4$. A representative curve from four independent biological replicates (n = 4) is shown in each panel.

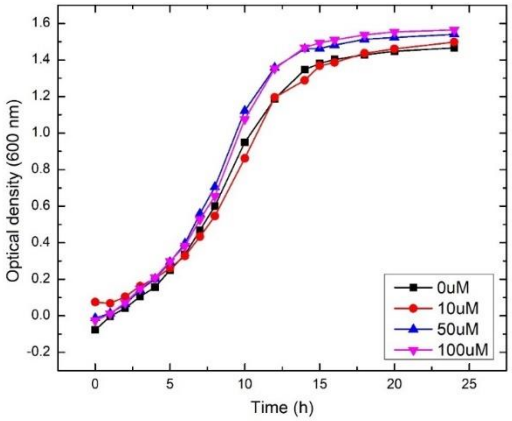

Figure 4.12: Growth curves of *S. cerevisiae Δhap4* cells cultured in YPD in the presence of $CuSO_4$. A representative curve from four independent biological replicates (n = 4) is shown in each panel.

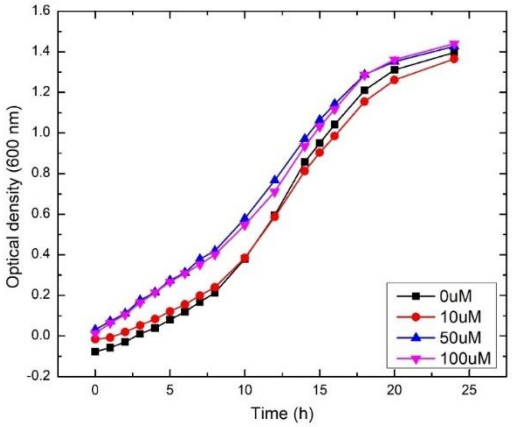

Figure 4.13: Growth curves of *S. cerevisiae Δrtg2* cells cultured in YPD in the presence of $CuSO_4$. A representative curve from four independent biological replicates (n = 4) is shown in each panel.

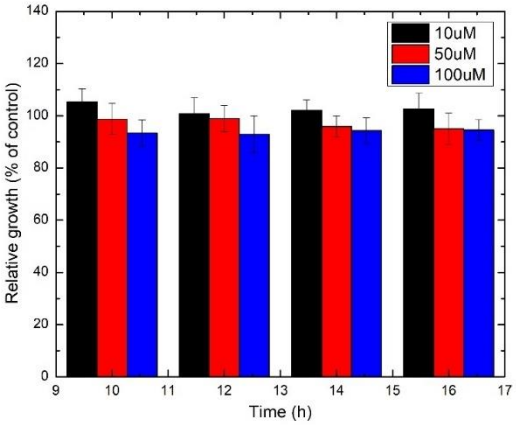

Figure 4.14: Relative growth of *S. cerevisiae WT* cells cultured in YPD in the presence of $CuSO_4$. Relative growth was calculated as the percentage of the OD_{600} of stressed/control cells. Each dataset shows the mean of four independent biological replicates (n = 4).

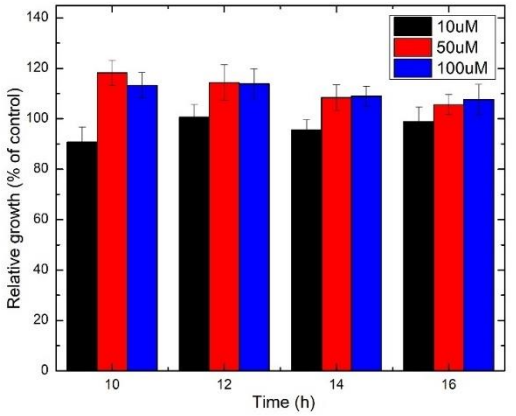

Figure 4.15: Relative growth of *S. cerevisiae Δhap4* cells cultured in YPD in the presence of $CuSO_4$. Relative growth was calculated as the percentage of the OD_{600} of stressed/control cells. Each dataset shows the mean of four independent biological replicates (n = 4).

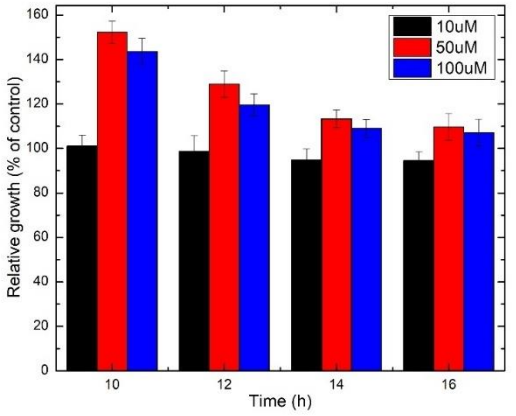

Figure 4.16: Relative growth of *S. cerevisiae Δrtg2* cells cultured in YPD in the presence of $CuSO_4$. Relative growth was calculated as the percentage of the OD_{600} of stressed/control cells. Each dataset shows the mean of four independent biological replicates (n = 4).

In the second analysis for different mutant strains, surprisingly, it was observed that both *Δhap4* and *Δrtg2* mutant strains also showed an increase in growth in the presence of mild and high $CuSO_4$ concentration with respect to control. After incubation of 12 h with $CuSO_4$ a boast in growth of almost 29 and 20 % was observed for *Δrtg2* strain in the presence of mild and high $CuSO_4$ concentrations, respectively (Figs. 4. 13 and 4. 16). In case of *Δhap4*, there was an increase in growth of almost 13 % in the presence of both medium and high $CuSO_4$ concentrations (Figs. 4.12 and 4.15). Although the growth decreased slightly overtime but it was still higher than control in both cases.

The results suggest that selected metabolic and genetic approaches can modulate the growth of biorecognition element and can be used to amplify the response of microbial cells in the presence of $CuSO_4$. It has been reported previously that depending on the amount, Cu^{2+} can either play a key role in enzymatic metabolic processes or exert varying level of cytotoxicity, cellular damage, and loss of viability, especially during bioproduction processes such as fermentation [43, 194]. In *S. cerevisiae*, increased level of the metalloenzyme superoxide dismutase (SOD) is directly linked to the presence of Cu^{2+} in the environment. Copper is an inorganic cofactor that helps SOD control the level of reactive oxygen species, thereby protecting the cells against oxidative stress [85]. This was supported by an increase in SOD1 mRNA transcript levels in the presence of bathocuproine sulphonate, a Cu^{2+} chelator [195]. However, the level of viability maintained in the presence of Cu^{2+} differs widely among strains of *S. cerevisiae,* depending on several factors such as habitat of isolation and genotype. For example, YPD medium supplemented with 1 mM Cu^{2+} did not significantly affect the growth rate and viability of 6 different yeast strains comprising four *S. cerevisiae* and two *Pichia pastoris*[196], whereas the growth of *S. cerevisiae BH8* exposed to 0.5 mM $CuSO_4$ was boosted in another study [194]. Also similar to our result, the levels of growth reported as OD_{600nm} varied insignificantly in *S. cerevisiae* strains *S288C*, *AWRI1631*, *RM11*, and *YJM339* exposed to 50 and 100 μM $CuSO_4$[193]. Generally, two mechanisms of metal detoxification have been identified in fungi; surface binding of metals (biosorption) or intracellular uptake during metabolic processes (bioaccumulation)[197], and these traits vary widely in strains of *S. cerevisiae* [43]. Exploiting these features, biosensor based on immobilized yeast cells for copper detection have been published and genetically modified *S. cerevisiae* cells have been immobilized in alginate beads to detect copper in the range 1-100 μM in drinking water and wastewater [198]. The insignificant effect of copper on yeast viability using optical detection and variable response of yeast strains to copper stress reported here and before offered the possibility of detecting copper by developing electrochemical biosensors at low concentrations.

4.3 Biosensor design

Having observed improvements in optical response of response of wild type and mutant yeast cells under different metabolic conditions we turned our attention towards preperation of SPE based bioelectrodes with proposed genetic and metabilic manipulations. The reason for using SPE instead of GCE was made considering the fact that for point-of-cure electrochemical biosensing applications the electrodes need to be cost-effective, able to withstand mechanical or fluidic impact, provide design flexibility and are ready to use. However, GCEs are usually costly and due to their smooth surface usually provide poor adhesion [199, 200]. Glassy carbon is known for its brittle nature thus GCE are available in limited shapes [201]. Moreover, in most cases GCE need pretreatment before use, making its infield application extremely challenging [202]. On the other hand, screen-printing technology involves applying layers of ink onto a solid substrate using a screen or mesh that defines the sensor's shape and structure. This method has several advantages, including flexibility in design, compatibility with automated processes, high reproducibility, and a wide selection of materials [203]. Screen-printed electrodes (SPEs) typically consist of three electrodes: a working electrode, a counter electrode, and a reference electrode printed on a single substrate to form a sensor and can be easily customized by using different commercial or homemade inks. Carbon paste is a popular choice due to its low cost, ease of modification, and chemical stability [204-206]. Additionally, these sensors can be

further customized by adding various coatings to their surfaces, including metal films, polymers, enzymes, and other substances [203]. Owing to above mentioned benefits, the immobilization protocols presented in section 3.3 were adopted for development of SP bioelectrodes (SPE Ref. TE100, Zensor, Taiwan) with 3 mm diameter carbon working electrode (WE), carbon counter electrode (CE) and silver (Ag) pseudo-reference electrode (RE). A multichannel potentiostat (EN035, multipalmsens4) was used for all bio-electrochemical characterizations and all potentials were reported vs. Ag pseudo-reference. The electrochemical polymerization step was performed by 20 repeated cyclic voltammetry between - 0.3 and + 0.5 V with a scan rate of 20 mV s^{-1}. The biosensors were later characterized using scanning electron microscopy (SEM), cyclic voltammetry, electrochemical impedance spectroscopy (EIS) and chronoamperometry (CA) as before.

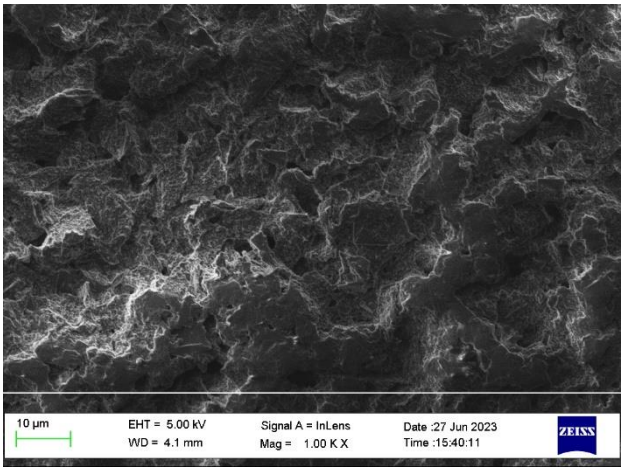

Figure 4.17: FE-SEM image of bare surface of SPE

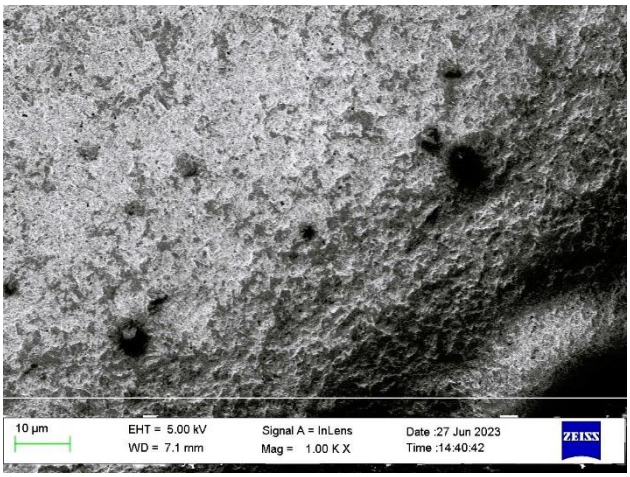

Figure 4.18: FE-SEM image of SPE coated with PDA

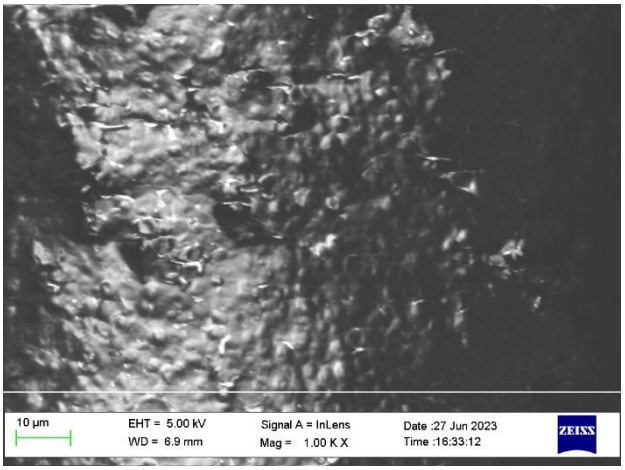

Figure 4.19: FE-SEM image of SPE with PDA immobilized *WT* yeast cells.

4.4 Assessment of PDA coating morphology

Following the preparation of bioelectrode using SPE, the morphology of the PDA coating used for immobilization of the cells was assessed by scanning electron microscopy. The morphology of PDA immobilization (cells embedded in PDA) was evaluated using FE-SEM (Sigma VP, ZEISS Company, Germany). Three different types of bioelectrodes: i) bare surface of SPE, ii) SPE coated with PDA, iii) yeast cells immobilized with PDA on SPE were analysed for morphological analysis. Bio-electrodes were prepared as stated in section 3.3 and were cut down to the size of stub/sample holder. The samples were fixed on stub using conductive double-sided tape and gold-coated using ion sputtering apparatus (SBC-12, KYKY, China) for 20 to 40 s at 5 - 10 mA. Samples were observed with an area width 3 to 10 mm at a magnification of 1000X under a vacuum pressure of 10 Pa. Other inspecting conditions like signal collected (In-lens), the conductor status (standard) and acceleration voltage (3 or 5 kV) were adjusted to obtain high quality images. Figs. 4.17 and 4.18 show bare SPE surface and PDA without cells drop-casted, respectively. The surface of bare SPE was rough while PDA drops casted on the surface of the SPE formed a plain layer of conductive coating. The roughness of the bare electrode surface is considered to be beneficial for electrochemical sensing applications as it significantly lowers the limit of detection by providing better immobilization [207], while PDA only sample filled the gapes and formed a uniform layer of polymer. Figs. 4.19 displays cells embedded in PDA, yeast cells were well-embedded in the PDA, at high cell density. These data demonstrated that the PDA coating was compact, homogeneous, and showed fully integrated morphology in the presence of the cells.

4.5 Electrochemical characterization of biosensors

Fig. 4.20 shows the image of a biosensor prepared by immobilizing yeast on SPE. For electrochemical characterization of biosensor, all experiments were performed at fixed temperature of 26 °C in 20 mL scintillation vials containing 18 mL electrolyte solution of 20 mM MOPS buffer (pH 5), 10 mM $MgCl_2$, 50 mM glucose, and $K_3[Fe\ (CN)_6]$ under aerobic conditions in the presence and absence of copper sulphate (0 to 100 µM). Copper sulphate was introduced in scintillation vials after electrochemical polymerization and magnetically stirred at 100 rpm for 120 seconds to obtain a homogenized solution. In order to improve the electrochemical response of electrochemical system, $K_3[Fe(CN)_6]$ was selected to act as extracellular redox mediator. $K_3[Fe(CN)_6]$ has been used both in microbial fuel cells (MFC) and electrochemical biosensors to increase extracellular electron transfer rate from biofilms to electrodes [208, 209].

.

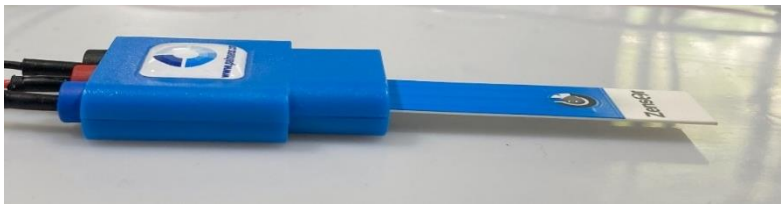

Figure 4.20: Image of SPE with immobilized yeast cells.

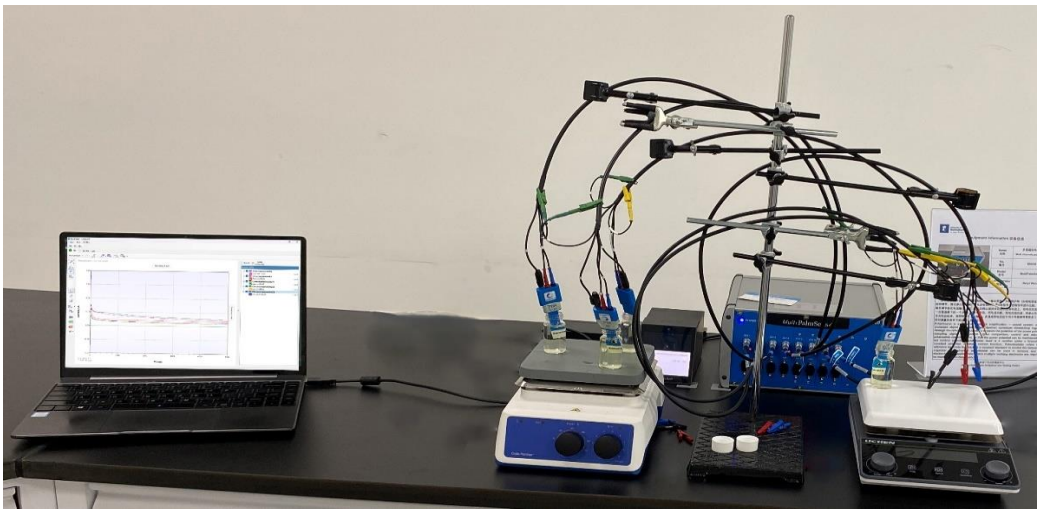

Figure 4.21: Assembly used for electrochemical characterization of biosensors prepared using immobilized yeast cells on the surface of SPE.

For example, a *S. cerevisiae* MFC showed improved performance when 50 mM $K_3[Fe(CN)_6]$ was added as external mediator [208]. Despite its toxicity, $K_3[Fe(CN)_6]$ was employed as redox mediator also with fungi *Candida albicans* at 100 µM concentration [210]. With respect to another biocompatible redox mediator like HNQ, it is more stable and has a faster turnover rate [211, 212]. Therefore, 50 µM $K_3[Fe(CN)_6]$ was used in all electrochemical experiments carried out in this part of the study. Control group experiments were performed following the same procedure for bio-electrode preparation stated in section 3.5 with dead cells (viable cells placed in a hot water bath for 1 hour at 100 °C) and PDA coating only. Fig. 4.21 shows the Assembly used for electrochemical characterization of biosensors prepared using immobilized yeast cells on the surface of SPE.

4.5.1 Voltametric analysis of biosensors

CV is a technique that not only provides quantitative analysis but also offers diagnostic information regarding metabolic activity of attached cells in electrochemical characterization [213-215]. Keeping that in mind, *S. cerevisiae WT* strain: dead cells, viable cells, and PDA only, immobilized on SPE surfaces were characterized to observe the voltametric response in the presence of the redox mediator (Fig. 4.22). Low scan rate (1 - 5 mV s^{-1}) is usually preferred while working with microbial applications as it can provide information regarding sluggish interfacial electron transfer. At 2 mV s^{-1} scan rate (- 0.3 V to + 0.52 V), the CVs at 14 h displayed sizeable differences in three groups. Control experiments with bioelectrodes prepared with dead cells and PDA coating only showed a smaller current density than yeast cells immobilized with PDA. These results were similar to our previous results obtained with glassy carbon electrode. However, the voltametric response demonstrated that bioelectrodes prepared using yeast cells embedded in PDA had almost 10 folds (16 ± 1 mA cm^{-2}) increase at + 0.4 V during anodic scan and SPE improved the current density compared to standard GCE.

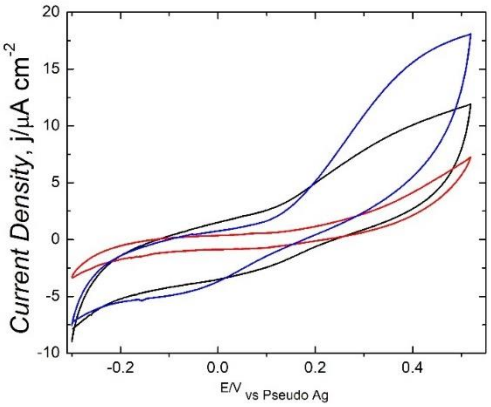

Figure 4.22: Cyclic voltammetry for the bioelectrode in the presence of redox mediator prepared with *WT S. cerevisiae* cells in the PDA matrix (blue), dead yeast cells in PDA (red), and sterile electrodes prepared with polydopamine alone (black). Results are the average of three independent biological replicates.

4.5.2 Impedimetric analysis of PDA immobilization

In order to study the facilitation of EET by PDA in current system, the EIS response was studied for four different samples based on the to evaluate the response of PDA coating i.e., Sample 1: viable yeast cells immobilized using PDA on SPE with redox mediator in electrolyte, Sample 2: viable yeast cells immobilized using PDA on SPE without redox mediator in electrolyte, Sample 3: PDA immobilized on SPE without redox mediator in electrolyte and Sample 4: Dead yeast cells immobilized using PDA on SPE without redox mediator. The EIS was performed as a potential scan from -100 mV to 400 mV with a step potential of 50mV between a frequency range of 0.05 Hz to 50 kHz.

4.5.2.1 Numerical results and discussion

Figs. 4.23 and 4.24 show the Nyquist and Bode plot for four samples. Nyquist plot showed both real and imaginary components increased from Sample 1 to sample 4, which indicates decrease in impedance during EET in the presence of viable cells and redox mediator. The plot shows depressed semi-circles for each sample indicating non-ideal capacitance [216]. Fig. 4.24 shows the bode phase plot with respect to frequency, indicating the characteristic time of different electrochemical effects at different frequencies.

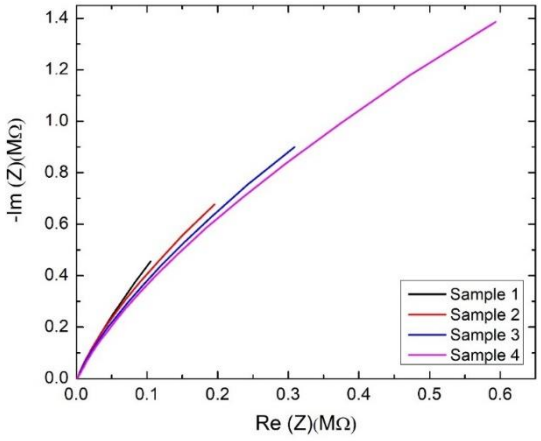

Figure 4.23: Nyquist plot for samples at OCP. Frequency range 0.05 Hz – 50 kHz, potential scan from -100 mV to 400 mV with a step potential of 50 mV.

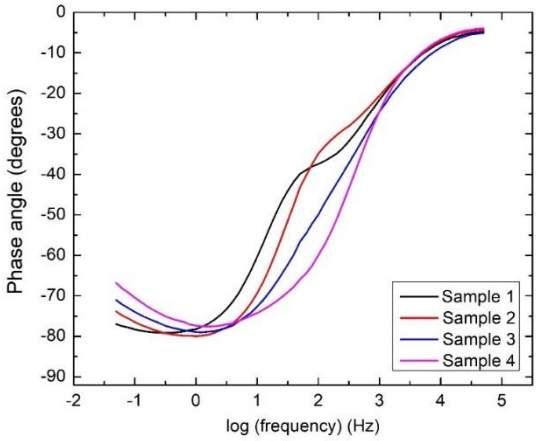

Figure 4.24: Bode plot for samples at OCP. Frequency range 0.05 Hz – 50 kHz, potential scan from -100 mV to 400 mV with a step potential of 50mV.

It is observed that EIS at low and medium frequency here represent charge transfer and double layer capacitance at the coating-electrode interface while the high frequency indicate charge accumulation on PDA-electrolyte interface and resistive behavior of electrolyte solutions to applied signal, respectively [217]. While looking at the phase angle, we noted that the phase angle never reached 90 which is an indication that the PDA-electrolyte interface behaved as a constant phase element CPE [216]. This also explains the depressed semi-circular feature observed in the Nyquist plot. The experimental data obtained from EIS was analyzed for distribution function of relaxation times (DFRT) and the corresponding number of time constants prior to modeling with equivalent circuit fitting (Fig. 4.25). Since the DFRT analysis showed two distinct time constants, a Randles equivalent circuit consisting of a series resistance (resistance of electrolyte) with two resistor-CPE circuits (Fig. 4.26) was selected to represent the electrochemical system [218].

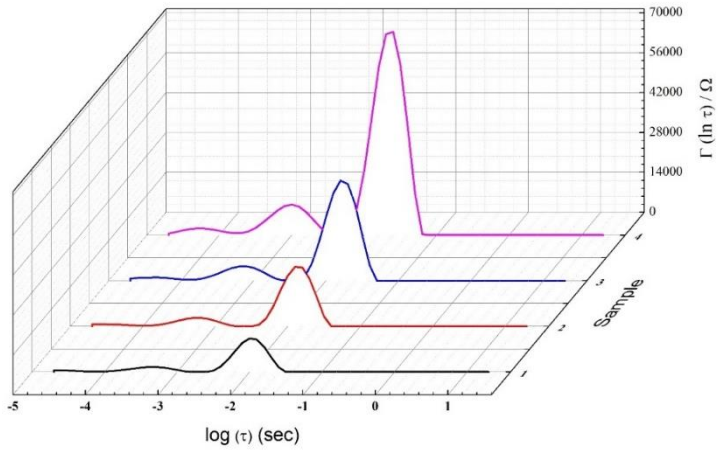

Figure 4.25: Representative DFRT plots for samples at OCP. Frequency range 0.05 Hz – 50 kHz, potential scan from -100 mV to 400 mV with a step potential of 50 mV.

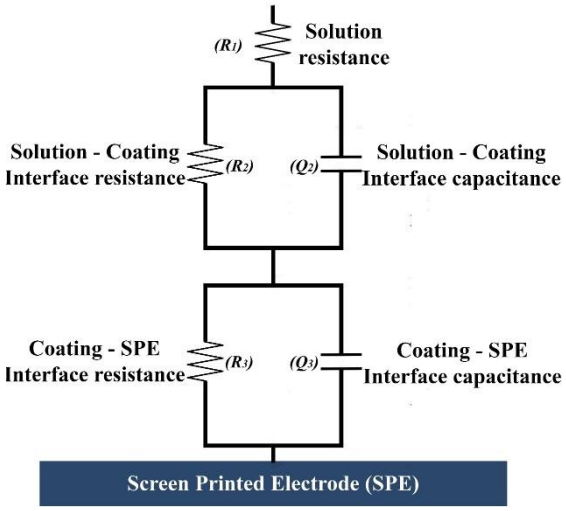

Figure 4.26: Schematic representations of equivalent circuit.

In equivalent circuit, R_1 represents the resistance of the electrolyte, Q_2 and α_2 represent CPE to model non-ideal capacitance at solution-coating interface, and R_2 is charge transfer resistance R_{ct} at the same interface. Similarly, Q_3 and α_3 represent the CPE to model the non-ideal capacitance at the coating-electrode interface, and R_3 is the resistance to charge transfer R_{ct} at the same interface [218]. CPE was used for modeling keeping in mind the depressed nature of semicircles during Nyquist plot with phase angles less than 90 degrees and to account for the for irregularities on the surface due to the roughness of the SPE and inhomogeneities on the composite layer [219]. As CPE was used for the modelling, capacitance was calculated using Hsu-Mansfeld equation because in equivalent circuit model resistance and CPE were in parallel, the CPE coefficients were between 0.65 and 1 and time constant was normally distributed in DFRT [217, 220].

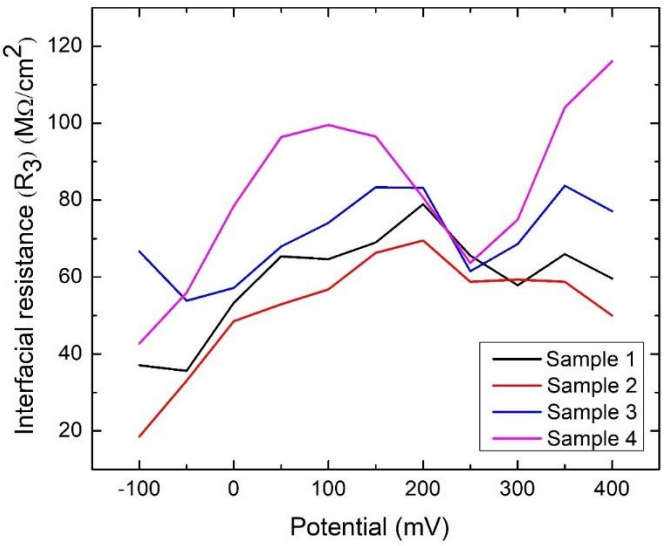

Figure 4.27: Interfacial resistance for samples at bias potential. Frequency range 0.05 Hz – 50 kHz, potential scan from -100 mV to 400 mV with a step potential of 50 mV.

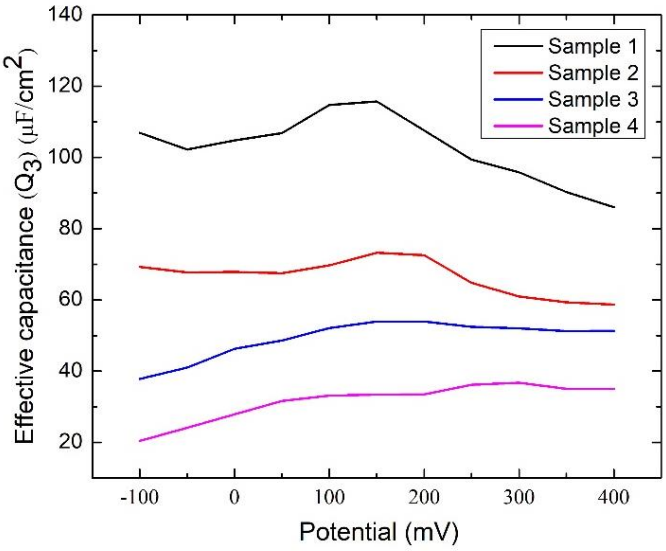

Figure 4.28: Effective capacitance for all samples at bias potential. Frequency range 0.05 Hz – 50 kHz, potential scan from -100 mV to 400 mV with a step potential of 50 mV.

As EET is potential dependent, Fig. 4.27 shows interfacial resistance between electrode and biofilm interface for four samples at different potentials for fitting data. It can be observed that the interfacial resistance for sample 4 (dead cells) is significantly higher with respect to samples 2 and 1 (viable cells) while sample 3 had the lowest resistance. From the results we hypothesize this effect shows facilitated charge-limited process and confirming the increase in EET from cells in sample 2 and 1. In contrast to interfacial resistance, effective capacitance displayed in Fig 4.28 showed inverse trend, where sample 1 and 2 (viable cells) showed higher capacitance for fitted data in comparison to sample 4 (dead cells). It indicates that there is formation of space charge layer in sample 1 and 2 (viable cells) due to higher EET resulting in double layer capacitance at electrode-biofilm interface. These results are consistent with our hypothesis and with the results obtained from CV and CA as well.

4.5.3 Amperometric analysis of biosensor

In this part of the study, our main focus was on the characterization of biosensors using CA as it provides the response of the system in steady state condition. Generally, in long-term experiments (e.g., 24 - 48 h), the current output is due to growth and respiration of the electricigens [221]. However, the inherent lack of repeatability of biofilm growth makes the long-term current output strongly dependent on the initial conditions. However, the current output for short term experiments with immobilizations, cell growth can be neglected and interpreted as steady-state respiration of the immobilized cells. Thus, short-term amperometry is an effective method to test constant respiration rate (e.g., for different environmental conditions and/or species or mutants) or detect rapid variation in the extracellular respiration following the application of chemical stress (e.g., $CuSO_4$). In the first set of experiments, *WT* cells were grown in rich medium YPD (with glucose as fermentative carbon source) and YPG or YPE (glycerol or ethanol as non-fermentative carbon sources). After 14 h cells from each culture media were immobilized on the SPE to prepare bioelectrodes of three different types, each having biorecognition element with different growth media. Having observed that respiratory metabolism might affect electrical cell response, chronoamperometric analysis of bioelectrodes with *WT* and two mutant strains, *Δhap4* and *Δrtg2,* lacking the catalytic subunit of the transcriptional complex Hap2-5 complex required for the control of tricarboxylic acid (TCA) cycle and electron transport and the upstream regulator of the mitochondrial retrograde

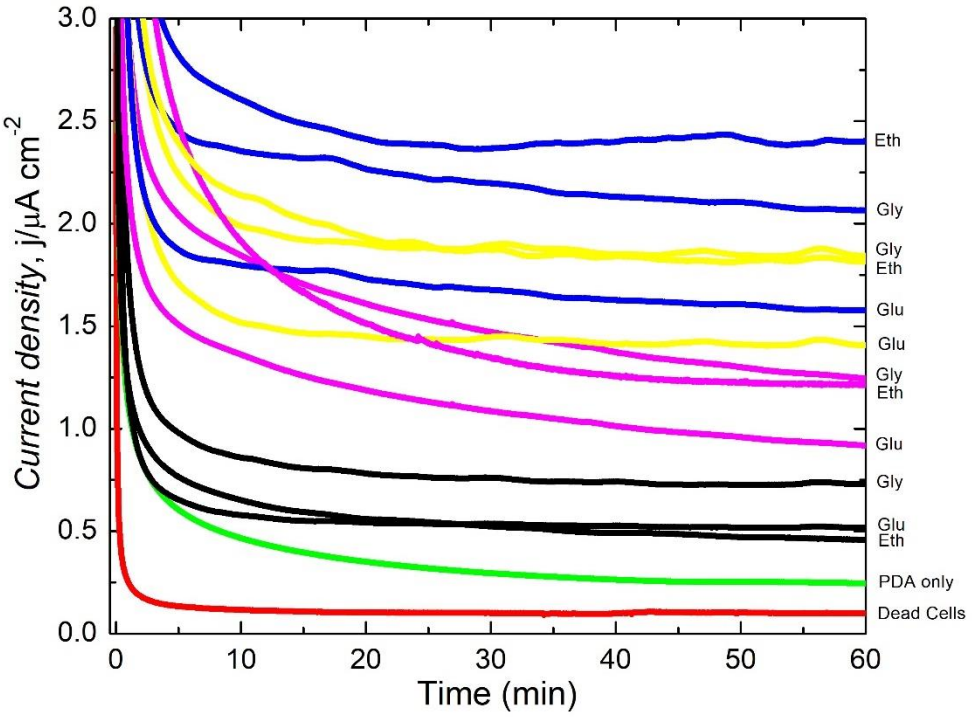

Figure 4.29: Amperometric i−t traces of *S. cerevisiae WT* cells grown in glucose, glycerol and ethanol as carbon source at 0.4 V versus CE, C; RE, Pseudo Ag with 0 µM (blue), 10 µM (yellow), 50 µM (pink), 100 µM (black) $CuSO_4$ under aerobic conditions.

pathway, respectively was performed. The three strains were cultured in medium containing glucose as sole carbon source and immobilized on the SPE to develop biosensors for electrochemical characterization. The characterization using CA was performed at 0.4 V for a period of 5000s for all samples.

4.5.3.1 Numerical results and Discussion

First, amperometric trace of biosensor prepared with *WT* cells cultured in YPD, YPG and YPE, and immobilized using PDA on the surface of SPE was performed as shown in Fig. 4.29. Differently from glucose, which is preferentially metabolized by yeast cells even in the presence of oxygen (glucose catabolite repression), glycerol and ethanol stimulate respiration (Figs. 4.5, 4.6 and 4.7). Obtained results showed that the chronoamperometric response, measured at 0.4 V for a period of 5000 s, was significantly improved by respiratory metabolism rather than fermentative metabolism (Fig. 4.29). Interestingly, it was reported before that *S. cerevisiae* respired aerobically in the mitochondria in the presence of glycerol as carbon source, producing 30% ATP higher than the medium containing glucose as carbon source [222]. Vasylkovska et al (2015) also demonstrated that the medium supplemented with glycerol and ethanol as carbon sources had 6.9 and 3.3 fold increase in metabolic rate compared to the medium containing glucose, respectively [223].

Table 4.1: Percentage increase of current densities at 2500 s in amperometric i–t traces of biosensors prepared using *S. cerevisiae WT* strain cultured in YPG and YPE with respect to YPD, at 0.4 V versus CE, C; RE, Pseudo Ag with different concentration of $CuSO_4$ (0, 10, 50, 100 µM) under aerobic conditions.

Name	Percentage increase in current density (YPG w.r.t YPD)	Percentage increase in current density (YPE w.r.t YPD)
0 µM	30.998	48.495
10 µM	30.987	30.154
50 µM	35.604	24.517
100 µM	40.444	-6.370

They also reported that although no significant difference was recorded in the SOD activity of the strains utilizing each of these carbon sources, the activity of catalase was found to be 3.3 higher in the glycerol medium relative to the medium containing glucose. This better response was maintained in the presence of copper sulphate, with less sensitivity at highest concentrations (Fig. 4.29 and Table 4.1). Relative growth data in these conditions indicate that copper had a stimulatory effect in glycerol or ethanol medium (Figs. 4.5, 4.6 and Fig. 4.7) according to [224]. Beyond its positive effect on respiratory rate, copper can also ameliorate oxidative stress. As earlier indicated, the presence of Cu^{2+} in trace amount could have led to increased SOD activity as reported by Liang and Zhou (2007), the high activity of catalase in the presence of glycerol could have better controlled the high amount of amount of H_2O_2 and molecular oxygen resulting from SOD activity, helping the cell achieve a more balanced redox state, and ultimately leading to the increase in current output (EET rate) [225]. The results of CA were compared at 2500 s, where the current output reached steady state for all samples, and the EET rate increase of about 30% for cells cultured in glycerol or ethanol for almost all concentrations of $CuSO_4$ with respect to glucose. However, at higher concentration the tolerance decreased for cell cultured in ethanol, and the current density showed a drastic inhibition particularly at 100 µM (Table 4.1 and Fig. 4.30).

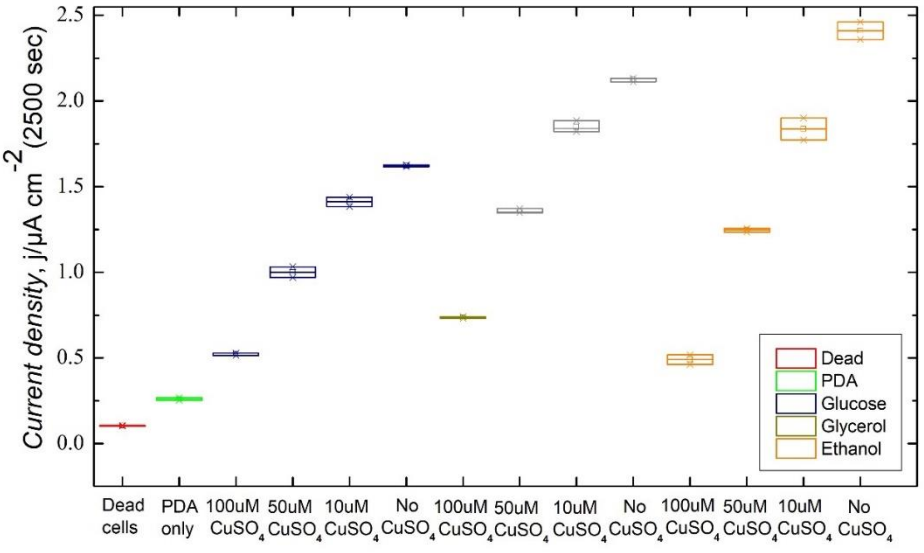

Figure 4.30: Current density of *S. cerevisiae WT* cells grown in glucose, glycerol and ethanol as carbon source at 0.4 V versus CE, C; RE, Pseudo Ag with different concentration of $CuSO_4$ (0, 10, 50, 100 µM) under aerobic conditions after 2500 s of incubation.

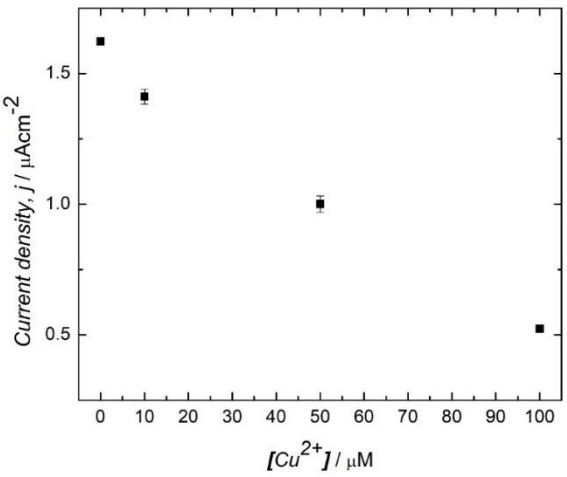

Figure 4.31: Relationship between $CuSO_4$ concentrations and current density during chronoamperometry at E_{APP}: +0.40 V. R^2: 0.998 for bioelectrodes prepared by immobilizing *WT* cell cultured in YPD. Error bars indicate one standard deviation.

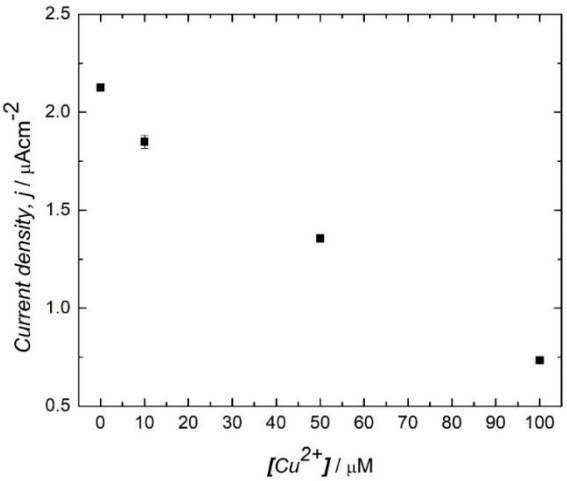

Figure 4.32: Relationship between $CuSO_4$ concentrations and current density during chronoamperometry at E_{APP}: +0.40 V. R^2: 0.996 for bioelectrodes prepared by immobilizing *WT* cell cultured in YPG. Error bars indicate one standard deviation.

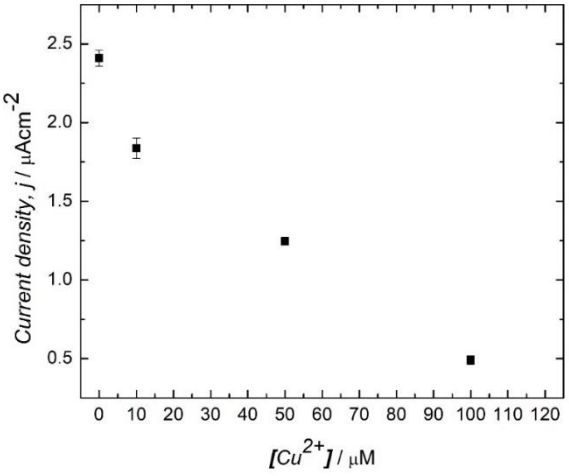

Figure 4.33: Relationship between $CuSO_4$ concentrations and current density during chronoamperometry at E_{APP}: +0.40 V. R^2: 0.947 for bioelectrodes prepared by immobilizing *WT* cell cultured in YPE. Error bars indicate one standard deviation.

Table 4.2: LoD, R^2, and sensitivity of bioelectrodes prepared by immobilization of *S. cerevisiae WT* strain cultured in glucose, glycerol and ethanol as carbon after 2500 s of incubation with different concentration of $CuSO_4$ (0, 10, 50, 100 µM) under aerobic conditions.

Name	LoD (µM $CuSO_4$)	R^2	Sensitivity ($\mu A*cm^{-2}*L*\mu mol^{-1}_{CuSO4}$)
YPD	2.2	0.998	$-10.9 \pm 0.3 \times 10^{-3}$
YPG	1.8	0.996	$-13.6 \pm 0.5 \times 10^{-3}$
YPE	1.4	0.947	$-17 \pm 2.3 \times 10^{-3}$

In order to better understand the response of biosensors, the current density values at 2500 s were analyzed for linear fitting as shown in Figs. 4.31, 4.32 and 4.33. The linear fitting data obtained from CA for all three groups is shown in Table 4.2. It was observed that the biosensors prepared using metabolic manipulations immobilized on SPE showed improvement in all aspects such LoD, R^2 and sensitivity in comparison to the results obtained by glassy carbon bioelectrode. The current set of biosensors provided at least 10 percent higher in LoD, improved R^2 (except ethanol) as well as a minimum of 2 fold increase in sensitivity.

Having observed that respiratory metabolism might affect electrical cell response, chronoamperometric analysis was performed with biosensors prepared using *WT* and two mutant strains, *Δhap4* and *Δrtg2,* respectively (Fig. 4.34). The three strains were cultured in medium containing glucose as sole carbon source and immobilized on the SPE for electrochemical characterization.

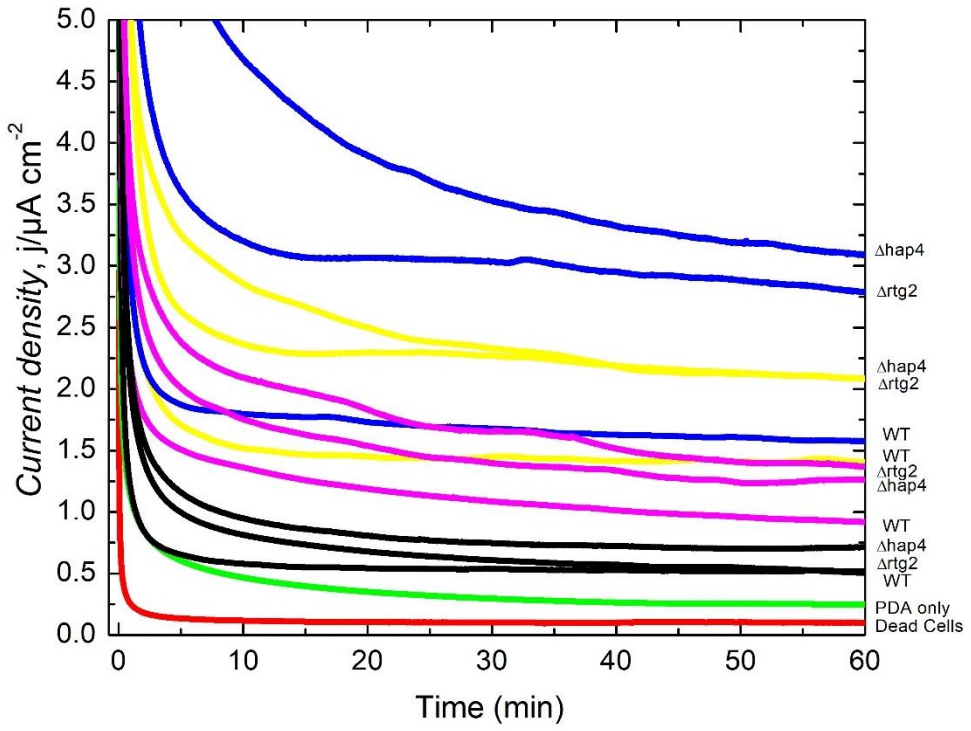

Figure 4.34: Chronoamperometric of *S. cerevisiae WT, Δhap4* and *Δrtg2* cells at 0.4 V versus CE, C; RE, Pseudo Ag with 0 µM (blue), 10 µM (yellow), 50 µM (pink), 100 µM (black) $CuSO_4$ under aerobic conditions.

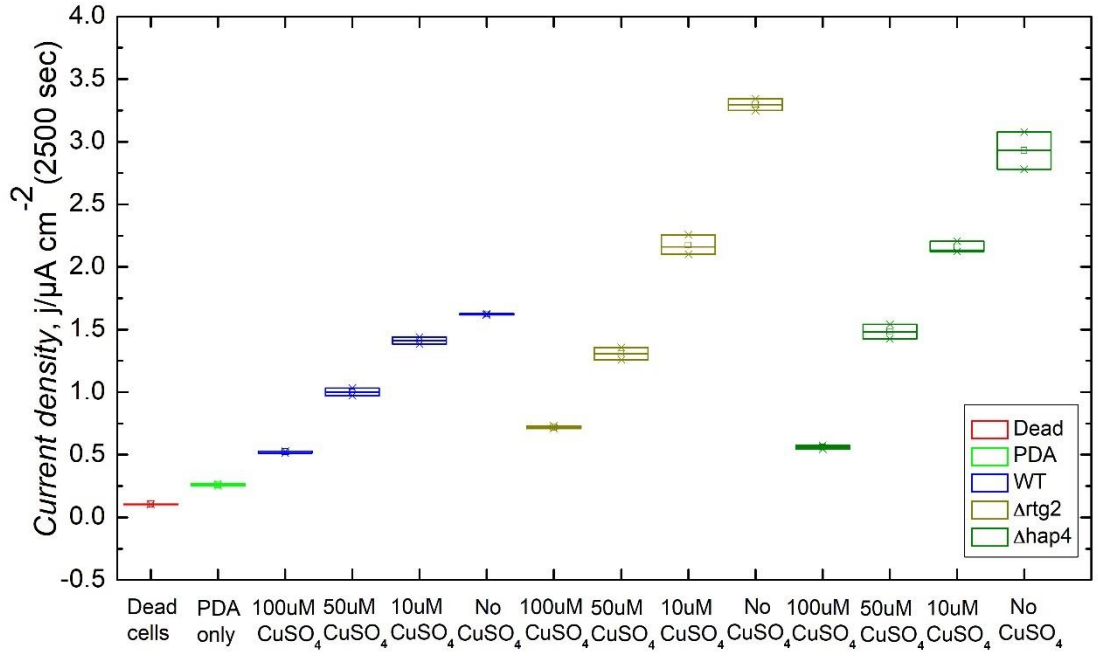

Figure 4.35: Current density of *WT, Δhap4* and *Δrtg2* cells at 0.4 V versus CE, C; RE, Pseudo Ag with different concentration of $CuSO_4$ (0, 10, 50, 100 µM) under aerobic conditions after 2500 s of incubation.

Table 4.3: Percentage increase of current densities at 2500 s in amperometric i–t traces of biosensors prepared using *S. cerevisiae Δhap4* and *Δrtg2* strains with respect to *WT*, at 0.4 V versus CE, C; RE, Pseudo Ag with different concentration of $CuSO_4$ (0, 10, 50, 100 µM) under aerobic conditions.

Name	Percentage increase in current density (*Δhap4* w.r.t WT)	Percentage increase in current density (*Δrtg2* w.r.t WT)
No	103.123	80.514
10 µM	54.003	52.579
50 µM	30.668	48.189
100 µM	37.160	7.174

Interestingly, both the mutations improved the EET response, measured at 0.4 V for a period of 5000 s (Fig. 4.34). The current density values were compared at 2500 s as shown in Fig. 4.35 and Table 4.3. An increase in EET response above 35 percent was observed for biosensors prepared with both mutant strains in comparison with *WT* for all concentration of $CuSO_4$. The current output of all the strains decreased with the increase in concentrations of $CuSO_4$, indicating a perturbation in their metabolic state associated with Cu^{2+} induced stress. As shown in Fig. 4.35 and Table 4.3, *Δhap4* and *Δrtg2* showed significant increased EET response in comparison with *WT* for concentrations of $CuSO_4$ except for 100 µM for *Δrtg2*. These observations were in agreement with cell growth data showing that copper can ameliorate cell growth in the two mutants with respect to *WT* (Figs. 4.11, 4.12 and 4. 13). On the other hand, the increased EET response in the presence of copper could be due to reduced oxidative stress in the mutants. The control experiments, bioelectrodes prepared using PDA with heat-killed cells and PDA-only showed negligible current output.

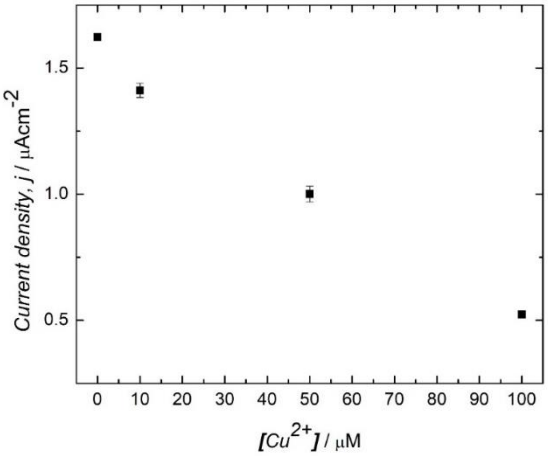

Figure 4.36: Relationship between $CuSO_4$ concentrations and current density during chronoamperometry at E_{APP}: +0.40 V. R^2: 0.998 for bioelectrodes prepared by immobilizing *WT* cell cultured in YPD. Error bars indicate one standard deviation.

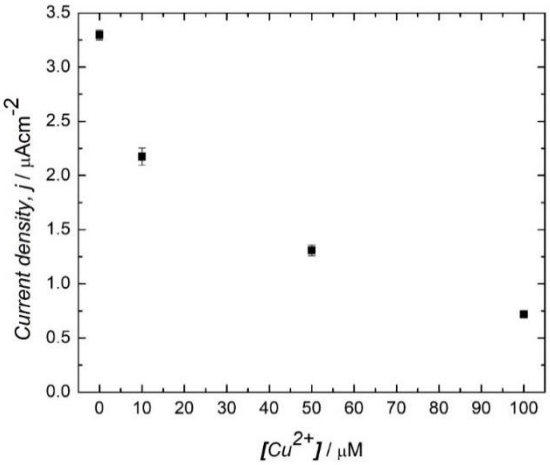

Figure 4.37: Relationship between $CuSO_4$ concentrations and current density during chronoamperometry at E_{APP}: +0.40 V. R^2: 0.902 for bioelectrodes prepared by immobilizing *Δhap4* cell cultured in YPD. Error bars indicate one standard deviation.

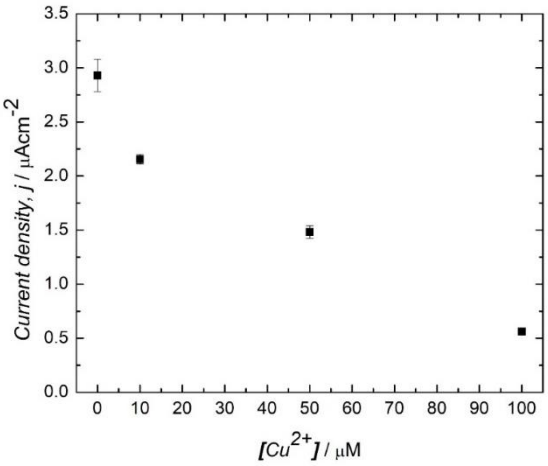

Figure 4.38: Relationship between $CuSO_4$ concentrations and current density during chronoamperometry at E_{APP}: +0.40 V. R^2: 0.986 for bioelectrodes prepared by immobilizing *Δrtg2* cell cultured in YPD. Error bars indicate one standard deviation.

Table 4.4: LoD, R^2, and sensitivity of biosensors prepared by immobilization of *S. cerevisiae WT, Δhap4* and *Δrtg2* strains cultured in glucose as carbon after 2500 s of incubation with different concentration of $CuSO_4$ (0, 10, 50, 100 µM) under aerobic conditions.

Name	LoD (µM $CuSO_4$)	R^2	Sensitivity ($*10^{-3}$ µA*cm^{-2}*L*µmol$^{-1}_{CuSO4}$)
WT	2.2	0.998	$-10.9 \pm 0.3 \times 10^{-3}$
Δhap4	1.1	0.902	$-22.1 \pm 4.1 \times 10^{-3}$
Δrtg2	1.3	0.986	$-18.3 \pm 1.2 \times 10^{-3}$

The higher rate of respiration observed in *Δhap4* and Δ*rtg2 (Table. 4.3)* is in agreement with Guaragnella et al (2021) and could be due to possession of higher mitochondrial mass, especially in *Δhap4* where the growth appeared accelerated with respect to *WT* in the absence of stress [170]. Also, the higher resistance to copper in both mutant strains might be an effect of dysfunctional mitochondria as previously observed in (Liang and Zhou, 2007). Overall, this confirms an interplay between *RTG2* and *HAP4* in controlling mitochondrial function [171]. Similar to previous case, we performed linear fitting and obtained calibration curves using current density values at 2500s as shown in Figs. 4.36, 4.37, 4.38 and Table 4.4. The data suggested a positive in all aspects i.e., as LoD, R^2 and sensitivity in comparison to the results obtained by glassy carbon bioelectrode. The current set of biosensors provided at least 10 percent higher in LoD, improved R^2 (except Δhap4) as well as a minimum of 2 fold increase in sensitivity.

Looking at results form CA analysis, either two or three phases can be observed: a) a rapid capacitive discharge in the initial 5 minutes; b) a slow decrease of the current output, which is longer at low $CuSO_4$ concentration and c) a plateau phase, in which the current remain stable with time. Virtually no current is observed for dead cells, indicating the biological origin of the current output. However, this current output is even lower than that of PDA only, likely due to the poor conductivity of the dead cells. The current observed for PDA seem due to the polyelectrolyte, which facilitate EET [155]. However, overall the current output remains low. The drift, i.e. the slope of the phase b) is small at both low (0 and 10 mM) and high (100 mM) concentrations of $CuSO_4$. In fact, the cell can tolerate low concentration of Cu^{2+}, although it decreases the respiration rate with respect to the control and it is likely that high concentration of $CuSO_4$ damages most of the cells quickly durring electrochemical analysis, leaving only a small residual repiration rate. This also corelate with the CFU counting results where the cells showed viability even after incubation with $CuSO_4$ after more than 20 h. On the other hand, at 100 µM, we are probably close to the MIC, thus cells are slowly dying/being inhibited under given conditions [50-52]. In an application, the concentration of the analyte should be kept lower than the MIC, to avoid damaging the sensing element. The comparision of result from CFU counting with CA analysis indicate that both show same trends but in case of CFU counting the inhabition in growith is very low as the percentage viability started to show slight decrease after 18 h (Fig. 4.4) of exposure while the presented method provide better sensitivity and rapid detection in comparison to conventional optical techniques. Moreover the results also correspond to our previous results presented in chapter 3 [177].

Chapter 5

PROTOTYPE AND WEB APPLICATION DESIGN

In this chapter we describe the description of the proposed prototype device, and the web application developed in this work for characterization of biosensor for in-situ detection of copper.

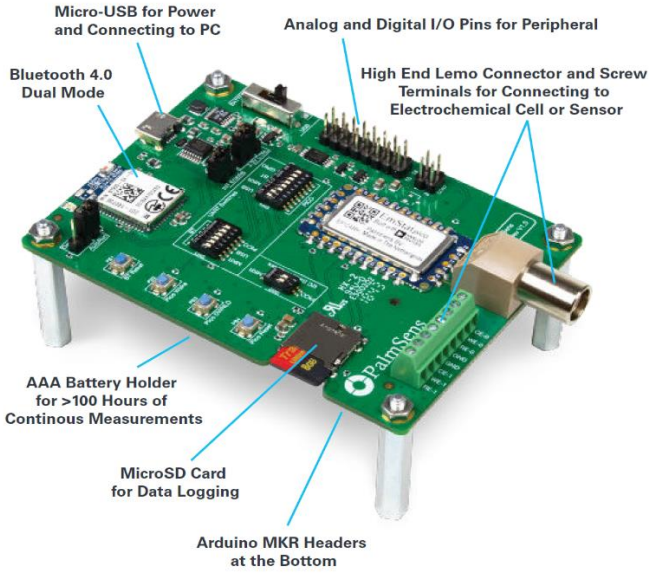

Figure 5.1: EmStat pico development board

5.1 State of the art

With the development of microelectronics, the instruments used for electrochemical measurements such as potentiostat have scaled down to handheld devices from desktop or rack mount machines. Modern instruments now a days have potentiostat fabricated into compact devices like PCBs, gas monitors, medical devices, or wearables [226]. One of the examples of such devices is Emstat pico development board with dimensions of 90 x 65 mm (Fig. 5.1). This board is equipped with already tested, calibrated, and proved potentiostat, EmStat Pico [227]. EmStat Pico, is a miniaturized potentiostat with a size of 30.5 mm × 18 mm × 2.6 mm (Fig. 5.2). This device is fabricated using Analog Device technologies like ADuCM355, ADP166, ADT7420, and AD8606 [228]. It has the ability to be connected with microcontroller based system and when integrated with EmStat Pico development board provides additional fatalities like Bluetooth (BT900 module) for communication with Android phones and tablets, real-time clock (On-board IC: S-35390A-T8T1G) for time-stamping, EEprom for calibration data storage, USB connection to interface with a PC, a header for direct insertion of an Arduino MKR, battery power (CR1225 and 2x AAA, 3V) and SD card (8GB) for standalone operations.

Figure 5.2: EmStat pico potentiostat.

Moreover, this kit comes with standard sensor cable with 2 mm banana pins, croc clips and connectors for in house SPE integration [227]. The EmStat Pico Development board is provided with a free to use software named PSTrace [229]. This software enables user to perform measurements using your own electrochemical sensor such as SPE similar to standard lab potentiostat. The software PSTrace works with human readable script namely MethodSCRIPT. This language for scripting is developed in order to provide adaptability of potentiostat for Original Equipment Manufacturer (OEM) users. The script can be generated using PSTrace software or with your own customized software. Additionally, for low lever communication libraries are available for integration of potentiostat with another instrument [230]. The Emstat Pico Development board has two working modes: low-speed mode (up to 100 Hz) and high-speed mode (up to 200 kHz). In low-speed mode two potentiostat circuits are used simultaneously while in high-speed mode each channel is used alternately [228]. To facilitate POC applications the kit is provided with a battery saving mode and have a small footprint with 2.54 mm (100 mil) connections along with castellations for ease-of-integration into prototype systems. EmStat Pico development kit, is capable of performing several voltametric, amperometric and impedimetric techniques especially Cyclic Voltammetry (CV), Chronoamperometry (CA) and Electrochemical Impedance spectroscopy (EIS) used for characterization in this work [227].

Figure 5.3: Working prototype of handheld device with in-house biosensors connected to android tablet for electrochemical quantification of $CuSO_4$.

5.2 Transfer of technology towards portable microelectronics prototype development

The benchtop results obtained from electrochemical characterization performed using standard potentiostat in this work lined the way for development of miniaturized microelectronic handheld prototype for point-of-care application. The form factor microelectronic prototype was assembled using EmStat Pico Development (bi-potentiostat) board which provides all the functionalities of a standard lab potentiostat in miniaturized form. Fig. 5.3 displays the working prototype with in-house SPE. In order to evaluate the response of prototype the EmStat pico development board was powered using 2x AAA, 3V batteries and connected to android tablet via bluetooth connection using PStouch application to pass instructions for electrochemical characterization. The biosensors (bioelectrodes) prepared with immobilized *WT* cells on the surface of Zensor SPE were mounting on the prototype device and dipping in the electrolyte containing different concentrations of $CuSO_4$. CA was performed at 0.4 V for a period of 5000 s and output was stored in the form of .CSV files on the Tablet.

5.2.1 Numerical results and discussion

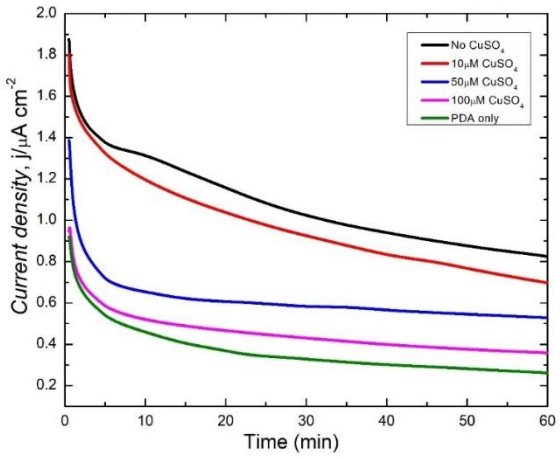

Figure 5.4: Amperometric i-t traces of SPE – yeast bioelectrode obtained from prototype with different concentrations of $CuSO_4$.

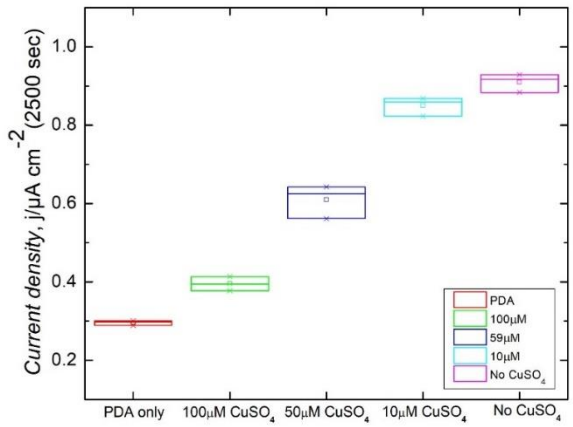

Figure 5.5: Box plot of current density values at 2500 s from chronoamperometric analysis of SPE – yeast bioelectrode obtained from prototype with different concentrations of $CuSO_4$.

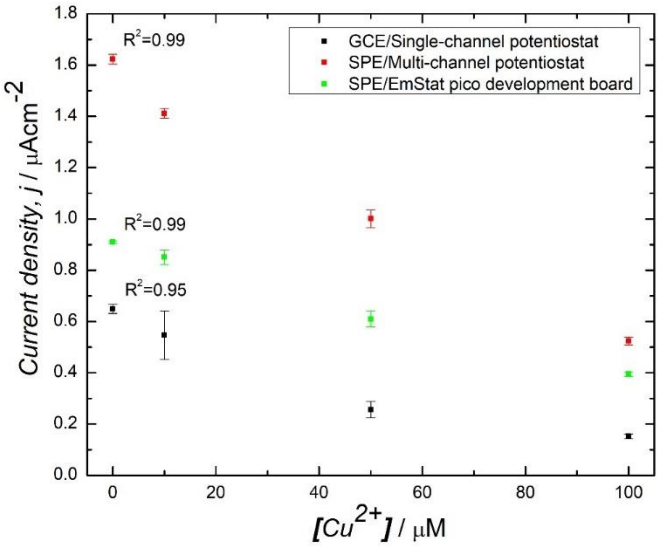

Figure 5.6: Relationship between $CuSO_4$ concentrations and current density during chronoamperometry at E_{APP}: +0.40 V for three cases. Error bars indicate one standard deviation.

The results obtained showed a dosage dependent inhibition in current density in the presence of different concentrations of $CuSO_4$ as in case of commercially available lab potentiostat. Figs. 5.4 and 5.5 display the i-t amperometric trace (3600 s) and box plot of current densities at 2500 s with different concentrations of $CuSO_4$, respectively. It can be observed that as the concentration of $CuSO_4$ increases the current densities keep on decreasing.

To further assess the response of the prototype in comparison with: GCE - yeast biosensors with single channel potentiostat (chapter 3) and SPE biosensor with multichannel potentiostat (chapter 4), the results of current densities obtained at 2500 s were analyzed and subjected to linear fitting to obtain calibration curve as shown in Fig 5.6. Then calibration curve data was used to calculate LoD, sensitivity and R^2 values and compared with previous cases. From Fig. 5.6 it was observed that the SPE based biosensors using prototype showed better current densities response in comparison with GCE based biosensors using single channel potentiostat evaluated in chapter 3. The improvement in signal is considered due to nature of electrode (SPE) that provides better immobilization and miniaturized prototype that has the ability for in house integration of biosensor, reducing the losses due to impedance.

Table 5.1: LoD, R^2, and sensitivity of bioelectrodes prepared by immobilization of *S. cerevisiae WT* strain cultured in YPD after 2500 s of incubation with different concentration of $CuSO_4$ (0, 10, 50, 100 µM) under aerobic conditions.

Name	LoD ($\mu MCuSO_4$)	R^2	Sensitivity ($*10^{-3}$ µA*cm^{-2}*L*µmol$^{-1}_{CuSO4}$)
SPE (multi-channel potentiostat)	2.2	0.998	10.9 ± 0.3
SPE (EmStat pico development board)	2.9	0.998	5.15 ± 0.1
GCE (Single channel potentiostat)	12.5	0.955	4.8 ± 0.6

However, SPE based biosensors using prototype displayed lower current densities response than SPE based biosensors using multichannel potentiostat discussed in chapter 4. The possible reason for lower current densities response in this case can be the absence of redox mediator. Table 5.1 shows the LoD, R^2 and sensitivity obtained for three different experimental setups used during this work. It can be observed that the biosensors evaluated with prototype display similar LoD and R^2 as in case of multichannel potentiostat with a lower sensitivity and better response in comparison to GCE biosensors with single channel potentiostat.

5.3 Web application

5.3.1 State of the art

To perform real-time, online monitoring of the data gathered by the prototype device, a web application has been developed. The decision of developing web application relies on the fact that a web application is platform independent and can be easily accessed via browser by any device (mobile phone, tablet, desktop computer) compared to a mobile application that is OS dependent. The application is developed by using Python Flask for the web server and Google's Firebase for the remote data storage [231]. Flask is a Python open-source micro-framework having a simple and high-performance core that provides fundamental features such as development server and debugger, routing, integrated unit testing support, protection against cross-site scripting (XSS) and the use of Jinja 2 as a template engine [232, 233]. Unlike full stack web frameworks such as Django [234], Flask does not include, for example, a database API, an authentication, upload, or form validation system: this type of functionality is included in a web app site written with Flask through the use of dedicated extensions, which once integrated into the project can be used easily as if they were part of the framework itself. Google's Firebase is a serverless platform for developing mobile and web applications. It is open source but supported by Google, leveraging Google's infrastructure and its cloud well suited for writing, analyzing, and maintaining cross-platform applications. In fact, Firebase offers features such as analytics, databases (using noSQL structures), messaging and crash reporting for managing web, iOS and Android applications. In this scenario, a real-time database will be used to host sensors' data. Moreover, the key-value paradigm of firebase makes it suitable to interact with a Python-based application that makes use of dictionary data structures [231].

5.3.2 Software architecture and working

Fig. 5.7. shows the schematic diagram of complete system architecture. The whole software architecture is composed of 3 different layers: user interface (UI) layer, logic layer and data layer. In the following sections, each part of the system will be described in detail.

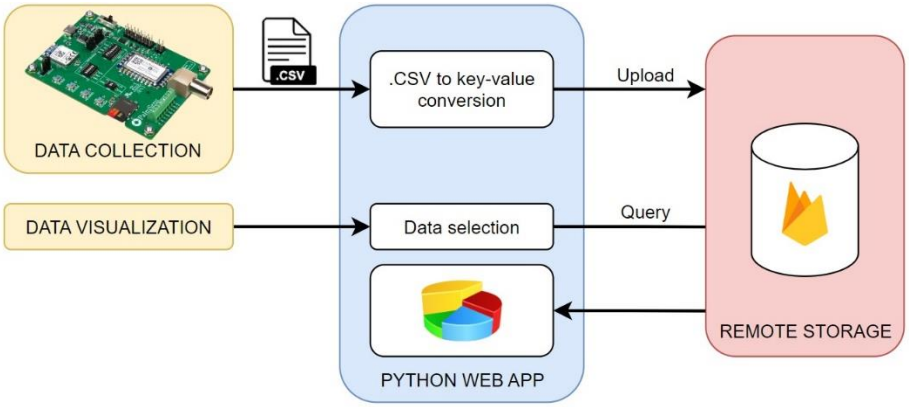

Figure 5.7: Block diagram of complete system architecture.

5.3.2.1 User Interface Layer

The User Interface comprises 2 different HTML pages: an index page and a data visualization page. Whenever the user accesses the index page, 2 different sections are shown as shown in Fig. 5.8. The first section allows uploading new files to the remote Firebase storage. The system requires all data to be structured into .csv files (coming from the Emstat PICO development board). Thus, the web interface allows to navigate through the filesystem and select the .csv file the user needs to upload. Once a file is selected, the upload button starts a routine to convert .csv format into key-value format.

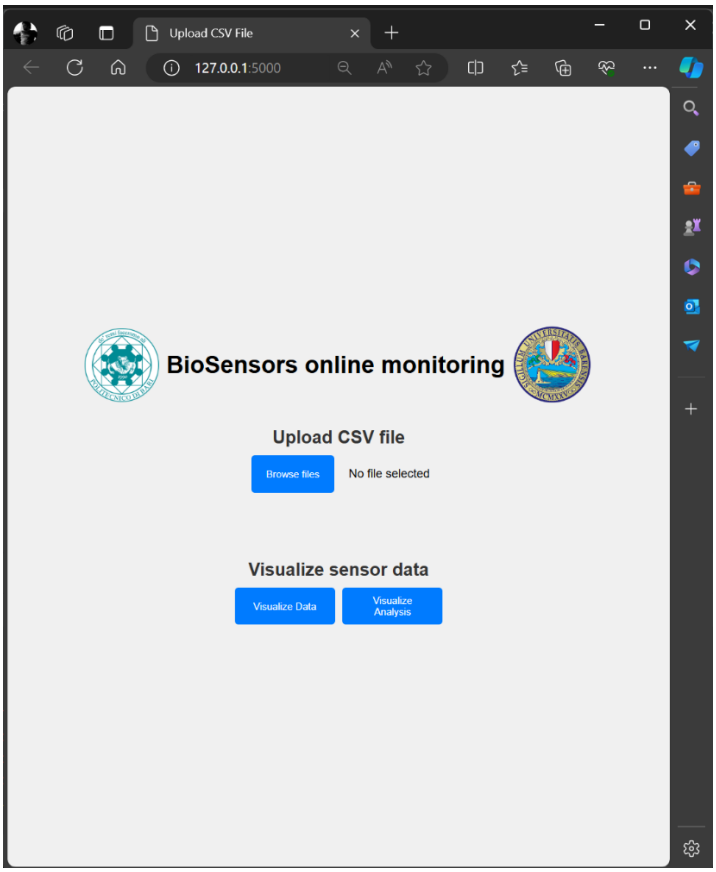

Figure 5.8: Display of index page of web application.

The whole backend logic is developed in python language, so behind the curtains of this process, there is a python method that creates a list containing all the current values from the file and, after converting all the values to current density, pushes the data into the real-time database. To do so, a new key is created in the database root, having the name of the file the user chose to upload. All current density data is then stored as a single value associated with the key, in order to speed up the process (saving each value as a new value in the db would slow down the system performance). Thus, once all data is uploaded, it can be retrieved via file name. The second section of the index web page allows data selection for online charts displaying. The "Visualize Data" and the "Visualize Analysis" buttons allow to display current density per unit time curves and a plot displaying concentration of $CuSO_4$ in each .csc based on current density values obtained from sample CA data, respectively as shown in Fig. 5.8.

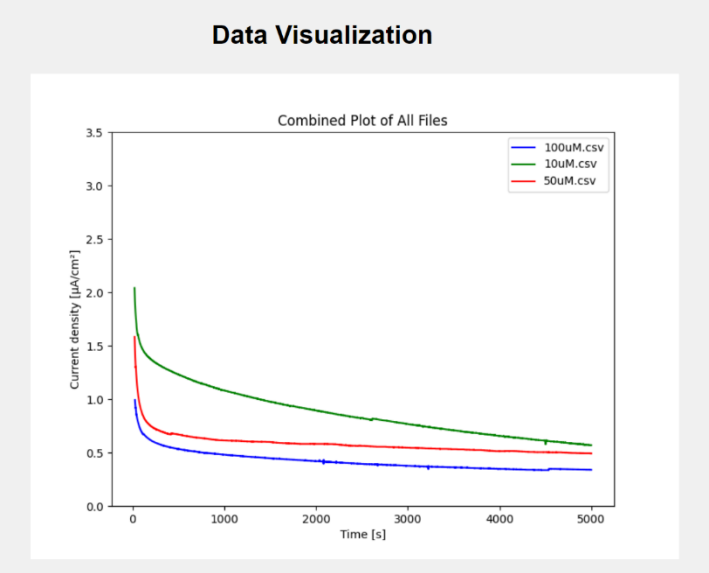

Figure 5.9: Display of data visualization page of web application showing i – t trace.

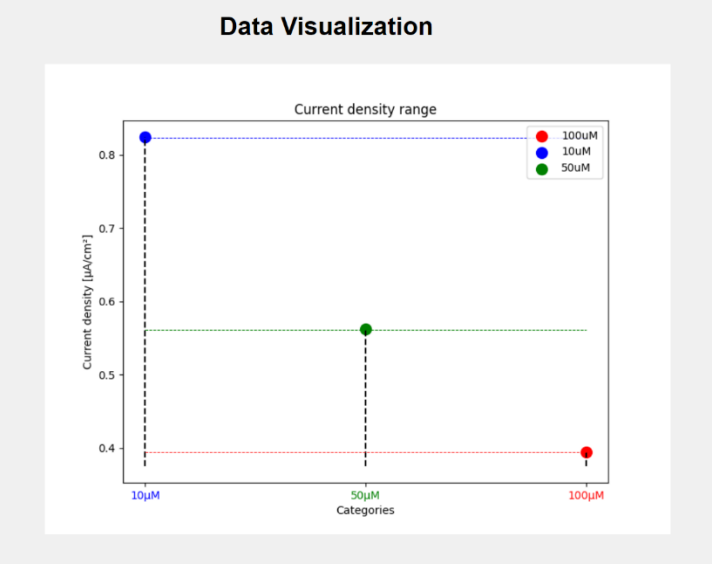

Figure 5.10: Display of data visualization page of web application showing classification of sample into different categories based on current density values at 2500 s of CA data.

When clicking both buttons, a JavaScript function is employed to retrieve all file names from the remote database. These are used to prompt a list of checkboxes where the user can select only the files to visualize and compare. Once the user has performed its selection, the buttons "Visualize Selected Data" or "Visualize Data Analysis" allows to redirect the user to the data visualization page. This page finally shows the graphs of sensors data as shown in Figs. 5.9 and 5.10.

5.3.2.2 Logic Layer

The backend logic of the whole web application is developed using the Python programming language. More specifically, the flask library allows you to associate a specific python method to each page, that is usually executed before rendering. The logic is therefore contained in a single python script where different methods handle all users' requests. This block does not only handle the web visualization, but also bridges the gap between the web server and the remote Firebase. The first step when loading the application is therefore to load all necessary authentication files to establish the connection with the remote database. This is done via the firebase_admin library: a suite of python methods to easily interact with a Firebase remote database. All different methods handling the logic are:

- Data uploading: the .csv file to be uploaded is opened and read row by row using the pandas library. All data is then concatenated into a single string having all values separated by a "/" symbol (again, for speed requirements). A file name key is finally created into the database a the string is finally stored as value.
- File retrieving: when the user needs to select data to be displayed, a JavaScript function creates a drop-down checklist with all the filename keys contained in the database. Behind the curtains, a python function is retrieving all the keys from the firebase and passing all the values back to the JS. This finally creates the selection list.
- Charts creation and data visualization: after creating the selection list, another JS function collects all file names selected by the user and starts the data visualization process. Specifically, this function passes all the file keys to the Python backend logic. The latter are used to retrieve from the realtime database all the values associated with each. During this process, all current values are retrieved from the unique string created during the data uploading process and converted to current density values. When all data from all files is gathered, it is time to create the final charts to be displayed. The matplotlib python library is used to create the plots. Two different functions have been created to differentiate whether the user want to visualize the current density curves over time or a box plot representing the current density distribution. In the first case, for each filename, all current density values are stored in a list. Once all lists are ready, a cumulative plot is created by overlapping the current density curves from all the selected files. In the second case instead, for each file, only the current density values corresponding to time instance 2500 (s) is collected. A scatterplot is finally created, by plotting a point for each file's current value. To display the charts, the base64 python library is used. This is a necessary step because matplotlib.pyplot is meant to display the generated plot in a dedicated GUI window. In this case instead, it is necessary to save these plots as standalone images and visualize them on the html page. To do so, the technique is to avoid calling the matplot displaying function. The final image is instead retrieved from the IO buffer that is created when matplot savefig() method was called. base64 is finally used to decode all image data from the buffer. This data is finally passed to the data visualization page that displays the plots.

5.3.2.3 Data Layer

The data layer is built on top of Google's Firebase. This publicly accessible database makes it possible to access the data of web applications from all over the world. The database structure is composed of a single root value called "/data", under which all files are saved as children nodes. The database interacts with the python flask application that handles all the CRUD (create, read, update and delete) functions. To do so, the firebase_admin library is used on the python side while the database rules are set to open to allow python to interact with it. Moreover, the web app is required to use an authentication file to have the rights to perform changes on the database. This consists of a json certificate that travels together with the source code of the application (without this file, the web app will no more be able to perform changes on the db).

5.3.3 Performance Assessment and discussion

In order to test the performance of web application, the .csv from the electrochemical experiments with known concentration of copper (10, 50, 100 μM) were uploaded and analyzed. The application was found to efficiently plot current density per unit time curves along with correct detection of concentrations of copper. Figs. 5.9 and 5.10 show the results obtained from analysis using a web application. It is worth mentioning here that, the application assign categories to sample data based on steady state current density at 2500 (s) by comparing it with values obtained from standard laboratory equipment. Moreover, initially the application is designed to classify the samples in three different concentration categories (10, 50, 100 μM) due to unavailability of standard data. However, the development of web applications and availability of prototype provides a way for point-of-cure applications of developed biosensors. Despite that, there is need for improvement in selectivity and selectivity of biosensors for analyte specific, repeatable and multiparametric sensing along with integration of prototype device with communication systems for standalone real-time remote operation. Therefore, the developed electrochemical yeast-based biosensors have significant potential for real-world applications and commercialization. By enabling rapid, low-cost, and on-site detection of analytes such as copper, these biosensors offer a substantial improvement over traditional methods, which often require complex, time-consuming, and costly procedures. In the context of PA, these biosensors can be employed to monitor soil and irrigation water in real-time, allowing farmers to make informed decisions regarding fertilization and pesticide use, thereby enhancing crop yields and reducing environmental impact. This capability is crucial for achieving sustainable agricultural practices and optimizing resource utilization. Moreover, the commercialization prospects for these biosensors are also promising due to their ease of miniaturization and integration with IoT technologies. The development of a handheld, low-power prototype device that can be operated via common consumer electronics such as smartphones and tablets broadens the potential user base, making advanced agricultural monitoring accessible to farmers of varying scales and technological expertise. Additionally, the inclusion of a Python-based web application for data visualization and analysis enhances the usability and appeal of the system, offering an integrated solution for data management and decision support. Moreover, the scalability of production and the robustness of yeast as a biorecognition element add to the commercial viability of these biosensors. Yeast cells, particularly S. cerevisiae, are easy to culture and maintain, making the biosensors cost-effective. The ability to produce these sensors in large batches may further reduces costs and allows for widespread adoption. The biosensors' versatility extends beyond agriculture, with potential applications in biomedical, industrial, and environmental monitoring, broadening their market potential. Overall, the integration of advanced biosensor technology with user-friendly, data-driven tools positions these devices as a transformative solution for modern agriculture and beyond.

Chapter 6

DESIGN AND CHARACTERIZATION OF MATLAB BASED APPLICATION FOR SPOTTING ASSAY QUANTIFICATION

6.1 State of the art

Evaluation of survival and growth is a crucial criterion applied in cell biology research. In micro-organisms, this can be achieved by the assessment of growth on both liquid and solid media. Specifically, the growth of cells from microorganisms, such as yeast and bacteria on solid media provide the same conditions as of real world environment [235]. Thus, evaluation of size and counting of colony provide a valid assessment by replicating real environmental conditions and acceptable for both low and high-throughput assessments for evaluation of cell fitness investigation scenarios [236-239]. Many different type of software have been developed for quantitative analysis of colony growth in yeast, such as ImageJ [240], Spotsizer [241], CellProfiler (a multi-purpose image analysis tool) [242], YeastXtract [243], HT Colony Grid Analyzer [244], Colonyzer [245], ScreenMill (an ImageJ macro) [246], Balony [247], SGAtools (web-based) [248] and gitter (R package) [249]. These software's use different criterions like definition of manual selection of radius of area to be quantified, generation of growth time relationship curve using size of colony, colony area/ colony size versus volume (i.e., integration of intensity obtained from each pixel) or use of manually prepared replica-plated arrays having bigger colonies versus robot arrays with small colonies [240-249]. However, some of these platforms do not provide user defined colony size and grid support [241, 243-249]. Other tools function with restricted image file formats and resolution, require specific equipment's for acquiring images and their results are dependent on environmental factors such as distortions introduced by imager/camera [240, 243-245, 247-249]. Moreover, the implementation of these platforms is technically challenging and/or use specific skills like programming without provision of graphical user interface (GUI) making their use to be limited by wet-lab researchers [240, 245, 249].

In this part of the work, we developed a dedicated platform using Matlab for quantification of yeast growth on solid media from analysis of spotting assay images. Spot plating assay is a classic method to assess growth of yeast in low-throughput laboratory settings, along with growth on different nutrient sources or treatment with specific stressors. Our platform was inspired by the image J-based method presented in Petropavlovskiy et al. (2020), providing an advancement to their protocol [240]. The developed Matlab application has the advantages of easy installation process, user friendly GUI with built-in image processing, provides selection of size of the spot, simple analysis steps, visual display of selected spots while providing the option to save the data as .jpg and .text file. The tool was tested with experimental data obtained in our laboratory from spotting assay experiments of *Saccharomyces cerevisiae* yeast cells exposed to osmotic stress, but it can be easily applied to any stress condition. Further validation has been performed by analyzing the same images with ImageJ software and comparison of results obtained from both tools.

6.2 Application overview

Spotting Assay Quantification (GUI) has been developed using MATLAB source code and is uploaded for download under BSD license (Berkeley Source Distribution), which provide Open-Source Software licenses with minimum restrictions from the MathWorks website [250]: our app is available for Windows, MacOs, and Linux. The App use already-developed method for quantification of spotting assay able to effectively process crowded cells and its adoptable design allows quantification of different conditions and phenotypes. It provides self-explanatory graphical interface with the benefit of shorter analysis steps generally absent in

most image analysis software (Fig. 6.1). Therefore, spot size can be quantified following few easy steps. The algorithm is developed to show quantification value and spots images. A brief comparison of available software platforms, including our Matlab based app, for yeast growth quantification on agar plate are presented in Table 6.1. Most prominent parameters like the file format, the defined grid and colony size, and the procedure for image acquisition have been compared. The absence of one or more of these limiting factors is considered as a bottleneck in analysis of colony size for wet lab researchers. Flexibility in image acquisition and file format: help reduce the need for dedicated instrumentation. User defined grid support and flexible size of colony: users can decide variable grids and sample size following their need aside from the conventional configurations resulting in simpler experimental setup. Operating systems and interface: provision of application for multiple operating system and availability of graphic user interface (GUI) provides flexibility to laboratory workers with no or minimum expertise in software installation as well as handling. The application developed in this work includes all the features mentioned in table while keeping the quantification results comparable to previously developed tool.

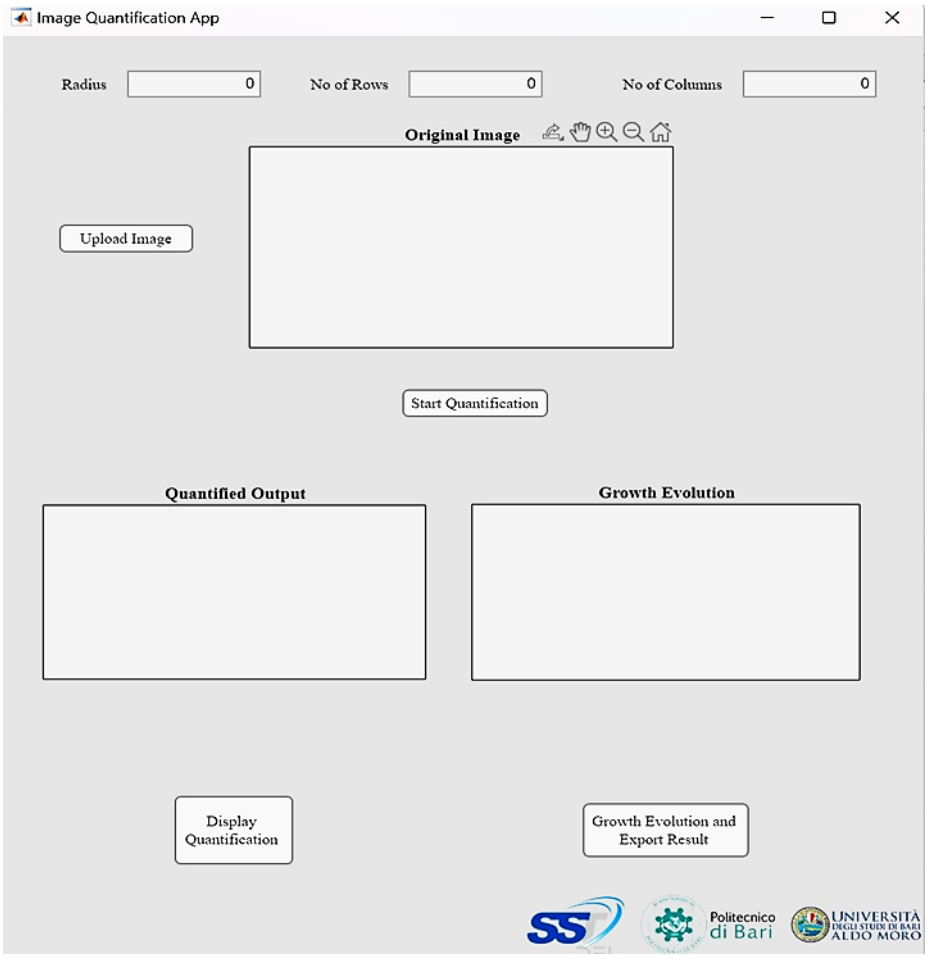

Figure 6.1: Display of Matlab-App interface for quantification of spotting assay.

Table 6.1: Comparison of available software tools for yeast growth quantification on agar plate.

Tool name	User defined grid	File format (JPEG/PNG)	User defined colony size	All operating systems	GUI	Flexible image acquisition	Ref
Spotting Assay Quantification	✓	✓	✓	✓	✓	✓	**Current study**
ImageJ	✓	×	✓	✓	×	✓	[240]
Spotsizer	×	✓	×	✓	✓	×	[241]
Balony	✓	×	×	✓	✓	×	[247]
CellProfiler	✓	✓	✓	✓	✓	×	[242]
Colonyzer	×	×	×	✓	×	×	[245]
Gitter	×	×	×	✓	×	×	[249]
HT Colony Grid Analyzer	×	×	×	✓	✓	×	[244]
ScreenMill	×	✓	×	✓	✓	×	[246]
SGAtools	×	×	×	✓	✓	×	[248]
YeastXtract	✓	×	×	✓	✓	×	[243]

6.3 The workflow of the algorithm

Fig. 6.2 shows the workflow of the algorithm used for development of Matlab based application. There are six basic steps used for quantification of images such as input, image processing, circular mask, thresholding, quantification of spot size and output (Fig. 6.2).

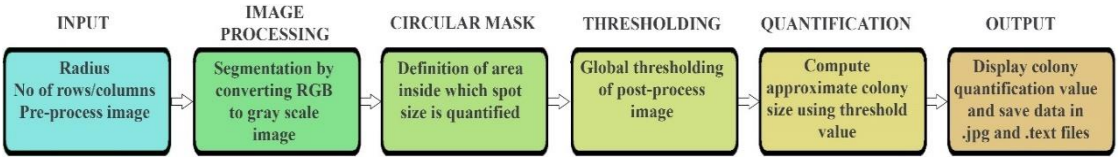

Figure 6.2: Flowchart diagram of Matlab-based algorithm for yeast growth quantification.

6.3.1 Input

The algorithm for quantification of images from spotting assay starts with input of the three variables: image of desired plate, number of rows/columns and radius. The application is developed such that it let user to choose area of Circular Mask (see section below) by manual input of radius. The user can input number of rows/columns (grid) of spots on the plate at the start of every quantification. This option is provided in the app to work with arbitrarily placed but equal volume of spots. After the selection of radius, the area of mask is fixed for the whole analysis. In the next step user selects the image and select the cultures spot by clicking in the centre of each spot on the plate under consideration. This helps accurate recognition of all colonies in image as visual investigation and manual selection is available.

6.3.2 Image acquisition/processing

Current application is designed to adopt images obtained from any acquisition such as mobile camera or dedicated instruments like gel imager ChemiDoc that output images in .jpg format. Adjustment of discrepancies in illumination plays a pivotal role in image analysis. Thus, in this application this aspect is addressed using standard method for correction in variations of illumination in acquired images. Plate images are segmented using white/black thresholding by converting the true colour image `RGB` to the grayscale image into colony area/background.

Matlab built-in *rgb2grey* function is used for transformation of standard images to grayscale by retaining the luminance and removing saturation and hue information. For further improvement, *double* function is used to add precision to the image. This method was used to improve the luminance of images under consideration as raw image intensity quantification may alter accurate analysis.

6.3.3 Circular Mask

Circular Mask is defined as the area within which spot size is analyzed based on the threshold value. The definition of mask is one of the most critical steps in quantification of spot size. The size of circular mask area is based on the radius that is chosen in the start of analysis. This concept is introduced as this method supports quantification of spots of your choice based on their size and discard irrelevant spots that are due to contamination. The size of masked area cannot be changed during one analysis, it is recommended to choose the size of masked area equal to or a little bigger than the biggest spot on the plate. It is important to state that the masked area (radius of area to be analyzed) is set before each quantification and maybe changed based on the experimental conditions.

6.3.4 Thresholding

In this step, each pixel of the image is compared with a predefined grey value, pixels are changed to black/white for separation of background from the yeast colonies on agar plate, this procedure is known as “thresholding”. The images are saved at an eight bits per pixel color depth, having a value between 0 and 255. An image from 3-D or 2-D grayscale image is generated by changing all values above a threshold with 1s and converting other values to 0s. We implemented Otsu's method using Matlab built-in command *imbinarize*. During this step, a “criterion function” is generated that ensures a clear separation between different regions. Otsu's method instinctively formulates restricting of a grayscale image to a binary or image clustering-based image thresholding. The algorithm considers backing bi-modal histogram (background pixels and foreground pixels) ensuring two classes of pixels; it then generates the optimum threshold that not only disconnects the classes but also keep the overall spread to a minimum value.

6.3.5 Quantification of spot size

The colony growth on plate is quantified as a function of spot sizes by analyzing all pixels within the masked area. When the quantification is started, the user is allowed to select the spot that is under consideration. When a spot is selected by clicking, the algorithm generates a masked area around the point of selection and compares the grey value of every pixel within the masked area with the threshold value. This app assumes that the intensity of the pixels of the area covered by each colony on each spot have higher values than the surrounding area. Every pixel above the threshold value is graded 1 and the other values are graded 0. The percentage of number of pixels having 1s compared to 0s in the total masked area is displayed as the size of spot in terms of numerical values.

6.3.6 Output

After all the spots are quantified, the app provides a graph, displaying the trend of growth treated, the numerical data saved in the form of simple table in a text file and cumulative image of spots analyzed in .jpg format.

6.4 Quantification of cell growth by Matlab application

Here we describe detailed steps for acquiring "Spotting Assay Quantification (GUI)" app and quantification of images obtained from spotting assay. Description of app is also available on YouTube at: https://youtu.be/7rCEfoEHrdw

(1) Open Matlab, go to "APPS" tab and click on "Get more apps". In the new window titled "Add-On Explorer" search by using keyword "Spotting Assay Quantification (GUI)". The App will appear in the drop-down menu, click on the App which takes us to app home page. Go to top right corner and click on "Add", accept the license and the App will automatically be added in the apps store of Matlab.
(2) Navigate the current directory of Matlab to the folder in which you have placed the image for analysis.
(3) Go to App store of Matlab and click on Spotting Assay Quantification application. App will open as shown in Fig. 6.1.
(4) Enter the radius size of the spot, number of rows and number of columns in the boxes in front of each section.
(5) Click upload image and select the image to be analyzed from the folder. The image will appear in the box in front of the "upload image" button.
(6) Click the start quantification button. A selection window appears showing input spotting assay image and a pointer. Drag the pointer to the center of the first spot of first row and left click. Similarly, click in the center of all the spots one after the other in all rows from left to right.
(7) When all spots are analyzed, three windows will appear: the first with the original image; the second with quantified values of each spot and the third with growth evolution graph.
(8) Click on display quantification to visualize quantified spots and values, in app display above display button.
(9) Click growth evolution and export results button for in app display of growth evolution graph and to save images in .jpeg format and quantification values in the form of a .text file in parent folder.
(10) Repeat steps 4 to 9 for the images of all other plates (that is, biological replicates).

The selection of value of radius must be kept same to perform analytical quantification in one experiment. Variation of radius may result in false quantification. Choice the radius of circle should be made such that the size of masked area is equal to the size of largest spot on the plate. In order to select appropriate size of radius for one experiment, multiple arbitrary radius values can be tried by selecting one row and one column prior to actual analysis. Select the largest spot on the image in the selection window and check if the masked area covers the whole spot. If not, change the radius accordingly.

6.5 Experimental design

6.5.1 Yeast strains and media

Two strains of the budding yeast *Saccharomyces cerevisiae* were used in this study: W303-1B wild type (*WT*) (MATα ade2 leu2 his3 trp1 ura3) and its derivative Δ*rtg2* (rtg2Δ::LEU2). Cells were grown at 30 °C with shaking (180 rpm) in YPD medium (1% yeast extract, 2% bactopeptone [Gibco, Life Technologies, Waltham, MA, USA]) and 2% glucose [Sigma-Aldrich, St. Louis, MO, USA]. For spotting assay, cell growth was performed on YPD medium with 2% agar (Invitrogen, Life Technologies Waltham, MA, USA) in the absence or presence of 0.4 and 0.8 M sodium chloride (NaCl). Optical density (600nm) was used to monitor cell growth in shaking flasks.

6.5.2 Spotting Assay

Spotting assay was performed as described by Guaragnella et al. (2021) [251]. Briefly, the optical density (OD_{600}) of overnight yeast cultures (30 °C, YPD medium, 180 rpm) was adjusted to OD_{600} = 1.0. Under sterile conditions, 5 uL of 1:10 serial dilutions were carefully spotted by using micropipette on YPD ± NaCl agar plates placed on a grid. The spotted plates were incubated at 30 °C for 2 days and plate images were taken every 24 h using ChemiDoc™ Touch Imaging System.

6.5.3 Data Analyses

All data are presented as mean ± standard deviation. All the experiments were performed with a minimum of three technical and biological replicates. The data were analyzed using one way ANOVA followed by Tukey's post hoc test to determine differences between and within groups. The data were analyzed using Microsoft Excel software, values of $p \leq 0.05$ (ANOVA-alpha) were considered significant. Since all the spots are quantified by the app, it is necessary to select a single dilution across the strains for data analysis. This should be the lowest dilution that shows distinct colonies. In the present study, the third dilution satisfied this condition (Fig. 6.3). Researchers should choose appropriate dilution based on the experimental conditions. The data obtained from the quantification was normalized by dividing the value of each spot from the test group (stressed cells) by the corresponding control at the same dilution.

6.6 Numerical results and discussion

To validate our Matlab application, we spotted replicates of *Saccharomyces cerevisiae* wild-type and mutant yeast strain lacking the *RTG2* gene on distinct agar plates with and without presence of mild (0.4 M NaCl) and high (0.8 M NaCl) salt stress. Results reported from distinct plates in Fig. 6.3 show an expected inverse correlation between cell growth and NaCl concentrations for both *WT* and *Δrtg2* cells. However, a higher sensitivity with respect to WT was observed in the mutant when comparing the same concentration of stressor. This agreed with previously reported data [251-253]. Images and values from spotting assay quantification are reported on top of each spot in Fig. 6.4.

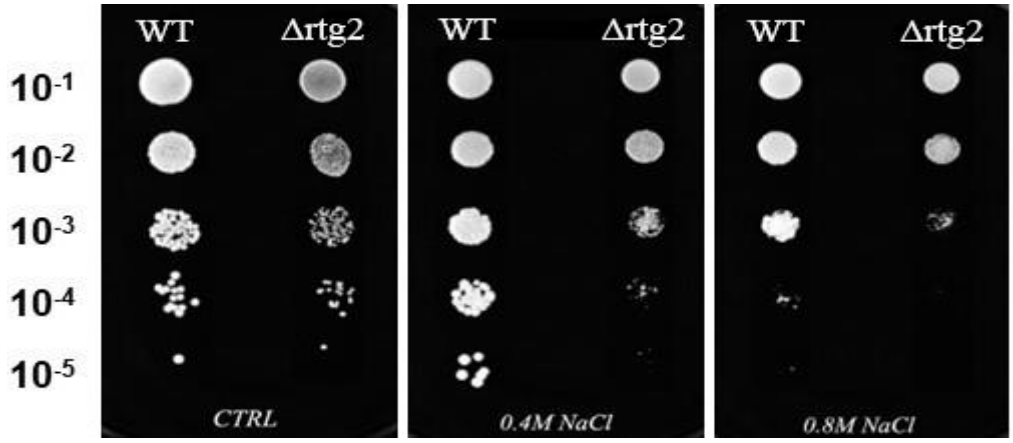

Figure 6.3: Effect of Sodium chloride on growth of *wild type* and *Δrtg2* cells. Wild type (*WT*) and RTG2-lacking cells (*Δrtg2*) were grown overnight in YPD medium and diluted to 1.0 OD_{600}. Ten-fold serial dilutions were spotted on YPD agar plates without (CTRL) or with 0.4 and 0.8 M sodium chloride (NaCl). Cell growth was analyzed after 2 days of incubation at 30°C. Images were acquired by ChemiDoc Touch Imaging System.

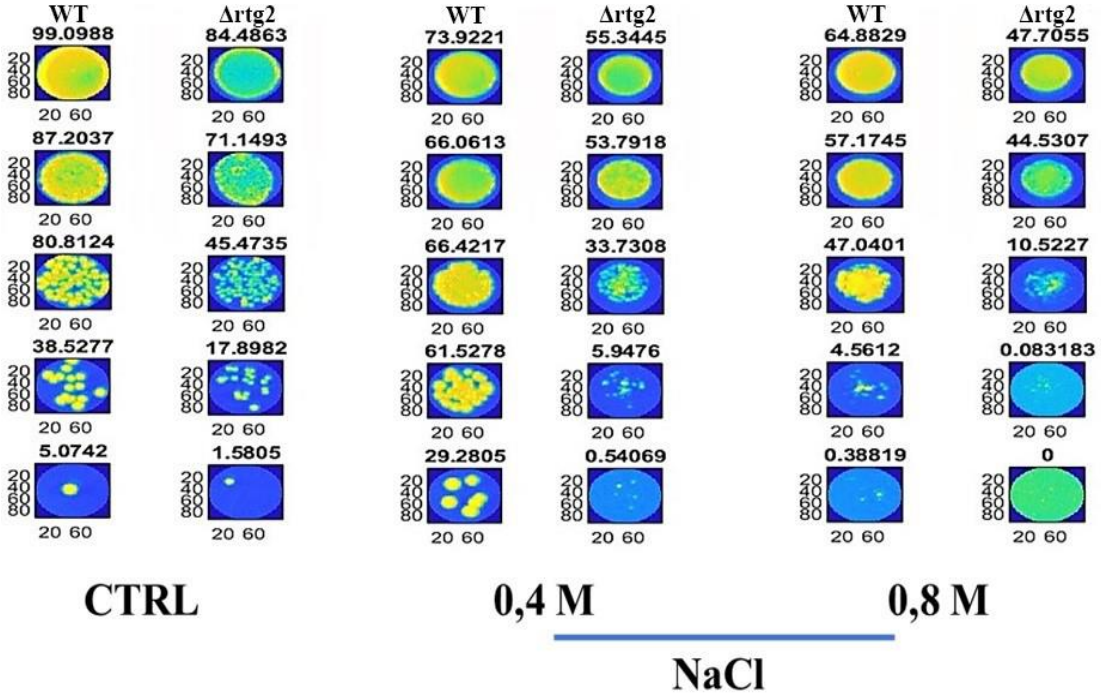

Figure 6.4: Spotting assay quantification. Masked area and numerical results from quantification process on wild type (*WT*) and RTG2-lacking strain (*Δrtg2*) with and without NaCl stress at the indicated concentrations using Spotting Assay Quantification (GUI).

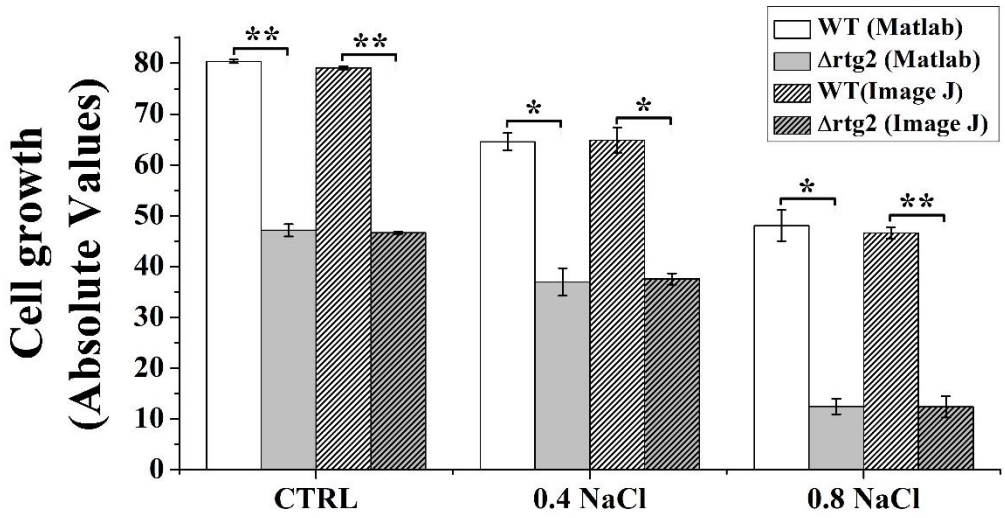

Figure 6.5: Cell growth of wild-type (*WT*) and RTG2-lacking strain (*Δrtg2*) using Matlab app and image J-based protocols. The third dilution on plate was selected to calculate absolute values. Average of three independent experiments is reported, $p < 0.05$ (ANOVA-alpha) is significant, *$p < 0.0001$ and ** $p < 0.00001$.

Table 6.2: Average quantification values and growth inhibition calculated via Matlab app or Image J protocol. Average quantification values were determined via Matlab app or Image J protocol and relative growth of control cells was set as 100%. Growth inhibition (GI) was calculated by measuring relative growth of stressed cells (exposed to 0.4 or 0.8 M NaCl) with respect to control and then subtracting to the value of 100.

Sample	CTRL	0.4 NaCl	0.8 NaCl	GI (%) 0.4 NaCl	GI (%) 0.8 NaCl
WT (Matlab-app)	80.4 ± 0.32	64.6 ± 1.71	48.1 ± 3.02	19.7	40.2
WT (imageJ)	47.1 ± 1.19	37 ± 2.71	12.5 ± 1.54	18.0	41.1
Δrtg2 (Matlab-app)	79.1 ± 0.31	64.9 ± 2.45	46.6 ± 1.13	21.5	73.6
Δrtg2 (imageJ)	46.7 ± 0.24	37.6 ± 1.11	12.4 ± 2.10	19.5	73.4

The values of quantification decreased proportionally in the serial dilutions, with lowest growth value observed for the highest dilution and vice versa. At the third dilution, Δ*rtg2* strain CTRL (non-treated cells), 0.4 and 0.8 M NaCl (treated cells) displayed a relative growth inhibition of 41%, 42% and 74% in comparison with WT strain CTRL, 0.4 and 0.8 M NaCl, respectively Fig. 6.5. Moreover, individual analysis of WT strain 0.4 and 0.8 M NaCl with respect to WT CTRL displayed relative growth inhibition of almost 20% and 40% in the presence of 0.4 M and 0.8 M NaCl, respectively. Conversely, 0.4 and 0.8 M NaCl inhibited the growth of Δ*rtg2* strain with respect to Δrtg2 CTRL by almost 22 and 74%, respectively (Table 6.2).
In *Saccharomyces cerevisiae*, mitochondrial RTG-dependent retrograde signaling plays an important role in yeast stress response and cellular adaptation under various environmental conditions [252, 254-256] . In particular, it has been shown that deletion of *RTG2*, the upstream positive regulator of RTG pathway, sensitized yeast cells to osmostress downstream of the mitogen-activated protein kinase Hog1 [251, 253]. These quantification results with growth inhibition for the different groups show that *RTG2*, the main upstream regulator of the RTG pathway, showed higher sensitivity to NaCl stress compared to wild type. This result revalidates the contribution of RTG pathway to osmoadaptation, as previously reported in both solid and liquid medium [251, 253]. Increasing sodium chloride concentration cause a proportional growth inhibition in both *WT* and Δ*rtg2* strains. Spotting assay quantification from replicates and separate experiments showed notable differences in growth between mild and high NaCl stress in the two strains, revealing subtle difference between the two strains when the same concentration was considered for the control and "stressed" groups as stated above (Fig. 6.5). It must be noted here that the developed method quantifies average growth present in a selected area unlike existing methods [241, 242]. Abnormal growth of colonies can perplex the results. So, after obtaining the results, researchers using our method should double check that the obtained results correspond to images. Moreover, the platform only provides insight about survival and growth, but it does not provide information about the mechanism of toxicity or genetic alteration in certain growth environments. For such studies, cell death staining and individual colony counting techniques can be considered [257, 258]. Matlab app was further verified by comparison of results with the ones acquired by the quantification of the same spotting images using ImageJ software (Fig. 6.6) [6]. In this case, Δ*rtg2* strain CTRL, 0.4 and 0.8 M NaCl samples displayed a relative growth inhibition of 41%, 42% and 73% in comparison with *WT* strain CTRL, 0.4 and 0.8 M NaCl, respectively (Fig. 6.5). In addition, the *WT* strain showed a relative growth inhibition of 18% and 41% in the presence of 0.4 M and 0.8 M NaCl with respect to *WT* CTRL, respectively. Conversely, 0.4 and 0.8 M NaCl inhibited the growth of Δ*rtg2* strain by 20 and 73% with respect to *Δrtg2* CTRL, respectively (Table 6.2).

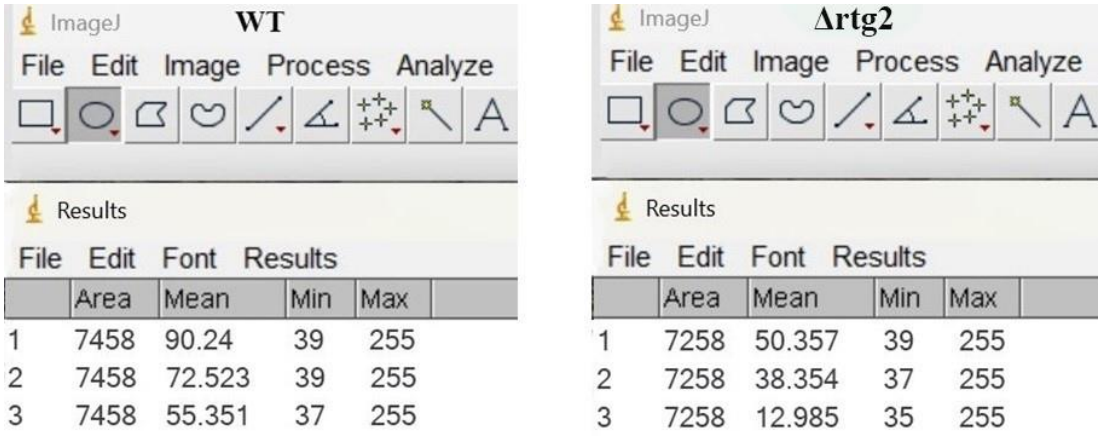

Figure 6.6: Numerical results from wild type (*WT*) and RTG2-lacking strain (*Δrtg2*) without and with NaCl stress using ImageJ software. In both panels (*WT* and *Δrtg2*), 1, 2 and 3 were referred to control cells, 0.4 and 0.8 M NaCl treated cells, respectively. The mean of each sample corresponded to the numerical results calculated using ImageJ protocol [240].

The similarity in results with previous experimental data obtained for liquid cultures and similar established methods proves the effectiveness of our method [240, 251]. The average quantification values calculated with Matlab app and Image J-based protocol were comparable in terms of relative growth for both WT and mutant as reported in Table 2. However, by comparing the two methodologies, the Matlab app provides several advantages, such as an interactive GUI, lower variations in quantification values due to fixed size of the spot and shorter quantification steps.

Chapter 7

CONCLUSION AND FUTURE PROSPECTIVES

7.1 Conclusions

Electrochemical yeast-based biosensors offer a promising alternative to conventional sensing technologies used for detection of analytes in biomedical, industrial, environmental, and especially PA applications due to nature of biorecognition element and flexibility of developing miniaturized devices for rapid, low power and point-of-cure applications. This thesis describes the design and characterization of yeast based electrochemical biosensors developed for detection of copper with the final aim to be implemented in PA. The main outcomes of this research are briefly summarized in the following paragraphs.

- A growth analysis of *WT S. cerevisiae* cells has been designed and analyzed through experimental setup in the presence of copper using standard optical detection (UV spectroscopy). The results indicated that optical detection cannot detect low concentration of copper (0 – 1 mM) and significant response is only observed at higher concentration (5 mM or above) of copper after incubation of 4 h.
- Immobilization protocols using PDA have been designed and characterized to attached biorecognition element with the transducer surface. Our proposed matrix not only provides cell immobilization but also facilitates extracellular electron transfer while keeping the biorecognition element viable.
- A bioelectrode acting as biosensor that includes immobilized *WT* yeast cells on the surface of GCE has been designed and characterized to detect copper. The biosensor is capable of electrochemical detection of copper at low concentrations (20 – 100 µM) in 2500 s with a LoD = 12.5 µM, $R^2 = 0.956$ and $4.8 \pm 0.6 \times 10^{-3}$ $\mu A*cm^{-2}*L*\mu mol^{-1}_{CuSO4}$ showing its superiority over standard optical detection. Although an R^2 of 0.956 is achieved, the results are considered promising because the system is yet to be optimized.
- With the aim to optimize biosensors response, multiple biosensors using SPE and immobilized yeast strain *WT* with different metabolic (fermentable and non-fermentable carbon sources in growth media) and respiratory (using Δ*hap4* and Δ*rtg2*) manipulations are designed and characterized. The SPE based biosensors developed with metabolic and respiratory approaches improved overall response as an LoD of 2.2 µM and lower is observed in some cases. Although an A LoD of 1.1 µM has also been achieved but R^2 worsens in such cases. Therefore, the overall best results is considered to be obtained with biosensors prepared using *WT* cells (cultured in standard media) immobilized on SPE with LoD = 2.2 µM, $R^2 = 0.998$ and sensitivity of $10.9 \pm 0.3 \times 10^{-3}$ $\mu A*cm^{-2}*L*\mu mol^{-1}_{CuSO4}$.
- A handheld prototype device using Emstat pico development board capable of in-house mounting of SPE based biosensors prepared in this work is assembled and presented for low power, rapid and point-of-cure detection of copper. The prototype is able to function standalone or the instructions can be passed using any Android, windows, or iOS device such as mobile phones, tablets, PC etc via Bluetooth/ USB connection. The prototype is tested using biosensors prepared by immobilizing WT cells on the surface of SPE in the presence of copper and an LoD of 2.9 µM with R^2 of 0.998 is achieved, almost similar to results obtained with standard lab potentiostat.
- A Python based web application is designed to visualize and analyze the obtained data from prototype. The data can be uploaded directly on the web application in the form

of .CSV files to obtain the concentration of copper present in tested sample. The application is also connected with a public database to store data files for use in future.

- A Matlab-based application is developed to provide rapid and robust quantitative yeast growth analysis from spot plating assay images. Spot plating assay is a typical procedure to evaluate yeast growth in low-throughput laboratory settings, including growth on different nutrient sources or treatment with specific stressors. The app has a one-step installation process, a self-explanatory interface and shorter analysis steps compared with previous established methods, providing a useful tool for quantitative assessment of growth and survival for both expert and non-expert yeast researchers.

7.2 Limitations and Challenges

Despite the promising advancements demonstrated in this study, several limitations and challenges need to be acknowledged.

- First, the sensitivity of the developed electrochemical biosensor is currently constrained by the use of non-engineered yeast cells. In this work the strains were selected by extensive literature review and using hit and trial method. Although the selected strain showed affinity towards the analyte of interest, it took us immense amount of time to identify strains that showed affinity towards $CuSO_4$. The challenge lies in improving this sensitivity through the preparation and implementation of engineered yeast cells specifically tailored to detect the analyte of interest.
- Second, while yeast-based biosensors, particularly those using *S. cerevisiae*, offer several advantages, including robustness and ease of modification, the detection capabilities still require improvement to meet the stringent demands of precision agriculture applications. In this study we achieved a limit of detection (LoD) as low as 2.2 μM for $CuSO_4$ concentration from 0 – 1 mM only in laboratory settings and further optimization is necessary to ensure consistent performance and broadened detection range across different environmental conditions and analyte concentrations.
- Third, the integration of biosensors with handheld prototype devices and web application presents challenges related to the standardization and scalability of such technologies. In this work, due to multidisciplinary nature of the project and lack of adequate time we used a commercially available potentiostat board for development of prototype which can be replaced with a customised board that may reduce the size and cost. Moreover, taking in account the ease of access, the web application developed in this work uses free public data base that is prone to data loss and there is need of dedicated data base. Hence, further testing and development ensuring that these systems can reliably collect, store, and analyse data in real-world agricultural settings is essential but challenging due to potential variations in field conditions.
- Finally, while the developed prototype demonstrated comparable performance to standard laboratory equipment, translating these findings into a commercially viable product requires addressing issues such as long-term stability, reproducibility, and cost-effectiveness of the biosensors and associated electronic components. Further research and collaboration with industry partners will be crucial to overcoming these hurdles and realizing the full potential of electrochemical yeast-based biosensors in precision agriculture.

7.3 Future prospects

The technological insights gained from current studies could pave the way to new opportunities for developing biosensors performing in situ monitoring of critical pollutants for the agriculture field and the environment. Below, we outline some potential opportunities for advancing the current work:

- The technological implications of current work may benefit from use of genetically engineered cells specific for detection of certain analyte of interest since selectivity of response in biosensor is related to nature of biorecognition element. The focus of research in this regard can also lead to the development of multiparametric sensors for environmental and agricultural circuits.
- The study of devices performance based on transducers and further optimization of immobilization could have a considerable effect on sensitivity leading to repeatable quantification from miniaturized device.
- Further development of this doctoral research will aim to address the communication systems that can be used to upload measurement to remote control platforms from the prototype to be integrated in IoT with particular focus on NB-IoT, LoRa and Sigfox. In this regard from preliminary studies, it has been observed that NB-IoT dominates in delivering reliable, high- bandwidth connectivity with extensive coverage. However, it is high cost and relies on cellular infrastructure. It is particularly well-suited for applications requiring frequent data exchanges and robust security measures, such as smart metering or asset tracking. LoRa, on the other hand leveraging its long-distance capabilities and low-power characteristics, is ideally suited for applications spanning vast areas, such as environmental monitoring or precision agriculture. While Sigfox, distinguished by its simplicity, cost-effectiveness, and global footprint, emerges as the preferred choice for applications demanding small, intermittent data transfers across multiple sites, such as supply chain management. Therefore, in depth study of frontrunner technologies in IoT solutions such as Sigfox, LoRa and NB-IoT are proposed and the decision should be guided by the specific project requirements, ensuring alignment for optimal functionality and success.

References

1. Wennberg, A., *Food and Agriculture Organization of the United Nations.* Encyclopedia of Toxicology, 2014.
2. Godfray, H.C., et al., *Food security: the challenge of feeding 9 billion people.* Science, 2010. **327**(5967): p. 812-8.
3. McBratney, A., et al., *Future Directions of Precision Agriculture.* Precision Agriculture, 2005. **6**: p. 7-23.
4. Gogos, A., K. Knauer, and T.D. Bucheli, *Nanomaterials in plant protection and fertilization: current state, foreseen applications, and research priorities.* J Agric Food Chem, 2012. **60**(39): p. 9781-92.
5. DeRosa, M.C., et al., *Nanotechnology in fertilizers.* Nat Nanotechnol, 2010. **5**(2): p. 91.
6. Chhowalla, M., *Slow Release Nanofertilizers for Bumper Crops.* ACS Cent Sci, 2017. **3**(3): p. 156-157.
7. Dimkpa, C.O. and P.S. Bindraban, *Nanofertilizers: New Products for the Industry?* J Agric Food Chem, 2018. **66**(26): p. 6462-6473.
8. Nair, R., et al., *Nanoparticulate material delivery to plants.* Plant Science, 2010. **179**: p. 154-163.
9. Rees, B., B. Griffiths, and A. McVittie, *Sustainable Intensification of Agriculture: Impacts on Sustainable Soil Management*. 2018. 7-16.
10. Garibaldi, L.A., et al., *Farming Approaches for Greater Biodiversity, Livelihoods, and Food Security.* Trends Ecol Evol, 2017. **32**(1): p. 68-80.
11. Duhan, J.S., et al., *Nanotechnology: The new perspective in precision agriculture.* Biotechnol Rep (Amst), 2017. **15**: p. 11-23.
12. Abobatta, W.F., *Precision Agriculture Age.* 2020. **2**: p. 1-5.
13. Luo, X., et al., *Improving agricultural mechanization level to promote agricultural sustainable development.* 2016. **32**: p. 1-11.
14. van Evert, F., et al., *Can Precision Agriculture Increase the Profitability and Sustainability of the Production of Potatoes and Olives?* Sustainability, 2017. **9**: p. 1863.
15. Ferrández-Pastor, F.J., et al., *Developing Ubiquitous Sensor Network Platform Using Internet of Things: Application in Precision Agriculture.* Sensors (Basel), 2016. **16**(7).
16. Silins, I., A. Korhonen, and U. Stenius, *Evaluation of carcinogenic modes of action for pesticides in fruit on the Swedish market using a text-mining tool.* Front Pharmacol, 2014. **5**: p. 145.
17. Steinborn, A., et al., *Development of a QuEChERS-Based Method for the Simultaneous Determination of Acidic Pesticides, Their Esters, and Conjugates Following Alkaline Hydrolysis.* J Agric Food Chem, 2017. **65**(6): p. 1296-1305.
18. Sawant, S., *Development of Biosensors From Biopolymer Composites*. 2017. 353-383.
19. Bhalla, N., et al., *Introduction to biosensors*. Vol. 60. 2016. 1-8.
20. Sharma, H. and R. Mutharasan, *Review of biosensors for foodborne pathogens and toxins.* Sensors and Actuators B: Chemical, 2013. **183**: p. 535–549.
21. Gonzalez-Rodriguez, J. and M. Raveendran, *Importance of Biosensors.* Biosensors Journal, 2015. **04**.
22. Ispas, C.R., G. Crivat, and S. Andreescu, *Review: Recent Developments in Enzyme-Based Biosensors for Biomedical Analysis.* Analytical Letters, 2012. **45**: p. 168-186.
23. Mehrotra, P., *Biosensors and their applications – A review.* Journal of Oral Biology and Craniofacial Research, 2016. **6**.
24. Viswanathan, S., H. Radecka, and J. Radecki, *Electrochemical biosensors for food analysis.* Monatshefte fuer Chemie/Chemical Monthly, 2009. **140**: p. 891-899.
25. CLARK, L.C. and C. LYONS, *Electrode systems for continuous monitoring in*

cardiovascular surgery. Ann N Y Acad Sci, 1962. **102**: p. 29-45.
26. Labib, M., E.H. Sargent, and S.O. Kelley, *Electrochemical Methods for the Analysis of Clinically Relevant Biomolecules.* Chem Rev, 2016. **116**(16): p. 9001-90.
27. Wu, J., et al., *Biomedical and Clinical Applications of Immunoassays and Immunosensors for Tumor Markers.* TrAC Trends in Analytical Chemistry, 2007. **26**: p. 679-688.
28. Minteer, S.D., *Advances in Electroanalytical Chemistry.* J Am Chem Soc, 2018. **140**(8): p. 2701-2703.
29. Adeniran, A., M. Sherer, and K.E. Tyo, *Yeast-based biosensors: design and applications.* FEMS Yeast Res, 2015. **15**(1): p. 1-15.
30. Jarque, S., et al., *Yeast Biosensors for Detection of Environmental Pollutants: Current State and Limitations.* Trends Biotechnol, 2016. **34**(5): p. 408-419.
31. Martin-Yken, H., *Yeast-Based Biosensors: Current Applications and New Developments.* Biosensors (Basel), 2020. **10**(5).
32. Roda, A., et al., *Analytical strategies for improving the robustness and reproducibility of bioluminescent microbial bioreporters.* Anal Bioanal Chem, 2011. **401**(1): p. 201-11.
33. Lian, J., S. Mishra, and H. Zhao, *Recent advances in metabolic engineering of Saccharomyces cerevisiae: New tools and their applications.* Metab Eng, 2018. **50**: p. 85-108.
34. Turcotte, B., et al., *Transcriptional regulation of nonfermentable carbon utilization in budding yeast.* FEMS Yeast Res, 2010. **10**(1): p. 2-13.
35. Raghavulu, S., et al., *Saccharomyces cerevisiae as anodic biocatalyst for power generation in biofuel cell: Influence of redox condition and substrate load.* Bioresour Technol, 2010. **102**: p. 2751-2757.
36. Sayed, E., et al., *Yeast Extract as an Effective and Safe Mediator for the Baker's-Yeast-Based Microbial Fuel Cell.* Industrial & Engineering Chemistry Research, 2015. **54**: p. 3116-3122.
37. Lovley, D., *Electromicrobiology.* Annual review of microbiology, 2012. **66**: p. 391-409.
38. Xie, X., C. Criddle, and Y. Cui, *Design and fabrication of bioelectrodes for microbial bioelectrochemical systems.* Energy Environ. Sci., 2015. **8**.
39. Li, C.Y., et al., *PCL film surfaces conjugated with P(DMAEMA)/gelatin complexes for improving cell immobilization and gene transfection.* Bioconjug Chem, 2011. **22**(9): p. 1842-51.
40. Geng, W., et al., *Single-cells in nanoshells for functionalization of living cells.* Nanoscale, 2018. **10**.
41. Wu, X.E., et al., *A Role for Microbial Palladium Nanoparticles in Extracellular Electron Transfer.* Angewandte Chemie (International ed. in English), 2011. **50**: p. 427-30.
42. Liu, S.R., et al., *Polydopamine coating on individual cells for enhanced extracellular electron transfer.* Chem Commun (Camb), 2019. **55**(71): p. 10535-10538.
43. Capece, A., et al., *Yeast Starter as a Biotechnological Tool for Reducing Copper Content in Wine.* Front Microbiol, 2017. **8**: p. 2632.
44. García Esparza, M., et al., *Copper content of grape and wine from Italian farms.* Food additives and contaminants, 2006. **23**: p. 274-80.
45. Probst, B., C. Schüler, and R. Joergensen, *Vineyard soils under organic and conventional management - microbial biomass and activity indices and their relation to soil chemical properties.* Biology and Fertility of Soils, 2007. **44**: p. 443-450.
46. Ash, C., et al., *Elevated Soil Copper Content in a Bohemian Vineyard as a Result of Fungicide Application.* Soil and Water Research, 2012. **7**: p. 2012-151.
47. Nogueirol, R.C., et al., *Sequential extraction and availability of copper in Cu fungicide-amended vineyard soils from Southern Brazil.* J Hazard Mater, 2010. **181**(1-3): p. 931-7.
48. Kim, B.E., T. Nevitt, and D.J. Thiele, *Mechanisms for copper acquisition, distribution*

and regulation. Nat Chem Biol, 2008. **4**(3): p. 176-85.
49. Claus, H., *Copper-Containing Oxidases: Occurrence in Soil Microorganisms, Properties, and Applications*. 2010. p. 281-313.
50. Ohsumi, Y., K. Kitamoto, and Y. Anraku, *Changes induced in the permeability barrier of the yeast plasma membrane by cupric ion.* J Bacteriol, 1988. **170**(6): p. 2676-82.
51. Azenha, M., M.T. Vasconcelos, and P. Moradas-Ferreira, *The influence of Cu concentration on ethanolic fermentation by Saccharomyces cerevisiae.* J Biosci Bioeng, 2000. **90**(2): p. 163-7.
52. Mrvcić, J., et al., *Optimization of bioprocess for production of copper-enriched biomass of industrially important microorganism Saccharomyces cerevisiae.* J Biosci Bioeng, 2007. **103**(4): p. 331-7.
53. Thi Minh Pham, H., et al., *Application of modified Arxula adeninivorans yeast cells in an online biosensor for the detection of estrogenic compounds in wastewater samples.* Sensors and Actuators B: Chemical, 2013. **185**: p. 628–637.
54. Balsiger, H.A., et al., *A Four-Hour Yeast Bioassay for the Direct Measure of Estrogenic Activity in Wastewater without Sample Extraction, Concentration, or Sterilization.* The Science of the total environment, 2010. **408**: p. 1422-9.
55. Colosi, J.C. and A.D. Kney, *A yeast estrogen screen without extraction provides fast, reliable measures of estrogenic activity.* Environ Toxicol Chem, 2011. **30**(10): p. 2261-9.
56. Li, J., et al., *A yeast bioassay for direct measurement of thyroid hormone disrupting effects in water without sample extraction, concentration, or sterilization.* Chemosphere, 2014. **100**: p. 139-45.
57. Marsafari, M., et al., *Genetically-encoded biosensors for analyzing and controlling cellular process in yeast.* Curr Opin Biotechnol, 2020. **64**: p. 175-182.
58. Daverey, A., K. Dutta, and A. Sarkar, *An overview of analytical methodologies for environmental monitoring*. 2019. 3-17.
59. Wangmo, C., et al., *In vitro assessment of sex steroids and related compounds in water and sediments - a critical review.* Environ Sci Process Impacts, 2018. **20**(2): p. 270-287.
60. Wahid, E., et al., *Biological and technical challenges for implementation of yeast-based biosensors.* Microbial Biotechnology, 2022. **16**.
61. Roda, A., et al., *A portable bioluminescence engineered cell-based biosensor for on-site applications.* Biosens Bioelectron, 2011. **26**(8): p. 3647-53.
62. Osman, A.G., et al., *Screening of multiple hormonal activities in water and sediment from the river Nile, Egypt, using in vitro bioassay and gonadal histology.* Environ Monit Assess, 2015. **187**(6): p. 317.
63. Vopálenská, I., L. Váchová, and Z. Palková, *New biosensor for detection of copper ions in water based on immobilized genetically modified yeast cells.* Biosens Bioelectron, 2015. **72**: p. 160-7.
64. Nie, M., et al., *Occurrence, distribution and risk assessment of estrogens in surface water, suspended particulate matter, and sediments of the Yangtze Estuary.* Chemosphere, 2015. **127**: p. 109-16.
65. Su, L., et al., *Microbial biosensors: a review.* Biosens Bioelectron, 2011. **26**(5): p. 1788-99.
66. Lehmann, M., et al., *Amperometric measurement of copper ions with a deputy substrate using a novel Saccharomyces cerevisiae sensor.* Biosens Bioelectron, 2000. **15**(3-4): p. 211-9.
67. Shetty, R.S., et al., *Fluorescence-based sensing system for copper using genetically engineered living yeast cells.* Biotechnol Bioeng, 2004. **88**(5): p. 664-70.
68. Park, J.N., et al., *Identification of the cadmium-inducible Hansenula polymorpha SEO1 gene promoter by transcriptome analysis and its application to whole-cell heavy-metal detection systems.* Appl Environ Microbiol, 2007. **73**(19): p. 5990-6000.
69. Gao, G., et al., *Development of a mediated whole cell-based electrochemical biosensor for joint toxicity assessment of multi-pollutants using a mixed microbial consortium.*

Anal Chim Acta, 2016. **924**: p. 21-28.
70. Furger, C., *Live Cell Assays: From Research to Health and Regulatory Applications*. 2016.
71. Hollis, R.P., K. Killham, and L.A. Glover, *Design and application of a biosensor for monitoring toxicity of compounds to eukaryotes.* Appl Environ Microbiol, 2000. **66**(4): p. 1676-9.
72. Nguyen, N.T., et al., *Effect of heavy metals, pesticides and pharmaceuticals on yeast's vacuoles as a biomarker for toxic detection.* Molecular & Cellular Toxicology, 2017. **13**: p. 287-294.
73. Goffeau, A., et al., *Life with 6000 genes.* Science, 1996. **274**(5287): p. 546, 563-7.
74. Botstein, D., S.A. Chervitz, and J.M. Cherry, *Yeast as a model organism.* Science, 1997. **277**(5330): p. 1259-60.
75. Hartwell, L.H., *Saccharomyces cerevisiae cell cycle.* Bacteriol Rev, 1974. **38**(2): p. 164-98.
76. MacKenzie, A.M. and S. Lacefield, *CDK Regulation of Meiosis: Lessons from.* Genes (Basel), 2020. **11**(7).
77. Wang, Z., et al., *Engineering Saccharomyces cerevisiae for improved biofilm formation and ethanol production in continuous fermentation.* Biotechnol Biofuels Bioprod, 2023. **16**(1): p. 119.
78. Cazzanelli, G., et al., *The Yeast Saccharomyces cerevisiae as a Model for Understanding RAS Proteins and their Role in Human Tumorigenesis.* Cells, 2018. **7**(2).
79. Karathia, H., et al., *Saccharomyces cerevisiae as a model organism: a comparative study.* PLoS One, 2011. **6**(2): p. e16015.
80. Tag, K., et al., *Amperometric detection of Cu2+ by yeast biosensors using flow injection analysis (FIA).* Sensors and Actuators B: Chemical, 2007. **122**: p. 403-409.
81. Fan, C., et al., *Engineering Saccharomyces cerevisiae-based biosensors for copper detection.* Microb Biotechnol, 2022. **15**(11): p. 2854-2860.
82. Linder, M.C., et al., *Copper transport.* The American journal of clinical nutrition, 1998. **67**: p. 965S-971S.
83. Puig, S. and D.J. Thiele, *Molecular mechanisms of copper uptake and distribution.* Curr Opin Chem Biol, 2002. **6**(2): p. 171-80.
84. Dancis, A., et al., *The Saccharomyces cerevisiae copper transport protein (Ctr1p). Biochemical characterization, regulation by copper, and physiologic role in copper uptake.* J Biol Chem, 1994. **269**(41): p. 25660-7.
85. Berterame, N.M., et al., *Copper homeostasis as a target to improve Saccharomyces cerevisiae tolerance to oxidative stress.* Metab Eng, 2018. **46**: p. 43-50.
86. Ebadi, M., et al., *Metallothionein, neurotrophins and selegiline in providing neuroprotection in Parkinson's disease.* Restor Neurol Neurosci, 1998. **12**(2-3): p. 103-11.
87. Emamverdian, A., et al., *Heavy metal stress and some mechanisms of plant defense response.* ScientificWorldJournal, 2015. **2015**: p. 756120.
88. Thiele, D.J., *ACE1 regulates expression of the Saccharomyces cerevisiae metallothionein gene.* Mol Cell Biol, 1988. **8**(7): p. 2745-52.
89. Dameron, C.T., et al., *A copper-thiolate polynuclear cluster in the ACE1 transcription factor.* Proc Natl Acad Sci U S A, 1991. **88**(14): p. 6127-31.
90. Dameron, C.T., et al., *Distinct metal binding configurations in ACE1.* Biochemistry, 1993. **32**(28): p. 7294-301.
91. Adamo, P., et al., *Bioavailability and soil-to-plant transfer factors as indicators of potentially toxic element contamination in agricultural soils.* Sci Total Environ, 2014. **500-501**: p. 11-22.
92. Lobsiger, N., et al., *YestroSens, a field-portable S. cerevisiae biosensor device for the detection of endocrine-disrupting chemicals: Reliability and stability.* Biosens Bioelectron, 2019. **146**: p. 111710.
93. Ostrov, N., et al., *A modular yeast biosensor for low-cost point-of-care pathogen*

detection. Sci Adv, 2017. **3**(6): p. e1603221.
94. Shing, W.L., L.Y. Heng, and S. Surif, *Performance of a cyanobacteria whole cell-based fluorescence biosensor for heavy metal and pesticide detection.* Sensors (Basel), 2013. **13**(5): p. 6394-404.
95. Yoetz, T., et al., *"Cells-on-beads": A novel immobilization approach for the construction of whole-Cell amperometric biosensors.* Sensors and Actuators B: Chemical, 2016. **232**.
96. Ahmed, E., *Hydrogel: Preparation, characterization, and applications: A review.* Journal of Advanced Research, 2013. **6**.
97. Ma, C., et al., *Hydrogel Microparticles Functionalized with Engineered.* Sensors (Basel), 2019. **19**(24).
98. Cevenini, L., et al., *A novel bioluminescent NanoLuc yeast-estrogen screen biosensor (nanoYES) with a compact wireless camera for effect-based detection of endocrine-disrupting chemicals.* Anal Bioanal Chem, 2018. **410**(4): p. 1237-1246.
99. Stocker, J., et al., *Development of a set of simple bacterial biosensors for quantitative and rapid measurements of arsenite and arsenate in potable water.* Environ Sci Technol, 2003. **37**(20): p. 4743-50.
100. Martín-Betancor, K., et al., *Microplate freeze-dried cyanobacterial bioassay for fresh-waters environmental monitoring.* Chemosphere, 2017. **189**: p. 373-381.
101. Prévéral, S., et al., *A bioluminescent arsenite biosensor designed for inline water analyzer.* Environ Sci Pollut Res Int, 2017. **24**(1): p. 25-32.
102. Siegfried, K., et al., *Field testing of arsenic in groundwater samples of Bangladesh using a test kit based on lyophilized bioreporter bacteria.* Environ Sci Technol, 2012. **46**(6): p. 3281-7.
103. Knecht, L.D., P. Pasini, and S. Daunert, *Bacterial spores as platforms for bioanalytical and biomedical applications.* Anal Bioanal Chem, 2011. **400**(4): p. 977-89.
104. Wynn, D., S. Deo, and S. Daunert, *Engineering Rugged Field Assays to Detect Hazardous Chemicals Using Spore-Based Bacterial Biosensors.* Methods Enzymol, 2017. **589**: p. 51-85.
105. Sangal, A., P. Pasini, and S. Daunert, *Stability of spore-based biosensing systems under extreme conditions.* Sensors and Actuators B-chemical - SENSOR ACTUATOR B-CHEM, 2011. **158**: p. 377-382.
106. Packer, M. and D. Liu, *Methods for the directed evolution of proteins.* Nature reviews. Genetics, 2015. **16**.
107. Rodriguez, E.A., et al., *The Growing and Glowing Toolbox of Fluorescent and Photoactive Proteins.* Trends Biochem Sci, 2017. **42**(2): p. 111-129.
108. Mirasoli, M., et al., *Internal response correction for fluorescent whole-cell biosensors.* Anal Chem, 2002. **74**(23): p. 5948-53.
109. Yoon, Y., et al., *Simultaneous detection of bioavailable arsenic and cadmium in contaminated soils using dual-sensing bioreporters.* Appl Microbiol Biotechnol, 2016. **100**(8): p. 3713-22.
110. Moscovici, L., et al., *Yeast-Based Fluorescent Sensors for the Simultaneous Detection of Estrogenic and Androgenic Compounds, Coupled with High-Performance Thin Layer Chromatography.* Biosensors (Basel), 2020. **10**(11).
111. Reyes, S., et al., *An Intact Cell Bioluminescence-Based Assay for the Simple and Rapid Diagnosis of Urinary Tract Infection.* Int J Mol Sci, 2020. **21**(14).
112. Goda, T. and Y. Miyahara, *Label-free and reagent-less protein biosensing using aptamer-modified extended-gate field-effect transistors.* Biosens Bioelectron, 2013. **45**: p. 89-94.
113. Kaisti, M., et al., *Hand-Held Transistor Based Electrical and Multiplexed Chemical Sensing System.* ACS Sensors, 2016. **1**.
114. Park, S., et al., *Detection of Avian Influenza Virus from Cloacal Swabs Using a Disposable Well Gate FET Sensor.* Adv Healthc Mater, 2017. **6**(13).
115. Prodromakis, T., Y. Liu, and C. Toumazou, *A Low-Cost Disposable Chemical Sensing Platform Based on Discrete Components.* Electron Device Letters, IEEE, 2011. **32**: p.

417 - 419.
116. Tarasov, A., et al., *A potentiometric biosensor for rapid on-site disease diagnostics.* Biosens Bioelectron, 2016. **79**: p. 669-78.
117. Sarangadharan, I., et al., *Single Drop Whole Blood Diagnostics: Portable Biomedical Sensor for Cardiac Troponin I Detection.* Anal Chem, 2018. **90**(4): p. 2867-2874.
118. Choi, S., et al., *Quantitative Studies of Long-Term Stable, Top-Down Fabricated Silicon Nanowire Ph Sensors.* Applied Physics A, 2012. **107**.
119. Fernandes, P., et al., *Effect of mobile ions on ultrathin silicon-on-insulator-based sensors.* Applied Physics Letters, 2010. **97**: p. 034103-034103.
120. Guan, W., X. Duan, and M.A. Reed, *Highly specific and sensitive non-enzymatic determination of uric acid in serum and urine by extended gate field effect transistor sensors.* Biosens Bioelectron, 2014. **51**: p. 225-31.
121. Zhou, W., et al., *Long term stability of nanowire nanoelectronics in physiological environments.* Nano Lett, 2014. **14**(3): p. 1614-9.
122. Kelley, S.O., et al., *Advancing the speed, sensitivity and accuracy of biomolecular detection using multi-length-scale engineering.* Nat Nanotechnol, 2014. **9**(12): p. 969-80.
123. Krishnan, S., et al., *Attomolar detection of a cancer biomarker protein in serum by surface plasmon resonance using superparamagnetic particle labels.* Angew Chem Int Ed Engl, 2011. **50**(5): p. 1175-8.
124. Liu, D., et al., *Trends in miniaturized biosensors for point-of-care testing.* TrAC Trends in Analytical Chemistry, 2019. **122**: p. 115701.
125. Routray, S., et al., *Internet of Things Based Precision Agriculture for Developing Countries*. 2019. p. 1064-1068.
126. Hassan, R.Y.A., F. Febbraio, and S. Andreescu, *Microbial Electrochemical Systems: Principles, Construction and Biosensing Applications.* Sensors (Basel), 2021. **21**(4).
127. Hubenova, Y. and M. Mitov, *Mitochondrial origin of extracelullar transferred electrons in yeast-based biofuel cells.* Bioelectrochemistry, 2015. **106**(Pt A): p. 232-9.
128. Mao, L. and W.S. Verwoerd, *Exploration and comparison of inborn capacity of aerobic and anaerobic metabolisms of Saccharomyces cerevisiae for microbial electrical current production.* Bioengineered, 2013. **4**(6): p. 420-30.
129. Ikebukuro, K., et al., *Microbial cyanide sensor for monitoring river water.* J Biotechnol, 1996. **48**(1-2): p. 73-80.
130. Mulchandani, *Principles of Enzyme Biosensors*. 1998, Totowa, NJ: Humana Press. 3--14.
131. Singh, M., et al., *Urea biosensors.* Sensors and Actuators B: Chemical, 2008. **134**: p. 345-351.
132. Giese, E.C., et al., *Immobilized microbial nanoparticles for biosorption.* Crit Rev Biotechnol, 2020. **40**(5): p. 653-666.
133. Zahirinejad, S., et al., *Nano-organic supports for enzyme immobilization: Scopes and perspectives.* Colloids Surf B Biointerfaces, 2021. **204**: p. 111774.
134. Liu, D., et al., *Immobilization of Biomass Materials for Removal of Refractory Organic Pollutants from Wastewater.* Int J Environ Res Public Health, 2022. **19**(21).
135. Hartmeier, W. and J. Wieser, *Immobilized Biocatalysts: An Introduction*. 2012.
136. D'Souza, S., *Microbial Biosensors.* Biosensors & bioelectronics, 2001. **16**: p. 337-53.
137. Mikkelsen, S.R. and E. Cortn, *Bioanalytical Chemistry*. 2016.
138. Ren, D., et al., *Recent environmental applications of and development prospects for immobilized laccase: a review.* Biotechnol Genet Eng Rev, 2020. **36**(2): p. 81-131.
139. Xue, J., et al., *Study on the degradation performance and kinetics of immobilized cells in straw-alginate beads in marine environment.* Bioresour Technol, 2019. **280**: p. 88-94.
140. Bouabidi, Z.B., M.H. El-Naas, and Z. Zhang, *Immobilization of microbial cells for the biotreatment of wastewater: A review.* Environmental Chemistry Letters, 2019. **17**(1): p. 241-257.
141. Datta, S., et al., *Immobilization of laccases and applications for the detection and*

remediation of pollutants: a review. Environmental Chemistry Letters, 2021. **19**: p. 521-538.
142. Zhou, W., W. Zhang, and Y. Cai, *Laccase Immobilization for Water Purification: A Comprehensive Review.* Chemical Engineering Journal, 2020. **403**: p. 126272.
143. Marie Hoarau and Somayesadat Badieyan and, E.N.G.M., *Immobilized enzymes: understanding enzyme – surface interactions at the molecular level.* Organic & Biomolecular Chemistry, 2017. **15**(45): p. 9539-9551.
144. Wu, E., et al., *Laccase immobilization on amino-functionalized magnetic metal organic framework for phenolic compound removal.* Chemosphere, 2019. **233**: p. 327-335.
145. Yang, Y., et al., *Immobilizing laccase to cellulose-biochar composite beads for removing phenol from an aqueous system.* Desalination and Water Treatment, 2021. **226**: p. 157-166.
146. Chen, X., et al., *Removal of nine pesticide residues from water and soil by biosorption coupled with degradation on biosorbent immobilized laccase.* Chemosphere, 2019. **233**: p. 49-56.
147. Holten-Andersen, N. and J.H. Waite, *Mussel-designed protective coatings for compliant substrates.* J Dent Res, 2008. **87**(8): p. 701-9.
148. Papov, V., et al., *Hydroxyarginine-containing Polyphenolic Proteins in the Adhesive Plaques of the Marine Mussel Mytilus edulis.* The Journal of biological chemistry, 1995. **270**: p. 20183-92.
149. Liu, Y., K. Ai, and L. Lu, *Polydopamine and Its Derivative Materials: Synthesis and Promising Applications in Energy, Environmental, and Biomedical Fields.* Chemical reviews, 2014. **114**.
150. Yang, S.H., et al., *Mussel-inspired encapsulation and functionalization of individual yeast cells.* J Am Chem Soc, 2011. **133**(9): p. 2795-7.
151. Fakhrullin, R., et al., *Cyborg cells: Functionalisation of living cells with polymers and nanomaterials.* Chemical Society reviews, 2012. **41**: p. 4189-206.
152. Wang, L., et al., *Polydopamine nanocoated whole-cell asymmetric biocatalysts.* Chem Commun (Camb), 2017. **53**(49): p. 6617-6620.
153. Du, Q., et al., *Protection of Electroactive Biofilm from Extreme Acid Shock by Polydopamine Encapsulation.* Environmental Science & Technology Letters, 2017. **4**.
154. Lee, H., et al., *Mussel-inspired surface chemistry for multifunctional coatings.* Science, 2007. **318**(5849): p. 426-30.
155. Buscemi, G., et al., *Bio-Inspired Redox-Adhesive Polydopamine Matrix for Intact Bacteria Biohybrid Photoanodes.* ACS Appl Mater Interfaces, 2022. **14**(23): p. 26631-41.
156. Malhotra, B. and M.A. Ali, *Nanomaterials in Biosensors*. 2018. 1-74.
157. Shanker, A., K. Lee, and J. Kim, *Synthetic Hybrid Biosensors*. 2014.
158. Grieshaber, D., et al., *Electrochemical Biosensors - Sensor Principles and Architectures.* Sensors (Basel), 2008. **8**(3): p. 1400-1458.
159. Chaubey, A. and B. Malhotra, *Mediated biosensor.* Biosensors & bioelectronics, 2002. **17**: p. 441-56.
160. Wang, B., et al., *Recent Advances in Electrochemical Biosensors for the Detection of Foodborne Pathogens: Current Perspective and Challenges.* Foods, 2023. **12**(14).
161. Pisoschi, A.M., *Potentiometric Biosensors: Concept and Analytical Applications-An Editorial.* Biochemistry & Analytical Biochemistry, 2016. **5**.
162. Arikawa, Y., K. Ikebukuro, and I. Karube, *Microbial Biosensors Based on Respiratory Inhibition*. 1998.
163. Simonian, A., E. Rainina, and J. Wild, *Microbial Biosensors Based on Potentiometric Detection*. 1998. 237-248.
164. Trimmer, W.S., *Micromechanics and MEMS: Classic and seminal papers to 1990*. 1997. 1-704.
165. Dzyadevych, S.V., et al., *Conductometric Enzyme Biosensors*. 2008: John Wiley & Sons Ltd.
166. Korpan, Y.I., et al., *Conductometric biosensor for ethanol detection based on whole*

yeast cells. Ukr Biokhim Zh (1978), 1994. **66**(1): p. 78-82.
167. Shul'ga, A.A., et al., *Thin-film conductometric biosensors for glucose and urea determination.* Biosens Bioelectron, 1994. **9**(3): p. 217-23.
168. Dzyadevych, S. and N. Jaffrezic-Renault, *Conductometric biosensors*. 2014. 153-193.
169. Radhakrishnan, R., et al., *Impedance Biosensors: Applications to Sustainability and Remaining Technical Challenges.* ACS Sustain Chem Eng, 2014. **2**(7): p. 1649-1655.
170. Guaragnella, N., et al., *Signaling Sustains Mitochondrial Respiratory Capacity in.* Microorganisms, 2021. **9**(9).
171. Di Noia, M.A., et al., *Inactivation of.* Int J Mol Sci, 2023. **24**(6).
172. Mensah, T.A. and S.M. Tagoe, *Measurement of Yeast Growth Using Spectrophotometer.* 2019.
173. Alupoaei, C.E. and L.H. García-Rubio, *Growth behavior of microorganisms using UV-Vis spectroscopy: Escherichia coli.* Biotechnol Bioeng, 2004. **86**(2): p. 163-7.
174. Perkampus, H.-H., *UV-VIS Spectroscopy and Its Applications*. 1992, Berlin, Heidelberg: Springer Berlin Heidelberg. 3--9.
175. De Caro, C.A. and C. Haller, *UV/VIS Spectrophotometry - Fundamentals and Applications*. 2015.
176. Liu, E., et al., *3.317 - Fluorescence Imaging of Cell–Biomaterial Interactions*, in *Comprehensive Biomaterials*, D. Paul, Editor. 2011, Elsevier: Oxford. p. 291-303.
177. Benjamin Ocheja, O., et al., *Polydopamine-immobilized yeast cells for portable electrochemical biosensors applied in environmental copper sensing.* Bioelectrochemistry, 2024. **157**: p. 108658.
178. *Yeast Fluorescence Microscopy*, ed. W. Xiao. 2006, Totowa, NJ: Humana Press. 85--96.
179. Tang, S.Y., et al., *High resolution scanning electron microscopy of cells using dielectrophoresis.* PLoS One, 2014. **9**(8): p. e104109.
180. Czerwińska-Główka, D. and K. Krukiewicz, *Guidelines for a Morphometric Analysis of Prokaryotic and Eukaryotic Cells by Scanning Electron Microscopy.* Cells, 2021. **10**(12).
181. Karimy, M.F., et al., *A simple method for analysis of Saccharomyces cerevisiae morphology by applying a high vacuum mode of the scanning electron microscopy and without chemical fixatives.* IOP Conference Series: Earth and Environmental Science, 2020. **462**: p. 012048.
182. Wang, B.B., et al., *Preparation of highly effective antibacterial coating with polydopamine/chitosan/silver nanoparticles via simple immersion.* Progress in Organic Coatings, 2020. **149**: p. 105967.
183. Magar, H.S., R.Y.A. Hassan, and A. Mulchandani, *Electrochemical Impedance Spectroscopy (EIS): Principles, Construction, and Biosensing Applications.* Sensors (Basel), 2021. **21**(19).
184. Wang, S., et al., *Electrochemical impedance spectroscopy.* Nature Reviews Methods Primers, 2021. **1**(1): p. 41.
185. Lee, J., *Electrochemical Sensing of Oxygen Gas in Ionic Liquids on Screen Printed Electrodes*. 2014.
186. Brett, C. and A.M.O. Brett, *Electroanalysis*. 1998: OUP Oxford.
187. Cozzi, R., P. Protti, and T. Ruaro, *Analisi chimica : moderni metodi strumentali*. Milano: CLUED ESU Zanichelli.
188. Harris, P., *Fullerene-Related Structure of Commercial Glassy Carbons.* Philosophical Magazine A-physics of Condensed Matter Structure Defects and Mechanical Properties - PHIL MAG A, 2004. **84**: p. 3159-3167.
189. Zhao, Z., et al., *Nanoarchitectured materials composed of fullerene-like spheroids and disordered graphene layers with tunable mechanical properties.* Nat Commun, 2015. **6**: p. 6212.
190. Awaji, H. and S.-M. Choi, *Thermal Shock Tests and Thermal Shock Parameters for Ceramics.* Journal of the Korean Ceramic Society, 2012. **49**.
191. Hubenova, E., M. Mitov, and Y. Hubenova, *Electrochemical performance of*

Paenibacillus profundus YoMME encapsulated in alginate polymer. Bioelectrochemistry, 2023. **150**: p. 108354.
192. Meyer, C.T., et al., *A high-throughput and low-waste viability assay for microbes.* Nat Microbiol, 2023. **8**(12): p. 2304-2314.
193. Rong-Mullins, X., et al., *Proteomic and genetic analysis of the response of S. cerevisiae to soluble copper leads to improvement of the antimicrobial function of cellulosic copper nanoparticles.* Metallomics, 2017. **9**(9): p. 1304-1315.
194. Sun, X., et al., *Effect of high Cu2+ stress on fermentation performance and copper biosorption of Saccharomyces cerevisiae during wine fermentation.* Food Science and Technology, 2018. **39**.
195. Montllor-Albalate, C., et al., *Extra-mitochondrial Cu/Zn superoxide dismutase (Sod1) is dispensable for protection against oxidative stress but mediates peroxide signaling in Saccharomyces cerevisiae.* Redox Biol, 2019. **21**: p. 101064.
196. Vulpe, C., et al., *Copper Accumulation Efficiency in Different Recombinant Microorganism Strains Available for Bioremediation of Heavy Metal-Polluted Waters.* International Journal of Molecular Sciences, 2023. **24**: p. 7575.
197. Tufail, M., et al., *Recent advances in bioremediation of heavy metals and persistent organic pollutants: A review.* Science of The Total Environment, 2022. **850**: p. 157961.
198. Vopálenská, I., L. Váchová, and Z. Palkova, *New biosensor for detection of copper ions in water based on immobilized genetically modified yeast cells.* Biosensors and Bioelectronics, 2015. **72**.
199. Sharma, S., *Glassy Carbon: A Promising Material for Micro- and Nanomanufacturing.* Materials, 2018. **11**: p. 1857.
200. Elitas, M., et al., *Dielectrophoresis-based purification of antibiotic-treated bacterial subpopulations.* Lab Chip, 2014. **14**(11): p. 1850-7.
201. Kim, J., et al., *Direct Metal Forming of a Microdome Structure with a Glassy Carbon Mold for Enhanced Boiling Heat Transfer.* Micromachines (Basel), 2018. **9**(8).
202. Jouikov, V. and J. Simonet, *Electrochemical conversion of glassy carbon into a poly-nucleophilic reactive material. Applications for carbon chemical functionalization. A mini-review.* Electrochemistry Communications, 2014. **45**: p. 32–36.
203. Alonso-Lomillo, M.A., O. Domínguez-Renedo, and M.J. Arcos-Martínez, *Screen-printed biosensors in microbiology; a review.* Talanta, 2010. **82**(5): p. 1629-36.
204. Wang, J., et al., *Performance of screen-printed carbon electrodes fabricated from different carbon inks.* Electrochimica Acta, 1998. **43**: p. 3459-3465.
205. Fanjul-Bolado, P., et al., *Electrochemical characterization of screen-printed and conventional carbon paste electrodes.* Electrochimica Acta, 2008. **53**: p. 3635-3642.
206. Kadara, R., N. Jenkinson, and C. Banks, *Screen printed recessed microelectrode arrays.* Sensors and Actuators B: Chemical, 2009. **142**: p. 342-346.
207. Police Patil, A.V., et al., *Recent Advances in Electrochemical Immunosensors with Nanomaterial Assistance for Signal Amplification.* Biosensors (Basel), 2023. **13**(1).
208. Gunawardena, A., S. Fernando, and F. To, *Performance of a yeast-mediated biological fuel cell.* Int J Mol Sci, 2008. **9**(10): p. 1893-1907.
209. Tharali, A., N. Sain, and J. Osborne, *Microbial fuel cells in bioelectricity production.* Frontiers in Life Science, 2016. **9**: p. 1-15.
210. Olaifa, K., et al., *Electroanalysis of Candida albicans biofilms: A suitable real-time tool for antifungal testing.* Electrochimica Acta, 2021. **389**: p. 138757.
211. Wark, A.W., et al., *Bioaffinity detection of pathogens on surfaces.* J Ind Eng Chem, 2010. **16**(2): p. 169-177.
212. Santoro, C., et al., *Sub-toxic concentrations of volatile organic compounds inhibit extracellular respiration of Escherichia coli cells grown in anodic bioelectrochemical systems.* Bioelectrochemistry, 2016. **112**.
213. Marsili, E., et al., *Microbial biofilm voltammetry: direct electrochemical characterization of catalytic electrode-attached biofilms.* Appl Environ Microbiol, 2008. **74**(23): p. 7329-37.
214. Babauta, J., et al., *Electrochemically active biofilms: facts and fiction. A review.*

Biofouling, 2012. **28**(8): p. 789-812.
215. Chalenko, Y., et al., *Electrochemistry of Escherichia coli JM109: Direct electron transfer and antibiotic resistance.* Biosensors & bioelectronics, 2011. **32**: p. 219-23.
216. Pires, L., et al., *Online monitoring of biofilm growth and activity using a combined multi-channel impedimetric and amperometric sensor.* Biosens Bioelectron, 2013. **47**: p. 157-63.
217. Hirschorn, B., et al., *Determination of effective capacitance and film thickness from constant-phase-element parameters.* Electrochimica Acta, 2010. **55**: p. 6218-6227.
218. Astorga, S., et al., *Electrochemical signature of Escherichia coli on Ni micropillar array electrode for early biofilm characterization.* ChemElectroChem, 2019. **6**: p. 4674-4680.
219. Salazar, P., M. Martín, and J. González-Mora, *In situ electrodeposition of cholesterol oxidase-modified polydopamine thin film on nanostructured screen printed electrodes for free cholesterol determination.* Journal of Electroanalytical Chemistry, 2019. **837**.
220. Dominguez-Benetton, X., et al., *The Accurate Use of Impedance Analysis for the Study of Microbial Electrochemical Systems.* Chemical Society reviews, 2012. **41**: p. 7228-46.
221. Sánchez, C., et al., *Microbial electrochemical technologies: Electronic circuitry and characterization tools.* Biosens Bioelectron, 2020. **150**: p. 111884.
222. Maslanka, R., R. Zadrag-Tecza, and M. Kwolek-Mirek, *Linkage between Carbon Metabolism, Redox Status and Cellular Physiology in the Yeast.* Genes (Basel), 2020. **11**(7).
223. Vasylkovska, R., N. Petriv, and H. Semchyshyn, *Carbon Sources for Yeast Growth as a Precondition of Hydrogen Peroxide Induced Hormetic Phenotype.* International Journal of Microbiology, 2015. **2015**: p. 1-8.
224. Kirchman, P.A. and G. Botta, *Copper supplementation increases yeast life span under conditions requiring respiratory metabolism.* Mech Ageing Dev, 2007. **128**(2): p. 187-95.
225. Liang, Q. and B. Zhou, *Copper and manganese induce yeast apoptosis via different pathways.* Mol Biol Cell, 2007. **18**(12): p. 4741-9.
226. Stratmann, L. and B. Heery, *EmStat Pico: Embedded Electrochemistry with a Miniaturized, Software- Enabled, Potentiostat System on Module.* 2022.
227. PalmSens. *EmStat Pico Development Kit*. [cited 2024 03/05/2024]; Available from: https://www.palmsens.com/product/oem-emstat-pico-development-kit/.
228. Palmsens. *EmStat Pico Module*. [cited 2024 03/05/2024]; Available from: https://www.palmsens.com/product/oem-emstat-pico-module/.
229. PalmSens. *PStouch*. [cited 2024 03/05/2024]; Available from: https://www.palmsens.com/software/pstouch/.
230. Palmsens. *MethodSCRIPT*. [cited 2024 03/05/2024]; Available from: https://www.palmsens.com/methodscript/.
231. Anshori, I., et al., *Web-based surface plasmon resonance signal processing system for fast analyte analysis.* SoftwareX, 2022. **18**: p. 101057.
232. Ronacher, A. *April 1st Post Mortem*. 2021 [cited 2024 03/05/2024]; Available from: https://lucumr.pocoo.org/2010/4/3/april-1st-post-mortem/.
233. Ronacher, A. *Jinja Project*. 2021 [cited 2024 03/05/2024]; Available from: https://jinja.palletsprojects.com/en/3.1.x/.
234. Django. *Django Project*. 2021 [cited 2024 03/05/2024]; Available from: https://www.djangoproject.com/.
235. Palkova, Z., *Multicellular microorganisms: Laboratory versus nature.* EMBO reports, 2004. **5**: p. 470-6.
236. Kamrad, S., et al., *Pyphe, a python toolbox for assessing microbial growth and cell viability in high-throughput colony screens.* eLife, 2020. **9**.
237. Miller, J., et al., *Using colony size to measure fitness in Saccharomyces cerevisiae.* PloS one, 2022. **17**: p. e0271709.
238. Zackrisson, M., et al., *Scan-o-matic: High-Resolution Microbial Phenomics at a*

Massive Scale. G3 (Bethesda, Md.), 2016. **6**.
239. Bean, G., et al., *Development of Ultra-High-Density Screening Tools for Microbial Omics.* PloS one, 2014. **9**: p. e85177.
240. Petropavlovskiy, A., et al., *A Quantitative Imaging-Based Protocol for Yeast Growth and Survival on Agar Plates.* STAR Protocols, 2020. **1**: p. 100182.
241. Bischof, L., et al., *Spotsizer: High-throughput quantitative analysis of microbial growth.* BioTechniques, 2016. **61**: p. 191-201.
242. Carpenter, A., et al., *CellProfiler: Image analysis software for identifying and quantifying cell phenotypes.* Genome biology, 2006. **7**: p. R100.
243. Shah, N., et al., *Accurate, precise modeling of cell proliferation kinetics from time-lapse imaging and automated image analysis of agar yeast culture arrays.* BMC systems biology, 2007. **1**: p. 3.
244. Collins, S., et al., *A strategy for extracting and analyzing large-scale quantitative epistatic interaction data.* Genome biology, 2006. **7**: p. R63.
245. Lawless, C., et al., *Colonyzer: Automated quantification of micro-organism growth characteristics on solid agar.* BMC bioinformatics, 2010. **11**: p. 287.
246. Dittmar, J., R. Reid, and R. Rothstein, *ScreenMill: A freely available software suite for growth measurement, analysis and visualization of high-throughput screen data.* BMC bioinformatics, 2010. **11**: p. 353.
247. Young, B. and C. Loewen, *Balony: A software package for analysis of data generated by synthetic genetic array experiments.* BMC bioinformatics, 2013. **14**: p. 354.
248. Wagih, O., et al., *SGAtools: One-stop analysis and visualization of array-based genetic interaction screens.* Nucleic acids research, 2013. **41**.
249. Wagih, O. and L. Parts, *gitter: A Robust and Accurate Method for Quantification of Colony Sizes From Plate Images.* G3 (Bethesda, Md.), 2014. **4**.
250. Wahid, E., *Spotting Assay Quantification (GUI)*. 2024, MATLAB Central File Exchange.
251. Guaragnella, N., et al., *RTG Signaling Sustains Mitochondrial Respiratory Capacity in HOG1-Dependent Osmoadaptation.* Microorganisms, 2021. **9**: p. 1894.
252. Guaragnella, N., et al., *Acid Stress Triggers Resistance to Acetic Acid-Induced Regulated Cell Death through Hog1 Activation Which Requires RTG2 in Yeast.* Oxidative Medicine and Cellular Longevity, 2019. **2019**: p. 1-9.
253. Di Noia, M.A., et al., *Inactivation of HAP4 Accelerates RTG-Dependent Osmoadaptation in Saccharomyces cerevisiae.* Int J Mol Sci, 2023. **24**(6).
254. Quesada Torelli, N., et al., *RTG1 and RTG2-Dependent Retrograde Signaling Control Mitochondrial Activity and Stress Resistance in S. cerevisiae.* Free radical biology & medicine, 2015. **81**.
255. Hijazi, I., J. Knupp, and A. Chang, *Retrograde signaling mediates an adaptive survival response to endoplasmic reticulum stress.* Journal of Cell Science, 2020. **133**: p. jcs.241539.
256. Ruiz-Roig, C., et al., *The Hog1 SAPK controls the Rtg1/Rtg3 transcriptional complex activity by multiple regulatory mechanisms.* Molecular biology of the cell, 2012. **23**.
257. Chadwick, S., et al., *A Toolbox for Rapid Quantitative Assessment of Chronological Lifespan and Survival in Saccharomyces cerevisiae.* Traffic (Copenhagen, Denmark), 2016. **17**.
258. Wloch-Salamon, D. and A. Bem, *Types of cell death and methods of their detection in yeast Saccharomyces cerevisiae.* Journal of applied microbiology, 2012. **114**.